VOLUME XLIV

GEMS & GEMOLOGY

SUMMER 2008

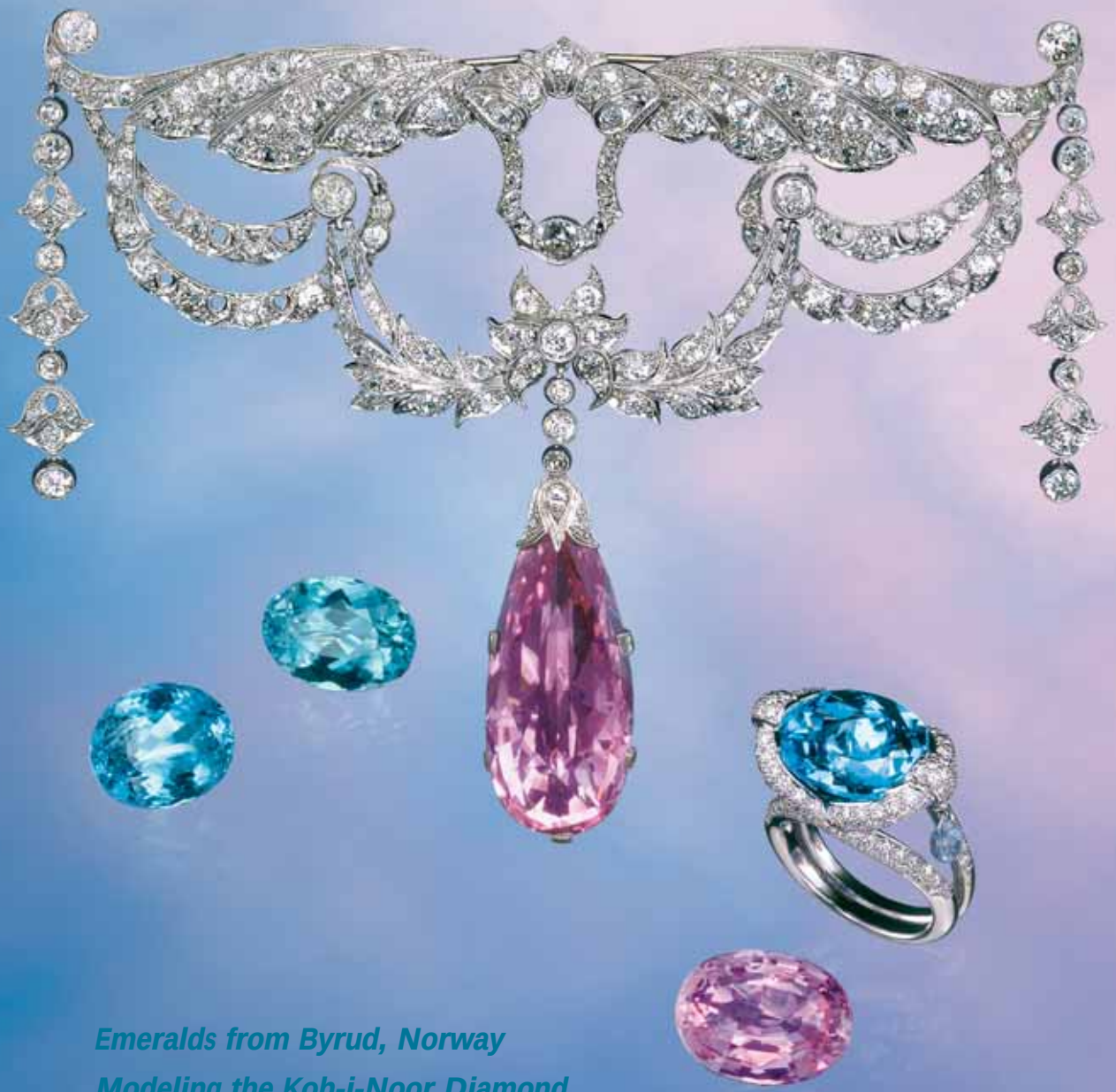

Emeralds from Byrud, Norway
Modeling the Koh-i-Noor Diamond
Coated Tanzanite
New Topaz Color Treatments

THE QUARTERLY JOURNAL OF THE GEMOLOGICAL INSTITUTE OF AMERICA

GEMS & GEMOLOGY®

Summer 2008

VOLUME 44, NO. 2

pg. 109

pg. 143

EDITORIAL

FEATURE ARTICLES

NOTES AND NEW TECHNIQUES

REGULAR FEATURES

pg. 159

pg. 178

GEMS & GEMOLOGY

www.gia.edu/gemsandgemology

SUBSCRIPTIONS

Subscriptions to addresses in the U.S. are priced as follows: **$74.95** for one year (4 issues), **$194.95** for three years (12 issues). Subscriptions sent elsewhere are **$85.00** for one year, **$225.00** for three years. Canadian subscribers should add GST.

Special rates are available for GIA alumni and current GIA students. One year: **$64.95** to addresses in the U.S., **$75.00** elsewhere; three years: **$179.95** to addresses in the U.S., **$210.00** elsewhere. Please have your student or Alumni number ready when ordering. Go to www.gia.edu/gemsandgemology or contact the Circulation Coordinator (see above).

Single copies of this issue (print or PDF) may be purchased for **$19.00** in the U.S., **$22.00** elsewhere. Discounts are given for bulk orders of 10 or more of any one issue. A limited number of back issues are also available for purchase. Please address all inquiries regarding subscriptions and single copy or back issue purchases to the Circulation Coordinator or visit www.gia.edu/gemsandgemology.

To obtain a Japanese translation of *Gems & Gemology*, contact GIA Japan, Okachimachi Cy Bldg., 5-15-14 Ueno, Taitoku, Tokyo 110, Japan. Our Canadian goods and service registration number is 126142892RT.

DATABASE COVERAGE

Gems & Gemology's impact factor is 1.381 (ranking 11th out of the 26 journals in the Mineralogy category), according to Thomson Scientific's 2006 Journal Citation Reports (issued July 2007). *Gems & Gemology* is abstracted in Thompson Scientific products (*Current Contents: Physical, Chemical & Earth Sciences* and Science Citation Index—Expanded, including the Web of Knowledge) and other databases. For a complete list, see www.gia.edu/gemsandgemology.

MANUSCRIPT SUBMISSIONS

Gems & Gemology welcomes the submission of articles on all aspects of the field. Please see the Guidelines for Authors on our Website, or contact the Managing Editor. Letters on articles published in *Gems & Gemology* are also welcome.

Gems & Gemology is published quarterly by the Gemological Institute of America, a nonprofit educational organization for the gem and jewelry industry, The Robert Mouawad Campus, 5345 Armada Drive, Carlsbad, CA 92008.

Postmaster: Return undeliverable copies of *Gems & Gemology* to GIA, The Robert Mouawad Campus, 5345 Armada Drive, Carlsbad, CA 92008.

ABOUT THE COVER

Concerns about topaz irradiation have led to the development of alternative color enhancement processes. In this issue, Dr. Harald Gabasch and a team of researchers examine the mechanisms by which a coating or a diffusion-induced layer near the surface can impart color to colorless topaz. Shown here is a selection of topaz jewelry and loose faceted stones from the GIA Collection. The 9.36 ct blue (GIA Collection no. 33563), 11.39 ct blue (no. 34302), and 14.47 ct pink topaz (no. 34304) are from the collection of Dr. Edward J. Gübelin. The blue topaz (11.54 ct) and sapphire ring set in 18K gold (no. 30973) is a gift of Jacques Prades. The Belle Époque platinum corsage ornament (no. 22746) features a 39.80 ct pink topaz and diamonds. A gift of Stephen and Eileen Silver, S. H. Silver Co., it is a founding piece in GIA's Historical Collection.

Photo © GIA and Harold & Erica Van Pelt. Composite image designed by Karen Myers.

Color separations for Gems & Gemology *are by Pacific Plus, Carlsbad, California.*
Printing is by Allen Press, Lawrence, Kansas.

 ISSN 0016-626X

GRC
GEMOLOGICAL RESEARCH CONFERENCE 2009
SAN DIEGO, CA ♥ AUGUST 21–23

Ten Reasons Why *You* Should Attend the 2009 GRC

The 2nd Gemological Research Conference will take place August 21–23, 2009, at the Town & Country Resort and Convention Center in San Diego, California. Co-chaired by GIA distinguished research fellow Dr. James Shigley and *G&G* editor Brendan Laurs, the GRC is a must-attend event for anyone involved in—or benefiting from—the broad range of research areas in gemology. Here are our top 10 reasons why you should plan now to attend the 2009 GRC:

1. Pure knowledge. New gem sources. Innovative technologies for gem treatment, synthesis, and identification. Emerging trends in gem marketing. The latest findings in analyzing and communicating cut and color. These are just some of the topics that will be explored at the GRC, through a program of lectures, panel discussions, and interactive poster sessions.

2. Session choices. The parallel-track format—one track for classical gemology and one for technical jewelry/business issues—means you can tailor the program to your own research interests or educational needs.

3. High-caliber keynote speakers. The GRC's compelling lineup of invited speakers features experts in a variety of technical and business-related fields. These include prominent scientists such as Caltech mineralogist Dr. George Rossman, CVD synthetic diamond developer Dr. Robert Linares, and spectroscopist Dr. Alexander Zaitsev, as well as appraisals specialist Gail Brett Levine, CAD/CAM whiz Jeff High, and representatives from major gemological laboratories in the United States, Europe, and Asia.

4. Exciting extracurricular activities. Field trips to the gem pegmatite mines of San Diego County, a gem photography contest and workshop, and various social events will be available to all participants.

5. Networking opportunities. Whether you're attending the social events or just enjoying a coffee break between sessions, you'll have the chance to form or renew valuable relationships with influential peers in the gemological community as well as experts from other sciences and elsewhere in the gem and jewelry industry.

6. Destination: San Diego. One of the most popular tourist destinations in the United States, San Diego is known for its sunny climate and beautiful Pacific beaches. Local attractions include the famous San Diego Zoo and Wild Animal Park, Sea World, and world-class golfing. This vibrant city lies just north of the Mexican border and is a two-hour drive south of Los Angeles. Accommodations at the Town & Country, which features several restaurants and swimming pools, are reasonably priced, and the hotel is located close to public transportation and shopping.

7. International flavor. The first GRC, held in August 2006, brought together hundreds of gemologists, researchers, and industry professionals from 32 countries. The 2009 GRC, with advisory committee members from five continents, already promises to have that same international quality.

8. Inspiration. What happens when you join a heady mix of academics and gem and jewelry industry leaders for three stimulating days in a place that's often called "America's Finest City"? You take away more than just insights and new contacts. You return home with renewed energy, creativity, and clarity of purpose.

9. The chance to take the stage. Do you have your own talk or poster you'd like to present? The GRC offers a unique forum for participants to share technical information with their colleagues. Submit a brief abstract of your presentation between September 1, 2008, and March 1, 2009. All abstracts will be reviewed by members of the GRC Advisory Committee; those that are accepted and presented at the conference will appear in a Proceedings volume.

10. Comments from 2006 GRC participants. I could give many more reasons why you should come to the GRC, but instead I'll close with a few words from participants at the first conference:

[I]t is a really unique opportunity to meet important researchers.

It was a very professional meeting. One of the best I have seen. . . .

[A] valuable summit meeting for our science. . . .

I thoroughly enjoyed myself, and everyone else I talked to was also very pleased.

Technology is advancing so rapidly it seems almost impossible to keep up. But keep up we must, and only by joining together in a forum such as the 2009 GRC can we harness our combined expertise to meet these challenges to the gem and jewelry industry. To learn more about this event, visit www.grc2009.gia.edu or e-mail grc2009@gia.edu.

If you can attend only one conference in 2009, make it the GRC.

Alice S. Keller
Editor-in-Chief
akeller@gia.edu

CHARACTERIZATION OF EMERALDS FROM A HISTORICAL DEPOSIT: BYRUD (EIDSVOLL), NORWAY

Benjamin Rondeau, Emmanuel Fritsch, Jean-Jacques Peucat,
Fred Steinar Nordrum, and Lee Groat

An emerald deposit at Byrud, in southern Norway, yielded significant quantities of crystals and gem rough in the late 19th and early 20th centuries. Complex multiphase inclusions in the emeralds consist of water, gaseous methane, halite, sylvite, calcite, and a sulfide assemblage (pyrrhotite, galena, and sphalerite). This sulfide assemblage makes it easy to distinguish Byrud emeralds from those from other localities with a binocular microscope. The chemical composition of Byrud emeralds is also characteristic: They are colored mostly by vanadium (up to 1 wt.% V_2O_3), and contain low sodium and magnesium (0.1 wt.% oxide or less). Moreover, the relative amounts of iron, magnesium, chromium, rubidium, and cesium appear to be diagnostic. Infrared absorption spectra show that they contain little water. Emeralds from the Byrud deposit are still occasionally recovered by hobbyist collectors from the mine dumps.

During the late 19th and early 20th centuries, the Byrud emerald deposit in Norway was mined commercially and produced many fine specimens (e.g., figure 1), as well as a limited amount of gem rough. Some of the crystals are housed in museum collections around Europe, and it is not uncommon to encounter a Byrud emerald in an antique jewelry piece. The mine is located on the shore of Lake Mjøsa, near Minnesund and a short distance from Eidsvoll, about 60 km north-northeast of Oslo, Norway (figure 2). The history, geology, and mineralogy of the deposit were comprehensively described by Nordrum and Raade (2006), and are summarized here. The aim of the present article is to characterize the emeralds from Byrud to make their unambiguous identification possible.

From a geologic and spectroscopic standpoint, emeralds from Byrud are interesting because they are vanadium-rich, as is also the case for emeralds from Colombia and some (or all) emeralds from a number of other deposits: Lened in the Northwest Territories, Canada; Salininha in Bahia, Brazil; Malipo in Yunnan, China; Panjshir, Afghanistan; and Gandao, Pakistan. In this article, we refer to "vanadian emeralds" as those that contain more vanadium than chromium, even when the vanadium content is somewhat low. The mechanisms of beryl coloration by Cr and V are very similar (Burns, 1993; Schwarz and Schmetzer, 2002); in 1988, after many years of controversy, vanadium joined chromium as an accepted coloring agent for emerald (CIBJO, 1988).

HISTORICAL BACKGROUND

The Byrud emerald deposit was probably discovered in the 1860s. During these early years, emerald specimens were obtained by several European natural history museums, including Stockholm in

See end of article for About the Authors and Acknowledgments.
GEMS & GEMOLOGY, Vol. 44, No. 2, pp. 108–122.

Figure 1. This 1.1-cm-long gem-quality emerald crystal on matrix, which was found by a collector at Byrud in the 1980s, is typical of emeralds from this locality. It is accompanied by quartz, feldspar, spheres of muscovite, and grayish fluorite. Courtesy of the Norwegian Mining Museum, Kongsberg; photo by Rainer Bode.

1868, Oslo in 1869, and London in 1870. Websky (1876) first described the morphology of the Byrud emeralds, and stated that the deposit was of commercial importance.

Preliminary prospecting and blasting took place around 1880 (Bull, 1952). Evelyn Aston inspected the almost forgotten occurrence in November 1898; at that time, the old workings consisted of an opening 2 m high and 1 m wide that accessed a room measuring about 3.5 m in diameter. On her next visit, she brought a miner who blasted further, and they found gem-quality emerald crystals in small clay-filled pockets (Cameron, 1963).

On April 5, 1899, the prospect (called Narum) was purchased by Evelyn's father, English mining prospector Edward Y. Aston. A London-based company—the Norwegian Exploration Co. Ltd.—was registered May 9, with Aston as a major shareholder in exchange for the property and rights to the emerald occurrence, as well as some additional prospects. Mining began in spring 1899 (figure 3). In June 1900, the company was renamed the Norwegian & General Exploration Co. Ltd. Edward Aston died on September 21, 1900, and on December 28, 1907, the company was liquidated and the assets sold to the Cornish Development Co. Ltd. The mine was subsequently abandoned in 1909 (Nordrum and Raade, 2006).

In the first years of mining, up to 30 miners were employed at Byrud. A crusher, washing plant, blacksmith's forge, administration building, and a small workshop were reportedly built at the mine, but few vestiges are visible today. However, production could not sustain this level of mining for very long, and by the time the mine closed 10 years later, it had only nine employees. It does not appear that the mine was ever profitable, even during the first few years (Nordrum and Raade, 2006).

Nevertheless, many gem-quality emeralds were recovered, some of which were displayed at the Paris World's Fair in 1900. Besides crystals, wrote Kunz (1902, p. 742), "Many cut stones, most of them pale in color, but generally free from flaws, were shown." Sinkankas (1981, p. 487) stated: "Only rarely were good stones found and then never

Figure 2. The Byrud emerald deposit is located on the western shore of Norway's Lake Mjøsa, close to Minnesund and a short distance from Eidsvoll, in southeastern Norway. Adapted with permission from Mineralien Welt *(Nordrum and Raade, 2006, p. 52).*

Figure 3. Commercial mining of the Byrud emerald deposit began in 1899, when this photo was taken. This building has since disappeared, but the tunnels are still visible. Courtesy of the Aston family archives.

more than about 6 mm in diameter, but the color quality was considered to be of the highest grade, and if anything a little too bluish. Selset (1963) cut some of the crystals himself and claimed that the gems matched the finest from any other source." Most of the transparent crystals from cavities were pale colored, but some were a fine, deep green. Cemented in feldspar, translucent crystals up to more than 1.2 cm in diameter and 5 cm in length with a deep green color were recovered. Translucent crystals were also commonly found in quartz.

A cut emerald from Byrud is said to have been used in a jewel belonging to the royal family of Great Britain, possibly in connection with the coronation of King Edward VII in 1902. The English companies sold the rough crystals and mineral specimens outside Norway, and no records of the sales have been found. The production data and names of the buyers are unknown (Nordrum and Raade, 2006).

Most of the emerald crystals pictured in this article were found by mineral collectors over the past 30 years (see, e.g., figure 4). For a small daily fee to the landowners, collectors have been allowed to search in the mine dumps. Several fine specimens and single crystals have been recovered over the years, but

the chances of making good finds are diminishing and gem-quality specimens are discovered only rarely today. The underground mine has not been worked since 1909.

GEOLOGY AND MINERALOGY

The emerald deposit is located in the northeastern part of the Oslo region, which is a rift structure of Permian age (Vogt, 1884; Goldschmidt, 1911; Nordrum and Raade, 2006). Flat-lying maenaite (syenitic) sills, usually ranging from 0.5 m to several meters thick, transect Cambrian alum shale (a black, clay-rich, iron sulfide–containing, carbonaceous sedimentary rock) over a distance of about 200 m. The sills generally dip 15–20° west but are nearly horizontal in places. They are present in at least three levels and have been intruded by small pegmatites, which also cross-cut the alum shales. Close to the pegmatites, the shales are often bleached. The pegmatites usually range from a few centimeters to 30 cm in thickness, but may locally reach up to 1 m. They form lenses or dikes that are commonly discontinuous and locally contain small cavities. The pegmatites have an alkali syenitic composition, consisting mainly of K-feldspar (microcline), and were intruded during the Permian Period in conjunction with alkaline magmatic activity in the area (Ihlen, 1978). A large alkaline granite intrusion occurs not far to the west of Byrud, and the pegmatites are most likely associated with this intrusive.

Emerald mining has taken place along the maenaite sills at various levels. Beryl occurs chiefly in the pegmatites (figure 5), and occasionally in the maenaites and in the shales adjacent to the pegmatites. The best-quality emeralds have been found in the northern part of the mining area (Lindaas, 1982), in small clay-filled pockets (Cameron, 1963). Vanadium and chromium, chromophores in the emeralds, were probably leached from the alum shales by the mineralizing fluids.

In addition to microcline, the pegmatites typically contain quartz and muscovite. Sodic plagioclase, pyrite, pyrrhotite, fluorite (purple and pale green), topaz, and beryl are also common in the pegmatites. Micro-crystals of laumontite and rutile ("ilmenorutile-strüverite") are frequently present as well. Goethite, jarosite, and gypsum are common secondary minerals. In all, 45 minerals have been reported from this deposit (Nordrum and Raade, 2006; Kvamsdal and Eldjarn, 2007). A complete list of minerals associated with the emerald mineralization is available on the *G&G* Data Depository (www.gia.edu/gemsandgemology).

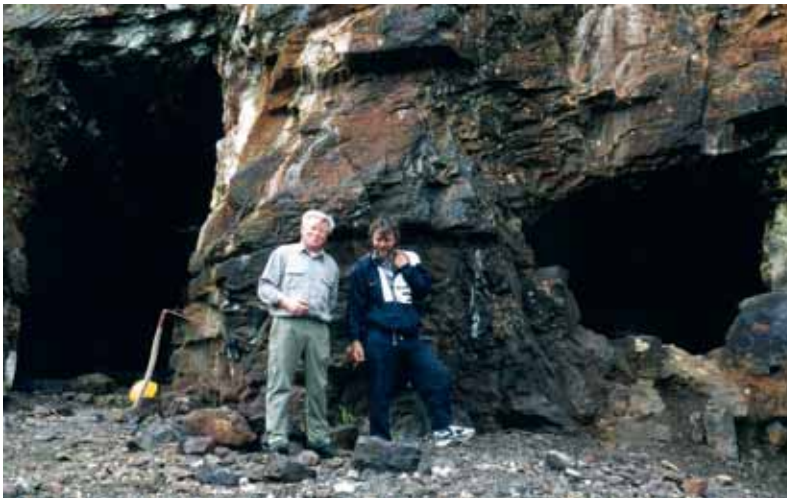

Figure 4. Galleries excavated for emerald extraction during the late 19th and early 20th centuries are still visible. Mineral collectors, such as Arnfinn Juliussen and Bjørn Skår in this photo, can visit the mine with the permission of the owners, Anne Grethe Røise and Ole Jørgen Bjørnstad. Photo by F. S. Nordrum.

MATERIALS AND METHODS

The authors studied three emerald-in-matrix specimens, collected more than a century ago, from the mineralogy collection of the Muséum National d'Histoire Naturelle (National Museum of Natural History) in Paris (collection nos. 106.718, 195.174,

Figure 5. Byrud emerald crystals are found mainly in small pegmatites intruding alum shales. This sample is 9.5 cm long, and the emerald crystals attain lengths of 9 mm. Courtesy of the Norwegian Mining Museum; photo by Gunnar Jenssen.

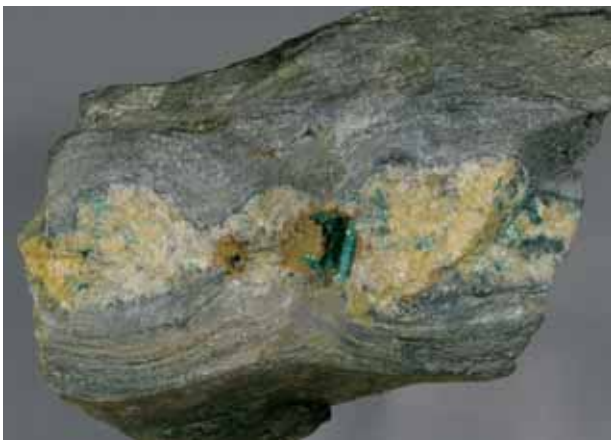

and 203.18). These idiomorphic bluish green crystals, each a few millimeters in length, are intergrown with feldspar, quartz, muscovite, and purple fluorite. One emerald crystal was removed from each of the matrix specimens and all three were polished to measure their gemological, chemical, and spectroscopic properties. In addition, we studied four loose transparent crystals, each measuring a few millimeters in length, that were recovered in the 1980s and belong to the collection of the Norwegian Mining Museum in Kongsberg (collection nos. BVM2378–A to D; figure 6). All seven samples studied were transparent and homogeneous in color, so we believe that they are representative of the material from which gems would be faceted. We did not study any cut stones or stones set in jewelry, as the very few that are known were not accessible.

Gemological data were acquired on various samples (see Results) using a Topcon refractometer, a 4-watt UV lamp with short-wave (254 nm) and long-wave (365 nm) bulbs, and an Olympus binocular microscope equipped with crossed polarizers and up to 1000× magnification. Specific gravity was determined by a combination of mass measurement using a precision scale and volume measurement using a classic pycnometer.

The composition of fluid inclusions in three samples (nos. 106.718, 195.174, and 203.18) was first determined by Raman spectroscopy using a Jobin-Yvon T64000 dispersive spectrometer equipped with a confocal-type apparatus. The Ar^+ laser (514 nm excitation) was operated with a power of 120 mW, and spectra were measured at a resolution of 2 cm^{-1}. Subsequently, one crystal (from sample 203.18) was broken to expose some of its fluid inclusions, and these were examined using a scanning electron microscope (SEM); the micro-crystals in about 30 of the inclusions were analyzed with an attached energy-dispersive spectrometer (EDS). We used a Zeiss Supra 55 VP SEM with an acceleration voltage of 7 or 22 kV, and a current of ~1 nA.

Electron-microprobe analyses of two samples (21 spots) were obtained with a fully automated Cameca SX-50 instrument, using the wavelength-dispersive mode with the following operating conditions: 15 kV excitation voltage, 20 nA beam current, 20 sec. peak count time, 10 sec. background count time, and 10 µm spot diameter. Data reduction was done using the "PAP" $\phi(\rho Z)$ method (Pouchou and Pichoir, 1991). Trace-element compositions of three emeralds (14 analyses) were measured using laser ablation–inductively coupled plasma–mass spectrometry (LA-ICP-MS) with an HP4500 spectrometer. The CETAC SLX200 ablation system used a Nd:YAG laser emitting at 1064 nm, frequency quadrupled to 266 nm. We limited our sampling to three emeralds, because this technique is somewhat destructive and cannot be applied to museum specimens.

Polarized ultraviolet–visible–near infrared (UV-Vis-NIR) absorption spectra of four samples (BVM2378–A to D) were acquired with a Varian Cary 5G spectrometer in the range 300–2500 nm, with a sampling interval of 1 nm and a spectral bandwidth of 1 nm, at a scan speed of 600 nm per minute, using 1 × 1 cm Glan-Thomson calcite polarizers. Infrared absorption spectra of three samples (nos. 106.718, 195.174, and 203.18) were acquired using a Nicolet 20SX spectrometer in the range 5800–1800 cm^{-1}. The spectra presented are directional (not polarized), with the beam (and not the electrical vector) parallel, and then perpendicular, to the optic axis.

Figure 6. These emerald crystals (sample nos. BVM2378–A to D), which are typical of those from Byrud, were characterized for this study. Note their rather homogeneous bluish green color. The longest crystal measures 9 mm. Photo by Alain Cossard.

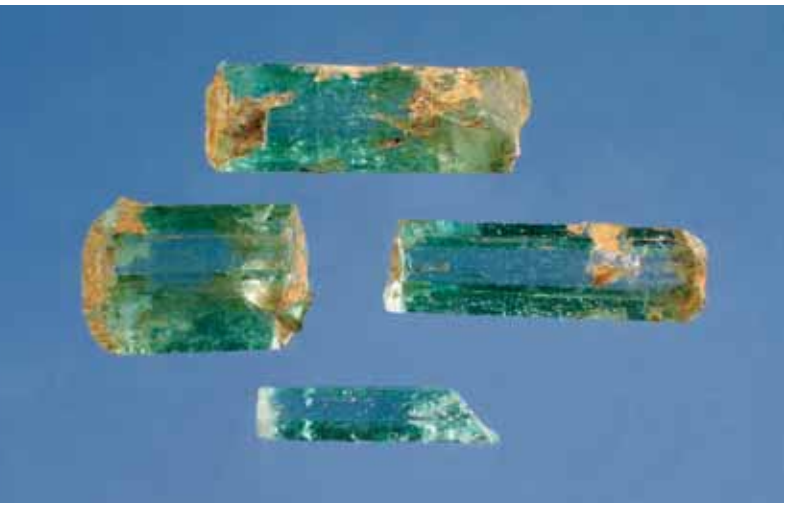

RESULTS

Gemological Properties. *Visual Appearance and Crystal Morphology*. The emerald crystals were translucent to transparent and formed hexagonal crystals with flat basal terminations (figures 7 and 8). Pyramidal faces have also been seen on the terminations of Byrud emeralds (figure 8, right-hand crystal). The studied crystals were green to bluish green, and

Figure 7. This 1.2-cm-long emerald crystal is partially embedded in a spherulitic muscovite matrix. Courtesy of the Norwegian Mining Museum; photo by Gunnar Jenssen.

showed weak but significant pleochroism, from bluish green to yellowish green. All samples studied were homogeneous in color, though we have observed some crystals (not included in this study) that exhibit very strong color zonation parallel to the basal plane, with some parts nearly colorless (again, see figure 8).

Figure 8. These two Byrud crystals (not studied for this report) show unusual features. The 5-mm-long crystal on the left has distinct color zonation, while the crystal on the right (3.5 mm in diameter) has a complex termination consisting of pedion and pyramidal faces. Courtesy of Bjørn Skår; photo by O. T. Ljøstad.

Refractive Indices. We measured the refractive indices from the natural prism faces of samples BVM2378–A to D and obtained identical values of n_o = 1.578 and n_e = 1.560. Three crystals from sample 203.18 were polished parallel to the c-axis, and we measured n_o = 1.587 and n_e = 1.579. In all cases, the birefringence was 0.008.

Specific Gravity. We measured a specific gravity of 2.75 on five fragments of sample 203.18. Additional SG measurements could not be done because many samples were crystals on matrix (in particular, samples BVM2378–A to D contained too much matrix material on their extremities).

UV Fluorescence. All samples were inert to both short- and long-wave UV radiation, as with most natural emeralds worldwide (Bosshart, 1991; Zylbermann, 1998).

Magnification. In the seven emerald samples studied with a gemological microscope, we observed a few solid inclusions; these showed a bright yellow metallic luster and were most probably pyrite. All the samples contained primary fluid inclusions, virtually all of which were multiphase (figure 9). We observed no secondary inclusions. Some inclusions had an irregular outline (figure 10), and others showed a somewhat hexagonal outline when viewed parallel to the c-axis of the host (again, see figure 9), indicating that crystal growth occurred mostly along the basal planes.

Figure 9. Multiphase inclusions are commonly observed in emeralds from Byrud. They typically show regular geometric outlines and contain a liquid and a gaseous phase, a cubic transparent solid phase, elongated transparent crystals, and opaque phase(s). Photomicrograph by B. Rondeau; magnified 200×.

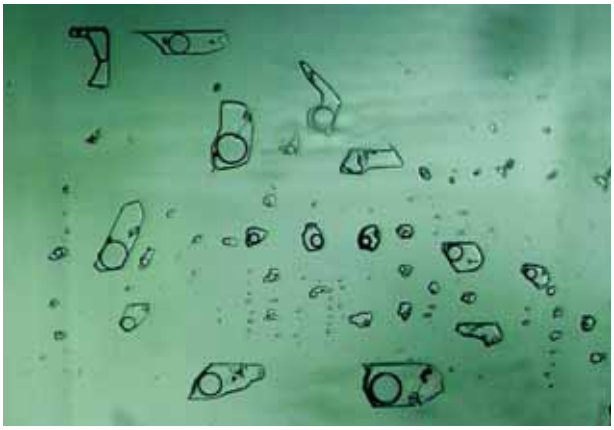

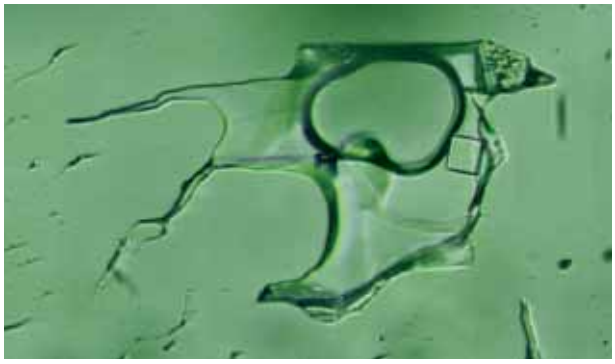

Figure 10. In rare instances, the multiphase inclusions in Byrud emeralds were observed to have irregular forms. Photomicrograph by B. Rondeau; magnified 500×.

The most characteristic multiphase inclusions (figure 11) contained predominantly a liquid phase, a gas bubble, an optically isotropic cube, some transparent, birefringent elongated material (as revealed between crossed polarizers, figure 11 right), and very small opaque phases. When these opaque phases are sufficiently large, one can see that they have a brownish yellow metallic luster (best observed using fiber-optic lighting from the side).

Composition of the Multiphase Inclusions. *Raman Spectroscopy.* Raman analyses revealed that the transparent cubes were halite and the aggregates of elongated opaque material were calcite (peaks at 1083, 279, 182, and 151 cm^{-1}). The liquid was water (broad band around 3600 cm^{-1}), and the gaseous phase was a mixture of water and methane (CH_4; broad band around 3600 cm^{-1} and sharp peak at 2915 cm^{-1}).

SEM-EDS Analysis. Fresh breaks on a fragment of sample 203.18 exposed numerous fluid inclusions. The liquid and gaseous phases were flushed out of the inclusions during sample preparation, and the solid phases were lost from some of the cavities as well. In those that still contained solids (figures 12 and 13), the most common phase identified was halite (NaCl); sylvite (KCl) was also found frequently. Several sulfide phases were observed: pyrrhotite ($Fe_{1-x}S$, hexagonal flakes), galena (PbS), and sphalerite (ZnS); these were often grouped together (again, see figure 12). Copper was also detected during the analysis, but we could not ascribe it to a specific mineral. Some rarer solid phases were also identified. In particular, we found one cassiterite crystal (SnO_2) and one crystal of a phase that contained phosphorus, oxygen, and scandium that we attributed to the very rare mineral pretulite ($ScPO_4$; again, see figure 13).

Chemical Composition. Electron-microprobe analyses are summarized in table 1, and LA-ICP-MS analyses are provided in table 2; additional data from both techniques are available on the *G&G* Data Depository (www.gia.edu/gemsandgemology). We measured relatively high concentrations of V (up to 2.44 wt.% V_2O_3, with a mean of more than 1 wt.%) and comparatively moderate concentrations of Cr (up to 0.33 wt.% Cr_2O_3). The V/Cr ratio was very high, ranging from 3.7 to 24.3. The emeralds also contained remarkably low concentrations of Mg and Na (about 0.1 wt.% oxide or less). Concentrations of Rb (21–61 ppm) and Cs (35–127 ppm) were quite high compared to other vanadian emeralds. Iron concentrations were low (467–1024 ppm) compared to emeralds from most other deposits.

Spectroscopy. *UV-Vis-NIR.* Typical polarized absorption spectra of a Byrud emerald (no. BVM2378-A) are presented in figure 14. The spectrum acquired with E⊥c shows V- (and partially Cr-) related absorption bands at 430 and 608 nm. With E∥c, the spectrum shows absorption bands at 423 and 630–642 nm (compare to Fritsch et al., 2002). A weak absorption band at 683 nm (spectrum E∥c) is attributed to chromium. The weak shoulders at 373 and 385 nm are due to Fe^{3+}.

In the near-infrared region, the three main absorption bands at approximately 1150, 1400, and 1896 nm are due to type I and type II water.

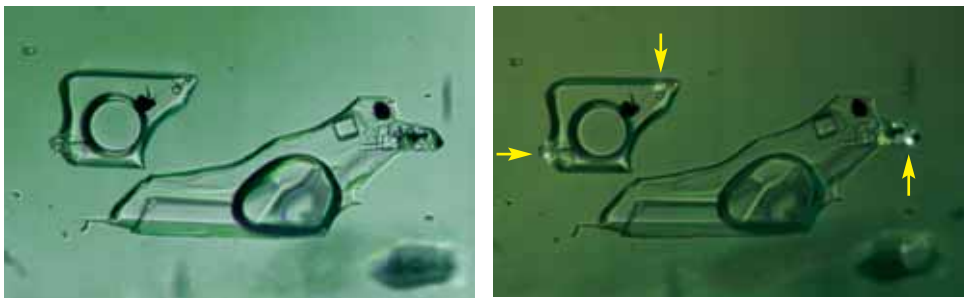

Figure 11. As shown in polarized light (left) and between partially crossed polarizers (right), the Byrud emerald's cubic phases are isotropic, whereas the elongated aggregates are anisotropic (yellow arrows). Note the opaque phases. Photomicrographs by B. Rondeau; magnified 500×.

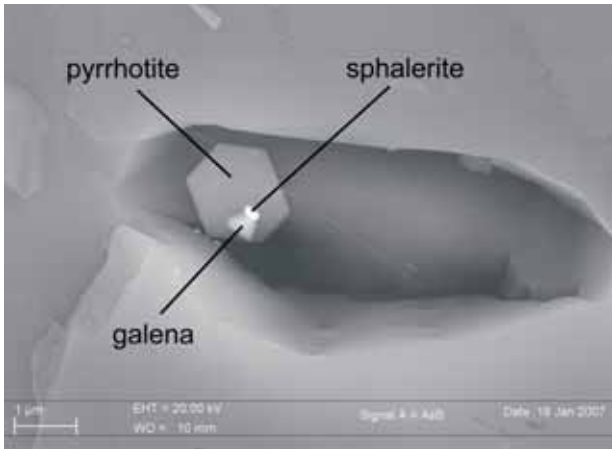

Figure 12. This multiphase inclusion in emerald sample 203.18 contains three sulfides: galena, sphalerite, and pyrrhotite. This assemblage is commonly found together in the multiphase inclusions within Byrud emeralds. Backscattered electron image.

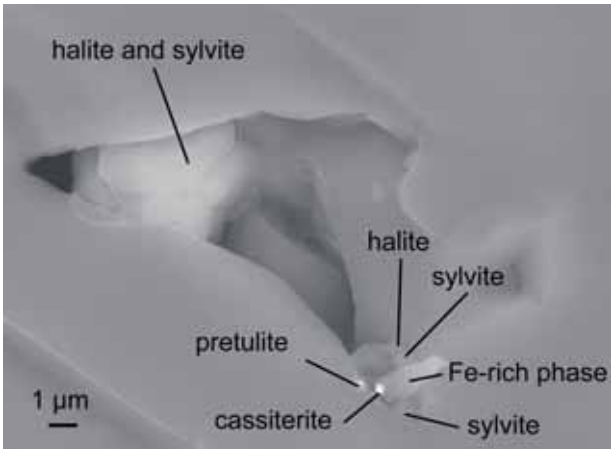

Figure 13. This inclusion in emerald sample 203.18 is a relatively rare example containing several phases including cassiterite (SnO_2) and pretulite ($ScPO_4$), as well as the common halite and sylvite. Backscattered electron image.

Infrared. Figure 15 shows two directional IR spectra in the 5800–1800 cm^{-1} range. Both H_2O and CO_2 absorptions are clearly visible. Details of the water-related absorptions in the range 4000–3000 cm^{-1} are given in figure 16. These spectra show typical absorptions due to both type I H_2O (3700–3694 and 3607 cm^{-1}) and type II H_2O (3657 and 3597–3595 cm^{-1}) molecules. The peak at 5273 cm^{-1} ($\nu_2+\nu_3$), attributed to type II water, is quite sharp and weak (figure 15), which means that there are relatively few type II water molecules in emeralds from Byrud.

Details of the absorptions in the 3000–2100 cm^{-1} range are given in figure 17. The CO_2 absorption at 2359 cm^{-1} is sharp; weak absorptions at 2372, 2345, and 2326 cm^{-1} are also attributed to CO_2. These are possibly due to isotopic effects (combination of the presence of ^{13}C and ^{18}O). The weak peak at 2818 cm^{-1} is attributed to chlorine (Schmetzer et al., 1997, and references therein; Fritsch et al., 1998). Several additional peaks shown in figure 17 (i.e., at 2928, 2854, 2739, 2687, and 2640 cm^{-1}) have never before been documented in the literature for natural emeralds. They may correspond to companion peaks of the 2818 cm^{-1} chlorine peak, even if their positions differ slightly from those observed in hydrothermal synthetic emeralds.

TABLE 1. Chemical composition of two Byrud emeralds, obtained by electron microprobe.[a]

Oxide (wt.%)	Sample 203.18			Sample 195.174		
	Range	Average	Std. dev.	Range	Average	Std. dev.
SiO_2	65.49–66.73	65.91	0.33	65.55–66.06	65.76	0.18
Al_2O_3	17.02–18.78	17.93	0.43	17.39–18.23	17.91	0.28
BeO[b]	13.69–13.92	13.77	0.06	13.71–13.78	13.74	0.03
V_2O_3	0.16–2.44	1.17	0.54	0.78–1.69	1.06	0.32
FeO	0.05–0.18	0.11	0.04	0.03–0.11	0.06	0.03
MgO	0.05–0.10	0.07	0.01	0.05–0.07	0.06	0.01
Na_2O	0.02–0.14	0.08	0.03	0.04–0.10	0.06	0.02
Sc_2O_3	nd–0.08	0.05	0.02	nd–0.08	nd	nd
Cr_2O_3	nd–0.30	0.13	0.09	0.17–0.33	0.26	0.06
H_2O[b]	0.85–0.96	0.91	0.02	0.87–0.92	0.89	0.02
Total	99.52–100.87	100.13	0.38	99.53–100.06	99.83	0.20

[a] *Total iron is shown as FeO. The detection limit for Sc_2O_3 is ~0.05 wt.%, and for Cr_2O_3 is ~0.06 wt.%. Abbreviations: Std. dev. = standard deviation, nd = not detected.*
[b] *BeO and H_2O were calculated, not measured.*

TABLE 2. Chemical composition of three Byrud emeralds, obtained by LA-ICP-MS.[a]

Element (ppm)	Sample 203.18		Sample 195.174		Sample 106.718		DL (ppm)
	Range	Average	Range	Average	Range	Average	
Li	20–28	24	15–21	18	17–19	18	0.8
Mg	277–474	389	306–486	386	348–488	395	3.8
K	23–92	55	26–684	199	63–98	82	23
Sc	126–332	266	160–278	202	146–195	175	0.2
Ti	23–270	146	12–16	14	14–21	18	0.2
V	4965–10021	7356	4496–6895	5485	1745–4211	3098	1.1
Cr	293–1208	579	1006–1654	1324	162–932	585	1.8
Mn	5–25	5737	18–25	22	33–109	67	0.7
Fe	573–1024	802	467–698	576	570–881	719	5.8
Ni	nd	nd	nd	nd	nd–1	nd	0.5
Zn	9–15	5291	15–23	18	13–45	33	1.1
Ga	9–27	5841	19–26	23	nd	nd	0.3
Rb	29–61	41	21–54	32	26–33	30	0.4
Sr	nd	nd	nd–7	3	nd–8	4	1.9
Zr	nd–1.1	nd	nd–1	nd	nd–1	nd	0.4
Cs	50–127	85	35–44	38	69–99	85	0.4
Pb	1.8–2.8	2.2	3–5	4.25	5–14	8.67	0.01
V/Cr	6–24.3	16.2	3.68–4.47	4.18	4.52–10.8	6.79	
V/(V+Cr)	0.9–1	0.9	0.79–0.82	0.81	0.82–0.92	0.86	
Fe/(Fe+Cr)	0.4–0.8	0.6	0.24–0.41	0.31	0.49–0.78	0.60	

[a] *Co, Cu, La, Ce, Gd, Th, and U were analyzed for but not detected. Na, Cl, F, P, and Ca could not be analyzed correctly by this technique. Si is taken as the reference at 650,000 ppm. Abbreviations: DL = detection limit, nd = not detected.*

DISCUSSION

Variations in Properties. The RI, SG, pleochroism, and fluorescence of our Byrud emeralds samples fall within the range of properties for emerald (Zylbermann, 1998). Higher values of RI were previously reported for Byrud emeralds (n_o = 1.591, n_e = 1.584; Webster, 1955).

Variations in color zonation, RI values, inclusion composition, and chemical composition may indicate that the mineralizing fluid was less homogeneous than is usual for emerald deposits. The relatively high concentration of chromophores (mostly V) may explain the high RI values sometimes observed, because—for example—V, which is heav-

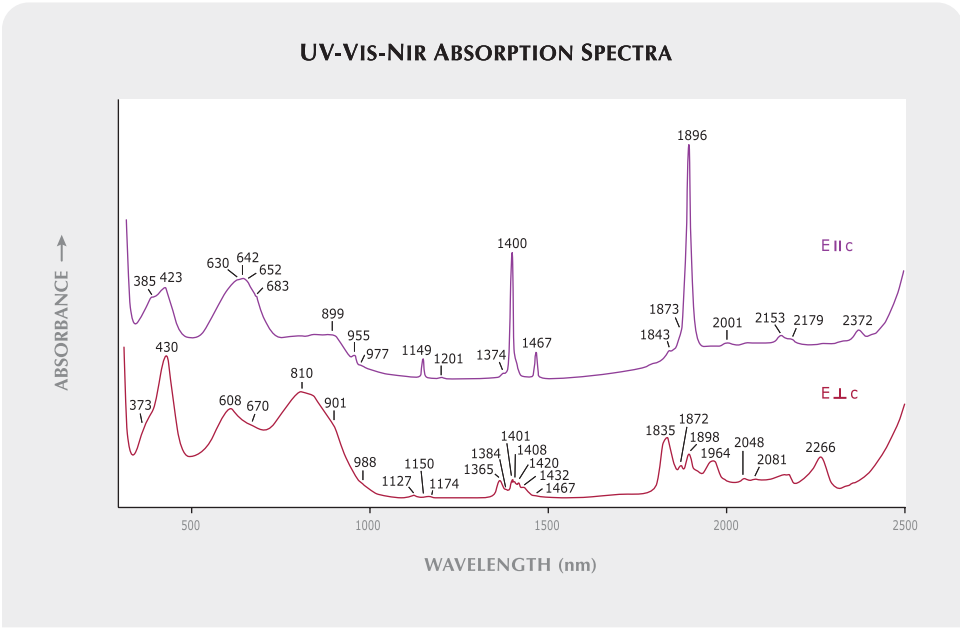

Figure 14. Polarized UV-Vis-NIR spectra of sample BVM2378-A show absorption bands at 430 and 608 nm (bottom) and 423 and 630–642 nm (top) that are due mostly to V^{3+}, and partly to Cr^{3+}. The weak shoulders at 385 (top) and 373 nm (bottom) are due to small amounts of Fe^{3+}. The sharp near-infrared peaks at approximately 1150, 1400, and 1896 nm are due to type II molecular water. Spectra have been shifted vertically for clarity. Sample thickness is 3 mm.

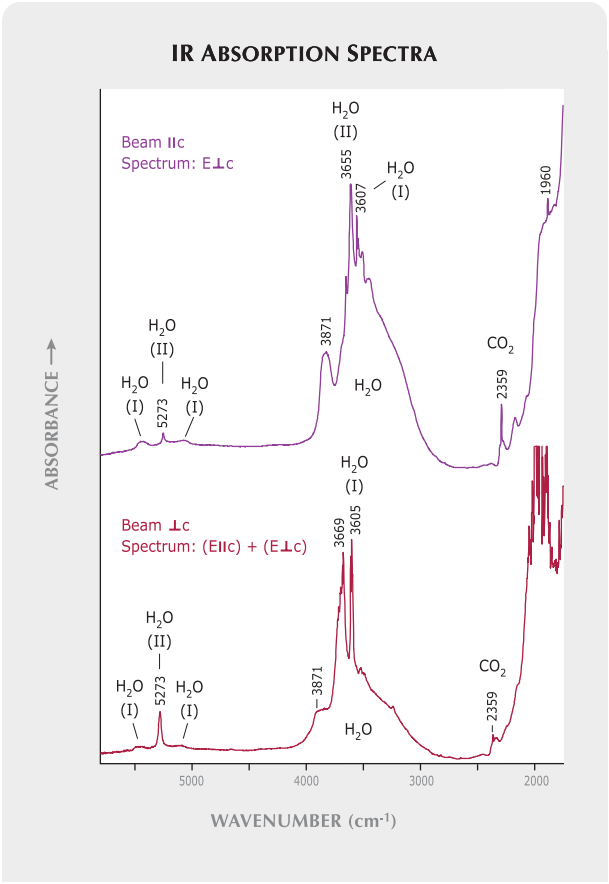

Figure 15. The IR spectra of Byrud emeralds clearly show absorptions due to H_2O and CO_2. Spectra have been shifted vertically for clarity.

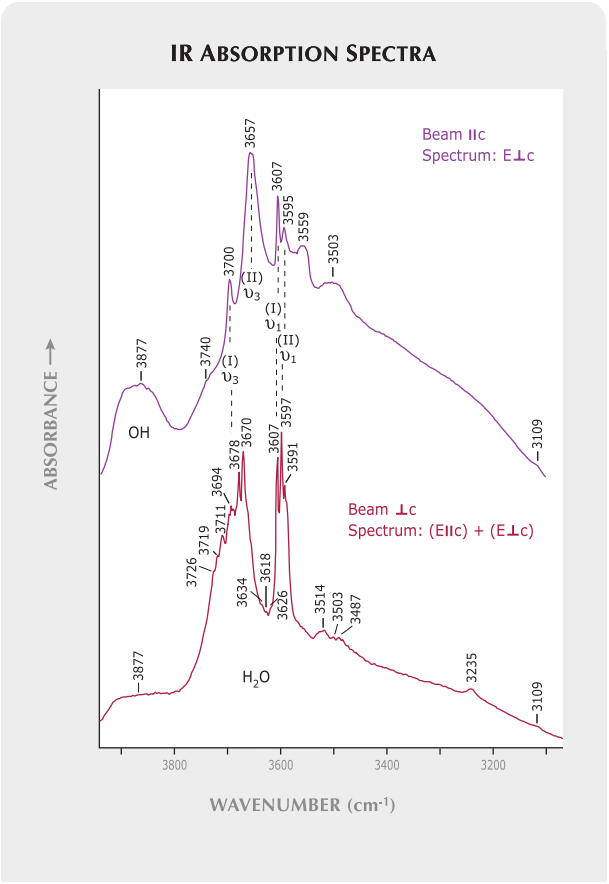

Figure 16. These IR spectra of emerald sample 195.174 in the 4000–3000 cm^{-1} range show the details of water-related absorptions. Spectra have been shifted vertically for clarity.

ier than the Al it substitutes for, may contribute to slowing down light as it passes through the emerald. However, the RI values are sometimes very low, as seen in samples BVM2378–A to D, which were not chemically analyzed. Their low RI values may be related to the water and CO_2 content in the channels of these emeralds, which are very low compared to those of other natural emeralds (B. Sabot, pers. comm., 2006; a value of 1.1 wt.% H_2O is given by Alexandrov et al., 2001). As these samples were vivid green, the channel content apparently may be more important than the chromophores for controlling RI. Nevertheless, our limited data set does not allow us to demonstrate a clear correlation between RI and water, CO_2, and V contents.

Some solids in the multiphase inclusions were identified only with Raman spectroscopy (calcite) and others only with EDS (sylvite and pretulite), simply because we did not analyze the same specimens with both methods. This illustrates the diversity of the solid phases in the multiphase inclusions. However, opaque, metallic-appearing sulfides were observed in the fluid inclusions of all seven samples studied.

Origin of Color. The main UV-Vis spectroscopic features are the absorption bands at 423 or 430 nm and at 608 or 642 nm. These positions prove that the color is due mainly to the presence of V. However, the weak peak at 683 nm indicates that Cr also contributes to the coloration. This was confirmed by chemical analyses: V was much more abundant than Cr.

Source of Vanadium and Chromium. Chromium in emerald typically originates from mafic and ultramafic rocks (e.g., Morteani and Grundmann, 1977; Laurs et al., 1996; Marshall et al., 2003), with the exception of Colombian-type deposits, where chromium is leached from sedimentary rocks (Giuliani, 1997). However, the geologic source of vanadium in emerald is not well documented. This element is usually concentrated in rocks that contain iron-rich

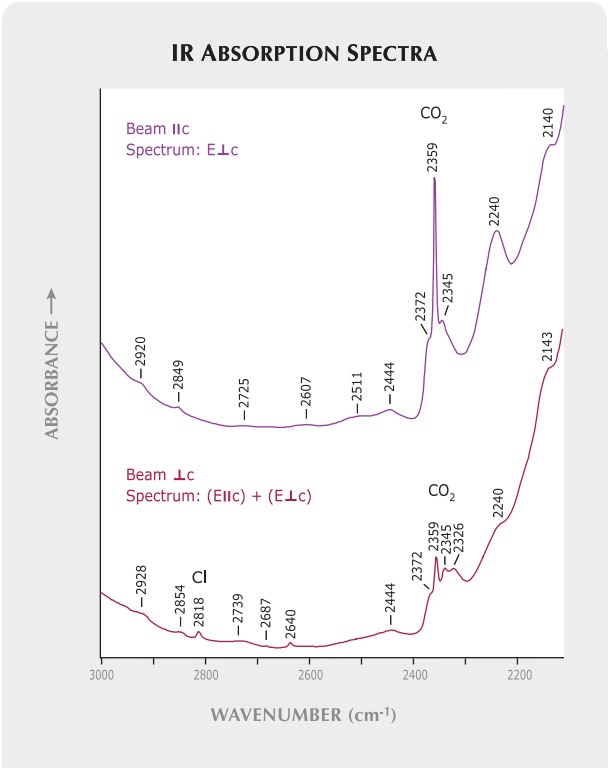

Figure 17. These IR spectra of emerald sample 195.174 in the 3000–2100 cm^{-1} range show the details of CO_2-related absorptions. Spectra have been shifted vertically for clarity.

minerals or organic compounds (e.g., Moskalyk and Alfantazi, 2003). Byrud's alum shales, rich in organic matter, are the most likely source of vanadium for these emeralds. By comparison, the source of vanadium in Colombian deposits is also related to organic matter in black shales (Campos Alvarez and Roser, 2007).

Trace-Element Geochemistry. Trace-element incorporation into beryl varies with geologic environment (Staatz et al., 1965; Calligaro et al., 2000). We plotted some trace-element pairs to detect possible correlations in their relative abundances within the three samples analyzed. Chromium and V showed a positive correlation (figure 18) in two samples but not in sample 203.18. Gallium and V showed a clear negative correlation in all three samples (figure 19). A less pronounced negative correlation was found for Zn, Pb, and Mn relative to V (figure 20). From these data (based on the analysis of only three samples, as mentioned above), the group of divalent ions Zn, Mn, Pb, and Ga seems to correlate negatively with V, but we did not observe any correlation with Cr. All this confirms that Cr and V do not have similar geochemical distribution properties. Also, this could indicate that Ga and V integrate into the beryl structure via the same crystallographic site.

We calculated a very low water content in our samples (0.85–0.96 wt.%). This is not inconsistent with the value of 1.1 wt.% reported by Alexandrov et al. (2001). It approaches the lowest water content recorded for emerald from any source (Schwarz, 1987, p. 43). The low water content in such emeralds is related to the very low amount of Na, as type II water incorporation directly correlates to Na concentration (Wood and Nassau, 1968; Charoy, 1998).

Figure 18. The contents of Cr and V in emeralds from Norway do not show a consistent correlation in the three Byrud emeralds tested.

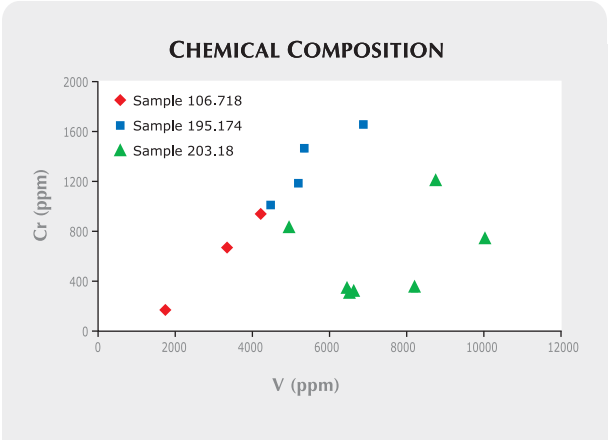

Figure 19. The concentrations of Ga and V clearly show a negative correlation in all three Byrud samples.

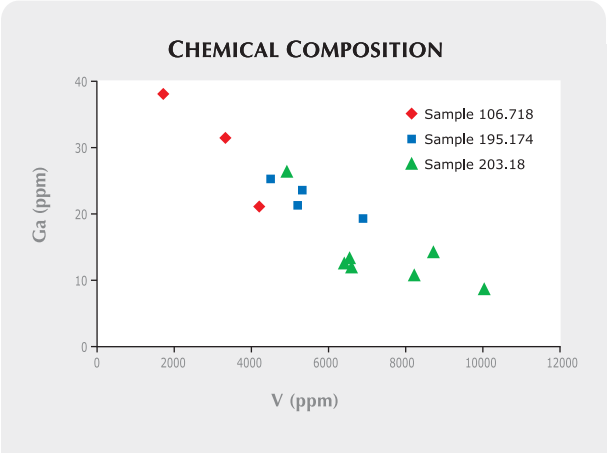

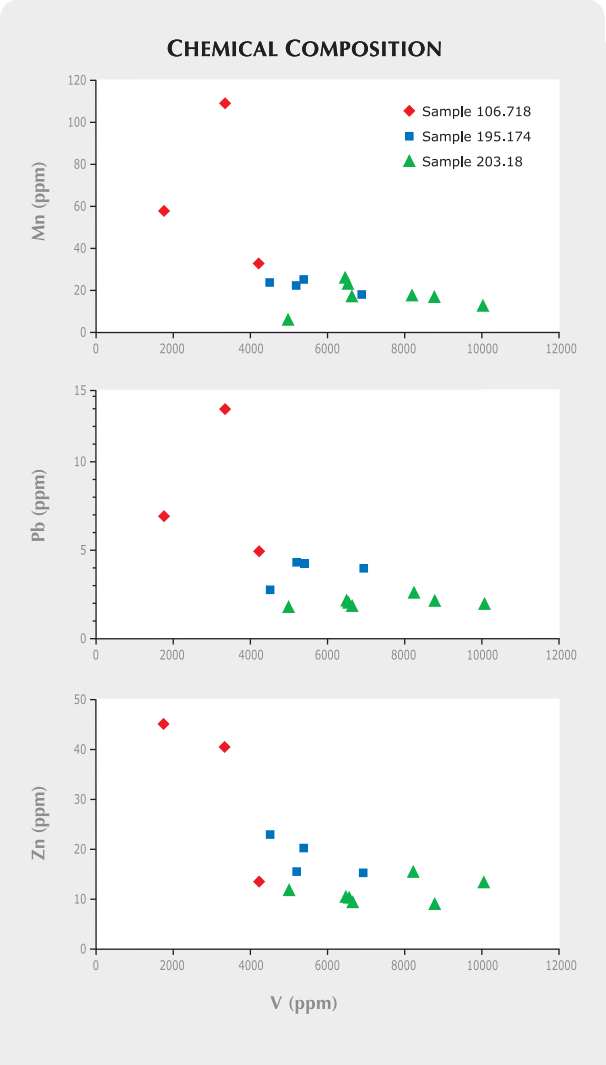

Figure 20. Concentrations of Mn, Pb, and Zn show a poorly pronounced negative correlation with V in the three Byrud emeralds.

IDENTIFICATION

We found several distinguishing criteria for Byrud emeralds. Most importantly, the presence of sulfides in the multiphase fluid inclusions is unique to emeralds from this locality and makes them straightforward to identify. With the optical microscope, we consistently observed a small (sometimes very small) black, opaque point somewhere in each multiphase inclusion. Three-phase and multiphase inclusions are known in emeralds from only a few other deposits: Colombia, Kaduna in Nigeria (Schwarz, 1998; Vapnik and Moroz, 2000; Sabot et al., 2000), Panjshir in Afghanistan (Seal, 1989; Bowersox et al., 1991), Kafubu in Zambia (Zwaan et al., 2005), and Xinjiang in China (Blauwet et al., 2005). Multiphase inclusions in these emeralds commonly contain halite cubes and sometimes carbonate crystals, but none of them systematically show the black, opaque phases seen in emeralds from Byrud. Sulfides have been described as solid inclusions in emeralds from several deposits (Giuliani et al., 1997; Rondeau et al., 2003), but never as part of a multiphase inclusion. Also, we observed that fluid inclusions in Norwegian emeralds are generally more regular in shape than those in Colombian emeralds, and the halite cube they contain is smaller. Hence, the careful use of a binocular microscope can be sufficient to ascribe Norwegian provenance to an emerald.

Among chemical criteria, the very low Na concentration (about 0.1 wt.% or less) is most significant. This is comparable to emeralds from Emmaville, Australia (Schwarz, 1998), and Delbegetey, Kazakhstan (Gravilenko et al., 2006), and is therefore not distinctive but certainly indicative. The appropriate data can be obtained by using either an electron microprobe or LA-ICP-MS.

In addition, the V content of the Byrud emeralds we tested was commonly high (a mean of more than 1 wt.% V_2O_3, with values ranging up to 2.4 wt.%), which is consistent with earlier data (Schwarz, 1991; Calligaro et al., 2000). This is among the highest of all emeralds, along with those from Malipo, China (Zhang and Lan, 1999). However, the V content is sometimes lower (down to 0.16 wt.% V_2O_3), particularly in light green stones, so this criterion cannot be considered a definitive identification tool. Moreover, a high V/Cr ratio (3 to 24 in our measurements) is not distinctive: Emeralds from other deposits (Salininha, Brazil, and Lened, Canada) also can show high V/Cr ratios, sometimes exceeding 100 (Marshall et al., 2004). However, the relative contents of Fe+Mg (low), Cr (low), and Cs or Rb (high) appear specific to the emeralds from Byrud, as shown in a ternary diagram that plots Fe+Mg, Cr, and Cs (figure 21). The trace-element composition of emeralds from Lened (Canada) has not yet been determined, but it may be useful to compare it to Byrud in this ternary diagram.

The oxygen isotopic composition of an emerald from Byrud has been reported in the literature (Giuliani et al., 1998; Groat et al., 2002). The $\delta^{18}O$ value of 9.4‰ is rather low, but overlaps that of many other deposits (Giuliani et al., 1998; Sabot, 2002), so this criterion alone is not distinctive.

According to the published literature, the emeralds from Emmaville and Torrington, Australia, share

many characteristics with emeralds from Byrud (Schwarz, 1991). They formed in pegmatite sills that intruded alum schist (Schwarz, 1991, and references therein; Grundmann and Giuliani, 2002), and their associated minerals include quartz, feldspars, micas, fluorite, topaz, cassiterite, wolframite, and arsenopyrite. These Australian emeralds contain very low concentrations of Na_2O and MgO (<0.1 wt.%; Schwarz and Henn, 1992; Brown, 1998). Such low concentrations are otherwise encountered only in emeralds from Byrud and in synthetic emeralds. Emerald crystals from Emmaville and Torrington typically show strong color zonation parallel to the basal face, which is rare in emeralds from Byrud. Also, emeralds from Emmaville contain more chromium and less vanadium (0.1 wt.% V_2O_3) than those from Byrud (Schwarz, 1991).

CONCLUSION

The gemological and spectroscopic properties of our Byrud samples did not differ on average from those of emeralds in general, either chromium- or vanadium-bearing. However, our study has shown that Byrud emeralds (e.g., figure 22) are colored mostly by vanadium. We also found a number of criteria that are diagnostic of these emeralds. Most importantly, we noted the presence of sulfide phases in multiphase fluid inclusions, together with halite, sylvite, calcite, liquid water, and gaseous CH_4. This is the first time that sulfide phases have been reported in multiphase inclusions in emeralds. They are seen with the optical microscope as minute black, opaque points. The chemical composition is also distinctive: The emeralds analyzed from Byrud had relative contents of Fe, Mg, Cr, Cs, and Rb that are specific to this locality and easily identified through LA-ICP-MS analysis. They also contained low Na and Mg and often high V.

These criteria make emeralds from Byrud unique and quite easy to distinguish using a microscope and/or chemical analysis. An unverified legend says that one of the emeralds in the jewels belonging to the British royal family comes from the Byrud deposit. Using the identification criteria provided in this article, it would now be quite easy to investigate this story.

When we compare our results with those reported in the literature for emeralds from other localities, it appears that those emeralds from Byrud that show a strong color zonation closely resemble emeralds from

Figure 22. Significant quantities of emerald were mined from Byrud, Norway, in the late 19th and early 20th centuries. As these two crystals (9.6 and 5.5 mm long) illustrate, some of the material was transparent enough for faceting. Courtesy of the Royal Ontario Museum, Toronto; photo by Robert Weldon.

Figure 21. The chemical composition field of the three analyzed emeralds from Norway is clearly distinct from that of V-rich emeralds from other deposits. The elements used in this diagram (Cr, Fe + Mg, and Cs) are the most useful for distinguishing their geographic origins (data from Peucat et al., in preparation).

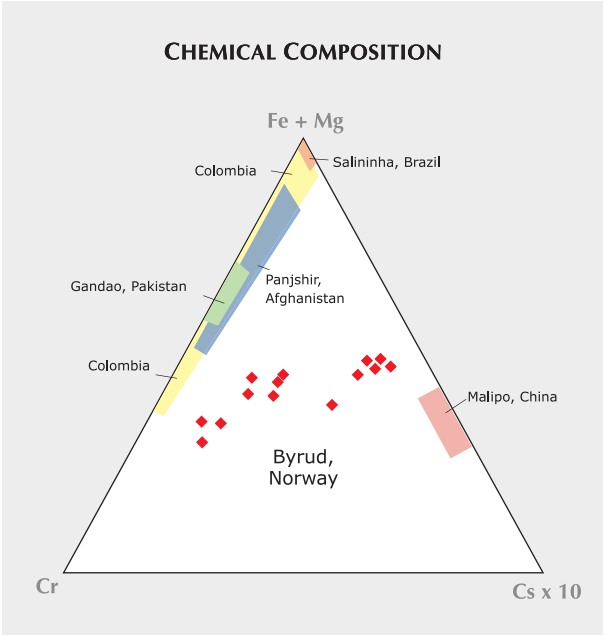

Emmaville and Torrington, Australia: similar color zonation, very low Na and Mg contents, similar geologic setting, and similar associated minerals. Hence, a detailed gemological study of emeralds from Australia would be very helpful in testing the identification criteria proposed here for the emeralds from Byrud. In general, much remains to be done on vanadium-bearing emeralds (except perhaps for some Colombian deposits), which are much less studied than their chromium-bearing counterparts.

ABOUT THE AUTHORS

Dr. Rondeau (benjamin.rondeau@univ-nantes.fr) is assistant professor at the Laboratoire de Planétologie et Géodynamique, University of Nantes, France, and belongs to the Centre National de la Recherche Scientific (CNRS), Team 6112. Dr. Fritsch is professor of physics at the University of Nantes, Institut des Matériaux Jean Rouxel (IMN)-CNRS. Dr. Peucat is a researcher in geochemistry at Géosciences Rennes, University of Rennes, France. Mr. Nordrum is curator at the Norwegian Mining Museum in Kongsberg, Norway. Dr. Groat is professor of mineralogy in the Department of Earth and Ocean Sciences, University of British Columbia, Vancouver, B.C., Canada.

ACKNOWLEDGMENTS

The authors are grateful to Mrs. M. Bouhnik-Le Coz (Géosciences Rennes) for performing LA-ICP-MS analyses. Special thanks to Dr. Bruno Sabot (Brioude, France) and Dr. Gaston Giuliani (INPG, Nancy, France) for their constructive comments on an early version of this article. Gunnar Raade (Oslo, Norway) kindly provided geological and mineralogical information, and Burny Iversen (Elverum, Norway), Atle Bergset (Langevåg, Norway), Knut Arne Eikrem (Grimstad, Norway), and Anne Grete Røise (Byrud farm, Eidsvoll, Norway) generously supplied historical background. Dr. Hanco Zwaan (National Museum of Natural History, Leiden, The Netherlands) is thanked for reviewing the original manuscript.

REFERENCES

Alexandrov P., Giuliani G., Zimmermann J.-L. (2001) Mineralogy, age and fluid geochemistry of the Rila emerald deposit, Bulgaria. *Economic Geology*, Vol. 96, pp. 1469–1476.

Blauwet D., Quinn E.P., Muhlmeister S. (2005) Gem News International: New emerald deposit in Xinjiang, China. *Gems & Gemology*, Vol. 41, No. 1, pp. 56–57.

Bosshart G. (1991) Emeralds from Colombia (Part 2). *Journal of Gemmology*, Vol. 22, No. 7, pp. 409–425.

Bowersox G., Snee L.W., Foord E.E., Seal II R.R. (1991) Emeralds of the Panjshir Valley, Afghanistan. *Gems & Gemology*, Vol. 27, No. 1, pp. 26–39.

Brown G. (1998) Les gisements d'émeraude en Australie [Emerald deposits in Australia]. In D. Giard, G. Giuliani, A. Cheilletz, E. Fritsch, and E. Gonthier, Eds., *L'émeraude*, Association Française de Gemmologie, Paris, pp. 201–204 [in French].

Bull E. (1952) Bygdehistorien 1800–1914. *Eidsvoll bygds historie* [*History of the Eidsvoll Parish*]. Vol. 1, Part 2, p. 537 [in Norwegian].

Burns R.G. (1993) *Mineralogical Applications of Crystal Field Theory*, 2nd ed. Cambridge Topics in Mineral Physics and Chemistry, Vol. 5, Cambridge University Press, Cambridge, UK.

Calligaro T., Dran J.-C., Poirot J.-P., Quérré G., Salomon J., Zwaan J.C. (2000) PIXE/PIGE characterization of emeralds using an external micro-beam. *Nuclear Instruments and Methods in Physics Research B*, Vol. 161–163, pp. 769–774.

Cameron E.A. (1963) Skattejaktminner fra Minnesund [Memories of a treasure hunt at Minnesund]. *Kvinner og Klær*, Vol. 40, pp. 33–54 [in Norwegian].

Campos Alvarez N.O., Roser B.P. (2007) Geochemistry of black shales from the Lower Cretaceous Paja Formation, Eastern Cordillera, Colombia: Source weathering, provenance, and tectonic setting. *Journal of South American Earth Sciences*, Vol. 23, No. 4, pp. 271–289.

Charoy B. (1998) Cristallochimie du béryl: L'état des connaissances [Beryl crystallochemistry: State of the art]. In D. Giard, G. Giuliani, A. Cheilletz, E. Fritsch, and E. Gonthier, Eds., *L'émeraude*, Association Française de Gemmologie, Paris, France, pp. 33–39 [in French].

CIBJO (1988) *Gemstone Book*. CIBJO Coloured Stones Commission, International Confederation of Jewellery, Silverware, Diamonds, Pearls and Gemstones, The Hague, Netherlands.

Fritsch E., Moon M., Wu T.S.-T., Liu Y., Park J.S. (1998) Les nouvelles émeraudes synthétiques d'Asie: Émeraude synthétique hydrothermale chinoise, émeraudes synthétiques par dissolution anhydre coréenne et taïwanaise [New Asian synthetic emeralds: Hydrothermal synthetic emeralds from China, anhydrous dissolution synthetic emeralds from Korea and Taiwan]. In D. Giard, G. Giuliani, A. Cheilletz, E. Fritsch, and E. Gonthier, Eds., *L'émeraude*, Association Française de Gemmologie, Paris, France, pp. 131–138 [in French].

Fritsch E., Rondeau B., Notari F., Michelou J.-C., Devouard B., Peucat J.-J., Chalain J.-P., Lulzac Y., De Narvaez D., Arboleda C. (2002) Les nouvelles mines d'émeraude de La Pita (Colombie), 2nde partie [The new emerald mines at La Pita, Colombia]. *Revue de Gemmologie a.f.g.*, No. 144, pp. 13–19 [in French].

Giuliani G. (1997) Genèse des gisements d'émeraude du Brésil et de Colombie [Origin of emerald deposits in Brazil and Colombia]. Thèse d'Habilitation, Institut National Polytechnique de Lorraine, Nancy, France, 147 pp. [in French].

Giuliani G., Cheilletz A., Zimmermann J.-L., Ribeiro-Althoff A.-M., France-Lanord C., Feraud G. (1997) Les gisements d'émeraude du Brésil: genèse et typologie [Emerald deposits in Brazil: genesis and typology]. *Chronique Recherche Minière*, Vol. 526, pp. 17–61 [in French].

Giuliani G., France-Lanord C., Coget P., Schwarz D., Cheilletz A., Branquet Y., Giard D., Martin-Izard A., Alexandrov P., Piat D.H. (1998) Oxygen isotope systematics of emerald: Relevance for its origin and geological significance. *Mineralium Deposita*, Vol. 33, pp. 513–519.

Goldschmidt V.M. (1911) Die Kontaktmetamorphose im Kristianiagebiet [Contact metamorphism in the Oslo region]. *Videnskapsselskapets Skrifter, I. Matematisk-naturvitenskapelig klasse*, Vol. 1, pp. 56, 357–358 [in German].

Gravilenko E.V., Calvo Pérez B., Castroviejo Bolibar R., Garcia del Amo D. (2006) Emeralds from the Delbegetey deposit (Kazakhstan): Mineralogical characteristics and fluid-inclusion study. *Mineralogical Magazine*, Vol. 70, No. 2, pp. 159–173.

Groat L.A., Marshall D.D., Giuliani G., Murphy D.C., Piercey S.J., Jambor L., Mortensen J.K., Ercit T.S., Gault R.A., Mattey D.P., Schwarz D., Maluski H., Wise M.A., Wengzynowski W., Eaton D.W. (2002) Mineralogical and geochemical study of the Regal Ridge emerald showing, southeastern Yukon. *Canadian Mineralogist*, Vol. 40, pp. 1313–1338.

Grundmann G., Giuliani G. (2002) Emeralds of the world. In G. Giuliani et al., Eds., *Emeralds of the World*, extraLapis English No. 2, pp. 24–35.

Ihlen P.M. (1978) Ore deposits in the north-eastern part of the Oslo region and in the adjacent Precambrian areas. In E.-R. R. Neumann and I. B. Ramberg, Eds., *Petrology and Geochemistry of Continental Rifts*, Proceedings of the NATO Advanced Study Institute, Oslo, July 27–August 5, 1977, D. Reidel Pub. Co., Dordrecht, Netherlands, pp. 277–286.

Kunz G.F. (1902) Precious stones. *Mineral Resources of the U.S. 1901*, U.S. Geological Survey, Bureau of Mines, Washington DC, pp. 729–771.

Kvamsdal L., Eldjarn K. (2007) Mineralene i smaragdgruvene ved Byrud gård, Minnesund, Norge [The minerals in the emerald mines at Byrud farm, Minnesund, Norway]. *Stein*, Vol. 33, No. 4, pp. 4–20 [in Norwegian].

Laurs B.M., Dilles J.H., Snee L.W. (1996) Emerald mineralization and metasomatism of amphibolite, Khaltaro granitic pegmatite-hydrothermal vein system, Haramosh Mountains, northern Pakistan. *Canadian Mineralogist*, Vol. 34, pp. 1253–1286.

Lindaas K.D. (1982) Gruvedrift etter smaragd på Byrud Minnesund [Mining for emerald at Byrud Minnesund]. *Romerikstun*, Romerike historielag Årbok 1982, pp. 90–93 [in Norwegian].

Marshall D., Groat L.A., Giuliani G., Murphy D., Mattey D., Ercit T.S., Wise M.A., Wengzynowski W., Eaton W.D. (2003) Pressure, temperature and fluid conditions during emerald precipitation, southeastern Yukon, Canada: Fluid inclusion and stable isotope evidence. *Chemical Geology*, Vol. 194, pp. 187–199.

Marshall D., Groat L.A., Falck H., Giuliani G., Neufeld H. (2004) The Lened emerald prospect, Northwest Territories, Canada: Insights from fluid inclusions and stable isotopes, with implications for Northern Cordilleran emerald. *Canadian Mineralogist*, Vol. 42, pp. 1523–1539.

Morteani G., Grundmann G. (1977) The emerald porphyroblasts in the penninic rocks of the central Tauern Window. *Neues Jahrbuch für Mineralogie Monatshefte*, Vol. 11, pp. 509–516.

Moskalyk R.R., Alfantazi A.M. (2003) Processing of vanadium: A review. *Minerals Engineering*, Vol. 16, pp. 793–805.

Nordrum F.S., Raade G. (2006) Das Smaragd-Vorkommen von Byrud (Eidsvoll) in Süd-Norwegen [The emerald deposit at Byrud (Eidsvoll) in South Norway.] *Mineralien-Welt*, Vol. 17, No. 4, pp. 52–64 [in German].

Pouchou J.-L., Pichoir F. (1991) Quantitative analysis of homogeneous or stratified microvolumes applying the model "PAP." In K.F.J. Heinrich and D.E. Newbury, Eds., *Electron Probe Quantitation*, Plenum Press, New York, pp. 31–75.

Rondeau B., Notari F., Giuliani G., Michelou J.-C., Martins S., Fritsch E., Respinger A. (2003) La mine de Piteiras, Minas Gerais, nouvelle source d'émeraude de belle qualité au Brésil [The Piteiras mine, Minas Gerais, a new source of gem-quality emerald in Brazil]. *Revue de Gemmologie a.f.g.*, No. 148, pp. 9–25 [in French].

Sabot B., Cheilletz A., de Donato P., Banks D., Levresse G., Barres O. (2000) Afghan emeralds face Colombian cousins. *Chroniques de la Recherche Minière*, Vol. 541, pp. 111–114.

Sabot B. (2002) Classification des gisements d'émeraude: Apports des études pétrographiques, minéralogiques et géochimiques [Classification of Emerald Deposits: Highlights of Petrographical, Mineralogical and Geochemical Studies]. PhD thesis, Institut National Polytechnique de Lorraine, Nancy, France, 172 pp. [in French].

Schmetzer K., Kiefert L., Bernhardt H.-J., Beili Z. (1997) Characterization of Chinese hydrothermal synthetic emerald. *Gems & Gemology*, Vol. 33, No. 4, pp. 276–291.

Schwarz D. (1987) *Esmeraldas: Inclusões em Gemas* [*Emeralds: Inclusions in Gems*]. Imprensa Universitaria Universidad Federal de Ouro Preto, Ouro Preto, Brazil, 439 pp.

Schwarz D. (1991) Die chemischen Eigenschaften der Smaragde, II. Australien und Norwegen [Chemical properties of emerald, II. Australia and Norway]. *Zeitung der Deutschen Gemmologischen Gesellschaft*, Vol. 40, No. 1, pp. 39–66. [in German].

Schwarz D. (1998) De l'importance des inclusions solides et fluides dans la caractérisation des émeraudes naturelles et synthétiques [The importance of solid and fluid inclusions in the characterization of natural and synthetic emeralds]. In D. Giard, G. Giuliani, A. Cheilletz, E. Fritsch, and E. Gonthier, Eds., *L'émeraude*, Association Française de Gemmologie, Paris, France, pp. 71–80 [in French].

Schwarz D., Henn U. (1992) Emeralds from Madagascar. *Journal of Gemmology*, Vol. 23, No. 3, pp. 140–149.

Schwarz D., Schmetzer K. (2002) The definition of emerald: The green variety of beryl colored by chromium and/or vanadium. In G. Giuliani et al., Eds., *Emeralds of the World*, extraLapis English No. 2, pp. 74–78.

Seal R.R. II (1989) A reconnaissance study of the fluid inclusion geochemistry of the emerald deposits of Pakistan and Afghanistan. In A. H. Kazmi and L. W. Snee, Eds., *Emeralds of Pakistan: Geology, Gemology and Genesis*, Van Nostrand Reinhold, New York, pp. 151–164.

Selset R. (1963) Emerald locality on Mjosa Lake, Norway. *Rocks & Minerals*, Vol. 38, pp. 608–609.

Sinkankas J. (1981) *Emerald and Other Beryls*. Chilton Book Co., Radnor, PA, 665 pp.

Staatz M.H., Griffitts W.R., Barnett P.R. (1965) Differences in the minor element composition of beryl in various environments. *American Mineralogist*, Vol. 50, pp. 1783–1795.

Vapnik Y., Moroz I. (2000) Fluid inclusions in emerald from the Jos complex (central Nigeria). *Schweizerische Mineralogische und Petrographische Mitteilungen*, Vol. 80, No. 2, pp. 117–129.

Vogt J.H.L. (1884) Undersøgelser ved den sydlige del af Mjøsen i 81 og 82 [Investigations at the southern part of Lake Mjøsen in 1881 and 1882]. *Nyt Magazin for Naturvidenskaberne*, Vol. 28, pp. 215–248 [in Norwegian].

Websky M. (1876) Über Beryll von Eidsvoll in Norwegen [On beryl from Eidsvoll in Norway]. *Tschermak's Mineralogischen und Petrologischen Abteilungen*, Vol. 6, No. 2, pp. 117–118 [in German].

Webster (1955) The emerald. *Journal of Gemmology*, Vol. 5, p. 303.

Wood D.L., Nassau K. (1968) The characterization of beryl and emerald by visible and infrared absorption spectroscopy. *American Mineralogist*, Vol. 53, pp. 777–800.

Zhang L., Lan Y. (1999) Gemological characteristics and deposit geology of Yunnan emerald. *Acta Mineralogica Sinica*, Vol. 19, No. 2 [in Chinese; no pagination].

Zwaan J.C., Seifert A.V., Vrána S., Laurs B.M., Anckar B., Simmons W.B., Falster A.U., Lustenhouwer W.J., Muhlmeister S., Koivula J.I., Garcia-Guillerminet H. (2005) Emeralds from the Kafubu area, Zambia. *Gems & Gemology*, Vol. 41, No. 2, pp. 116–148.

Zylbermann N. (1998) Tableau synoptique comparatif des propriétés gemmologiques des gisements majeurs et des principales syntheses [A comprehensive comparison of the gemological properties of major deposits and principal synthetics]. In D. Giard, G. Giuliani, A. Cheilletz, E. Fritsch, and E. Gonthier, Eds., *L'émeraude*, Association Française de Gemmologie, Paris, France, pp. 227–233 [in French].

THE USE OF LASER AND X-RAY SCANNING TO CREATE A MODEL OF THE HISTORIC KOH-I-NOOR DIAMOND

Scott D. Sucher and Dale P. Carriere

For centuries, the Koh-i-Noor was one of the world's largest diamonds. It was recut in 1852 from its historic form of 186.1 old carats to an oval of 105.60 modern carats. While the modern shape is well documented, the original form is not. Fortunately, the Natural History Museum in London commissioned a mold of the diamond in 1851 before it was recut. Using one of two plaster replicas made from this mold, the present study captured the surface topology of the original Koh-i-Noor through photography plus laser and X-ray scanning methods. A crystallographic analysis of the major facets determined the diamond's orientation within a "perfect" diamond crystal, which was used to refute one theory about the diamond's genealogy. Computer modeling established the orientation of the recut diamond within the historic version. Information from this study was used to create an accurate replica from cubic zirconia.

The Koh-i-Noor is one of the great historic diamonds (figure 1), a gem that has figured prominently in south Asian history for hundreds of years. The precise history of the Koh-i-Noor prior to the mid-1500s is in doubt (Mawe, 1815; Balfour, 2000). Some sources claim the stone was discovered in India 5,000 years ago, while others place it in the 1300s or 1500s. It was owned by a long succession of rulers and warlords over the ensuing centuries, finally ending up as part of the English Crown Jewels after the British conquest of the Punjab. Queen Victoria had the stone recut to its current form in 1852 (see box A for more information on the diamond's history).

Although much is known about the original Koh-i-Noor, drawings of its form are scarce and contradictory (figure 2). As a result, there is insufficient historical data to recreate the diamond with any accuracy.

However, the Natural History Museum in London created a plaster mold of the diamond in 1851, prior to the recutting, and from this two plaster casts were made. The discovery of a firebrick mold in December 2007 suggests that at least one lead model was also made, but there is no documentation to confirm this. The two plaster casts are the only replicas known to have been made from the original stone (a cubic zirconia [CZ] replica has been cut based on one of these plaster forms, as described in Hatleberg, 2006, but no details as to the specific techniques used were provided in that report). One of the plaster casts is on permanent display at the museum, but the other was analyzed for this study using a combination of photographic techniques and laser and X-ray scanning technologies to create a computer model of the original Koh-i-Noor. This model was used to determine the alignment of the historic stone within the original diamond crystal (and test one theory of its origin), analyze the

See end of article for About the Authors and Acknowledgments.
GEMS & GEMOLOGY, Vol. 44, No. 2, pp. 124–141.

Figure 1. The Koh-i-Noor, currently the centerpiece of the Queen Mother's crown in the English Crown Jewels, is perhaps the most famous diamond in the world. It was recut to its current size of 105.60 ct in 1852. A replica of its historic form (inset) was prepared as part of this article. Crown ©/ The Royal Collection © Her Majesty Queen Elizabeth II; inset photo by S. Sucher.

recutting of the stone, and create a CZ replica to evaluate historical reports of its optical performance.

MODELING BACKGROUND

Famous diamonds have been replicated from glass, crystal, lead, and plaster for hundreds of years. More recently, various computer-aided techniques have been added to the modeler's tools (e.g., Attaway, 2005). Some, such as photography, photogrammetry, and photomodeling, rely on photos to reconstruct the stone. Laser and X-ray scanners, as well as optical scanners, can be used with either the original stone or a model to scan the surface topography and generate reflections from which a digital three-dimensional (3-D) model of the original can be created.

The study described here combined photography with laser and X-ray scanning. Initially, only the photographic process was employed. This consisted of photographing the plaster model from many angles and using these photos to generate line drawings of the facet pattern and other surface features. The line drawings served as design templates, on the basis of

BOX A: THE STORY OF THE KOH-I-NOOR

Although it is neither the largest nor the most dazzling diamond ever found, the Koh-i-Noor's fame and colorful background are unsurpassed. The stone's origins and early history have never been conclusively established—apocryphal accounts have placed its discovery as early as 3000 BC. It is widely believed to have come from India's Golconda region, an early source of high-quality colorless diamonds. The first reliable reference to the Koh-i-Noor is believed to be in the memoirs (circa 1526) of Babur, founder of the Mogul dynasty, who wrote of the Sultan of Delhi capturing the then-unnamed diamond in 1304 (Streeter, 1882). Babur himself had captured the stone in 1526 after defeating its previous possessor, the Rajah of Gwalior (Balfour, 2000).

For centuries, the original 186 ct (191.03 modern carats) diamond changed hands repeatedly and often by violence, a coveted spoil of the wars between the Mogul empire, India, Afghanistan, and Persia. Its name, said to have been exclaimed by the Persian Emperor Nadir Shah upon seeing the gem for the first time after the sack of Delhi in 1739, is Persian for "Mountain of Light." The British East India Company acquired the Koh-i-Noor in 1849 with the British conquest of the Punjab. In 1850, it was presented to Queen Victoria at a ceremony marking the 250th anniversary of the founding of the East India Company (Copeland, 1974), and it has remained in British possession ever since.

The Koh-i-Noor first went on public display at the Great Exhibition, held in London's Hyde Park from May to October of 1851. The diamond was displayed in a large glass case and illuminated by either candles or gas lamps, hardly suitable conditions for brilliance or sparkle. *The Times* reported that while the gem drew the exhibition's largest crowds, many were disappointed by its rather ordinary appearance (Balfour, 2000). The following year, Prince Albert gave it to the crown jewelers, Garrard & Co., for recutting (Blair et al., 1998). Garrard's brought several master cutters from Coster Diamonds in Amsterdam to London to oversee the job (figure A-1), and 38 days later the Koh-i-Noor had been trimmed to 105.60 (modern) ct, just over half the original size. The resulting oval-cut diamond was set in a tiara for the queen.

Opinions of the recutting were mixed. Prince Albert, who had been closely involved with the operation, was openly dissatisfied with the outcome, especially the great loss of weight it had entailed (Streeter, 1882). There is also a perhaps-apocryphal story that when the Sikh Prince Dhulip Singh, the Koh-i-Noor's last non-British owner, was shown the recut diamond by Queen Victoria, he was rendered speechless for some minutes afterward (Blair et al., 1998). That the recutting was unnecessarily rushed seems clear, judging by the number of correction facets on the stone (Blair et al., 1998).

Gemologically, the Koh-i-Noor is a D-color type IIa stone (Blair et al., 1998). Unlike similar classic "Golconda diamonds" that show pinkish orange fluorescence (Fritsch, 1998), the Koh-i-Noor is inert to long-wave UV radiation but shows a weak green reaction to short-wave UV. Although it has not been given a clarity grade, it shows several feathers/gletzes and a black inclusion under its table (Blair et al., 1998).

Since the Koh-i-Noor's acquisition by the British,

which the diamond could be virtually "cut" using a software program designed for three-dimensional gem modeling. The data from this computer model were then used to create a CZ replica that more closely mimicked the diamond than the materials historically used.

The complexity of the plaster model's surface topography made it extremely difficult to resolve the Koh-i-Noor's features photographically. Although photos alone can be used to produce a computer-generated and physical replica of any original, any assumptions as to facet settings based on the photos have a high probability of causing errors. These can be minimized through extensive iterations (i.e., "trial and error") of the resultant computer model—making adjustments to each facet until the computer model matches the photos as best as possible—but this is extremely time consuming for a stone of such complexity. It became apparent that a different technique was needed to improve accuracy, as this would be our only opportunity to have unfettered access to the 150+-year-old plaster replica. The technique had to be objective and generate highly accurate data that precisely captured the diamond's surface topology. Laser and X-ray scanning methods meet both these criteria.

METHODS AND RESULTS

The Photographic Method. We applied the photographic method to capture the outline of the plaster replica and every surface detail, including the pattern,

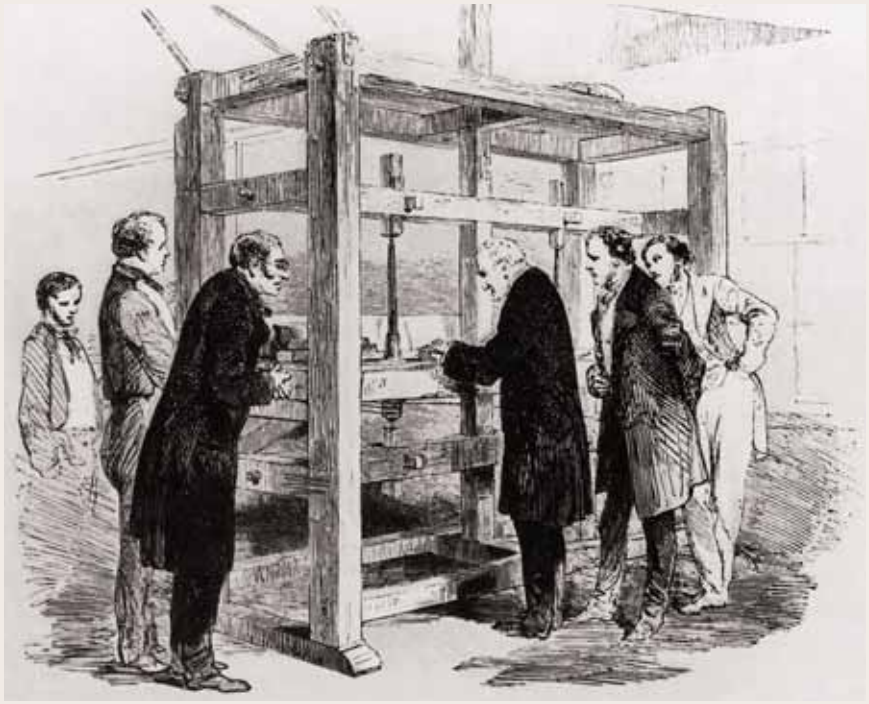

Figure A-1. This drawing from The Illustrated London News *(July 1852) depicts the recutting of the Koh-i-Noor by a team from Garrard & Co., the Crown Jewelers, and Coster Diamonds of Amsterdam.*

only female members of the royal family have worn it. This may be because the diamond is said to carry a curse that brings its male possessors great misfortune—though the Indian legend is the exact opposite, reflecting the many powerful men who possessed it (Balfour, 2000).

Today, the Koh-i-Noor resides in the Tower of London, where it is the centerpiece of the Queen Mother's 1937 coronation crown (again, see figure 1), seen by millions of visitors each year. Yet the diamond's future is still not entirely settled, as the governments of India, Pakistan, Iran, and Afghanistan have all claimed ownership of it and demanded its return at various points over the past few decades. Controversy flared up again in 2002, after the Queen Mother's funeral. Her crown, including the Koh-i-Noor, was placed atop her casket during the ceremony, a gesture that angered Indian politicians, who considered it an unnecessary flaunting of imperial plunder ("Diamond teaser. . .," 2002).

Even as the legendary diamond enjoys a seemingly quiet "retirement," its notoriety continues to grow.

shape, and size of the facets, as well as four surface cavities that held the original diamond in its prong setting (Tennant, 1852, p. 82). Using a Canon Powershot A40 digital camera with 2-megapixel resolution, we took 10 series of photos from different perspectives—top, bottom, and side views at every 45° of rotation—to create the line drawings (e.g., figure 3).

Many facets on the plaster replica were difficult to discern in the photos. Plaster is a soft material that erodes over time. Facet edges become rounded, often making the outlines difficult to see. In addition, the angular difference between adjacent facets was minimal, in many cases less than 3°, causing one facet to "blend" into its neighbors. This was resolved by taking many photos under low-illumination, low-angle conditions. A 40 watt incandescent light source was rotated about the model in a darkened room, causing facet junctions to alternately appear and disappear (figure 4, photos). Over 700 pictures were taken in various lighting conditions.

Next, we created the line drawings by importing a baseline photo into Adobe Illustrator 9.0 and tracing all visible surface details. Then we imported another photo from that series, with the light in a different position, and the newly visible features were added to the line drawing. Additional photos were imported until all features visible with the changing light positions had been incorporated and the resulting line drawing was complete (see, e.g., figure 4, bottom).

The line drawings captured the facet details, stone outline, and all other features necessary to describe the surface topology of the plaster replica.

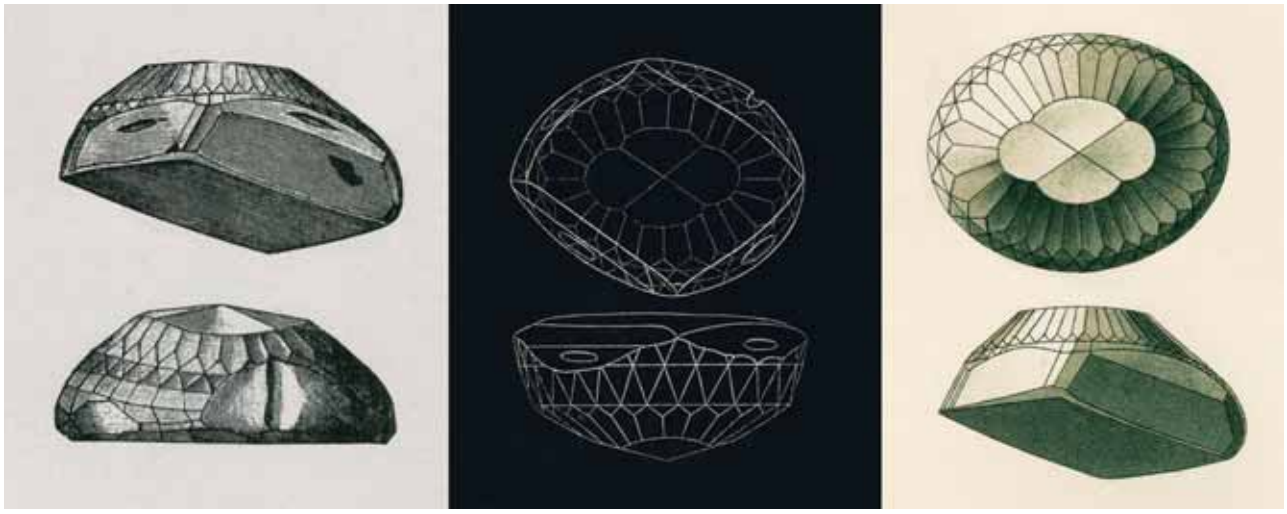

Figure 2. These historic drawings of the original Koh-i-Noor diamond show conflicting appearances: left—Tennant (1852, p. 83); center—Dieulafait (1874, p. 95); and right—Bauer (1968, plate X).

As noted earlier, though, relying on photography alone to generate line drawings introduces additional sources of error. These were addressed as follows:

Viewing Angle. Photos could not be taken randomly; they had to be shot from specific viewing angles that were accurately reproducible. The solution was a compass rose with graduated markings like those of the index wheel on a faceting machine. The plaster replica was placed on this compass rose and held stationary (figure 5). Photos were taken from different angles by rotating the compass rose around a fixed axis and maintaining the camera in a fixed position.

Parallax. Parallax (the apparent displacement of a feature as seen from two different points) was especially acute for facets visible on the far left or right in any photo, due to the diamond's pronounced curvature. This was mitigated by giving priority to those facets in the center of a photo whenever there was a discrepancy between adjacent views.

Perspective. All photos had to be taken orthogonal to a diamond axis. Side views were directly from the side (again, see figure 4), with the camera and replica positions kept fixed. Any angling up or down would distort facet shapes.

Depth of Field. All photos had to be in focus. An out-of-focus picture causes a slight displacement of surface features when the line drawing is generated. This effect is especially acute on sharply curved surfaces such as those of the Koh-i-Noor, which became apparent during computer modeling. A facet visible in one photo would be slightly displaced on the computer model in an adjacent view. The center facets in the picture would be in focus, but those on either side would be blurred and their

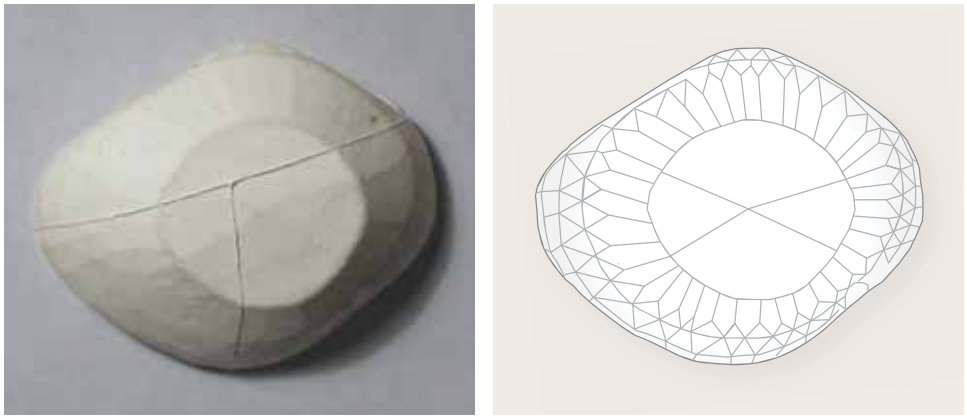

Figure 3. Photos of the plaster model (left) served as a guide to generate line-drawing templates, from which facet pattern and other surface features could be derived (right). Not all facets could be discerned from the photos. Photo by S. Sucher.

apparent positions in the photo slightly different from their real positions. Again, priority was given to facets in the center of any photo.

Line Drawings. Creating a line drawing that captures diamond outline, facet junctions, and other features is highly subjective when these features are not well defined. Misplacing the endpoint of a facet junction by even one pixel has a cumulative effect in introduced error. This was mitigated by expanding the photos approximately 5× in Illustrator to trace the facet junctions. The resultant drawing was exported as a .wmf (Windows Metafile Format) file, as this vector-based format allows expansion and contraction of the line art without the associated ragged lines of raster-based drawings. The wmf drawing was used as the overlay graphic during computer modeling.

Indistinct Facets. Determining facet shape and size from the photos was very difficult because each facet tended to blend in with adjacent ones, as described above. Low-angle lighting (again, see figure 4) mitigated most of this effect. Approximately 10 facets were so indistinct as to be nonexistent, but they could be inferred. A study of ancient Indian cutting techniques (Meen, 1968) revealed several historic diamonds in the Iranian Crown Jewels that were cut similarly to the Koh-i-Noor. All have four main crown facets surrounded by long facets, which in turn were bounded by very small triangular facets. The succeeding rows consist of small triangular or rectangular facets. On the Koh-i-Noor, most of the "missing" facets were the long facets and the very small triangular ones adjacent to them. However, the row of facets below these was sufficiently defined to create the boundaries of the missing facets by emulating the pattern found on the other diamonds (figure 6).

The Scanning Process. Although with the photos we were able to successfully capture the surface topography of the plaster cast, the limitations of the photographic method required a more accurate method of capturing data for computer modeling, so we turned to commercially available laser and X-ray scanners. The Helium 1:4 digital laser scanner by OctoNus Software Ltd. offered the necessary precision and was able to accommodate an object roughly 41 × 31 × 17 mm. A sister company, SkyScan, manufactures a high-resolution X-ray scanner (model 1172) with similar capabilities. The resulting scan data could be interpreted using a proprietary software program, Diamond Calculator 3.0 (also referred to as DiamCalc 3.0), which gives the angle and index of each planar surface generated by the scan data. (The *angle setting* is the placement of the cutting angle in relation to a horizontal reference; the *index setting* refers to the degree of rotation around a central axis.)

The plaster replica was scanned on both the laser and X-ray machines in Belgium. Afterward, the replica was mailed directly back to the museum in London and the data were forwarded to the authors for analysis.

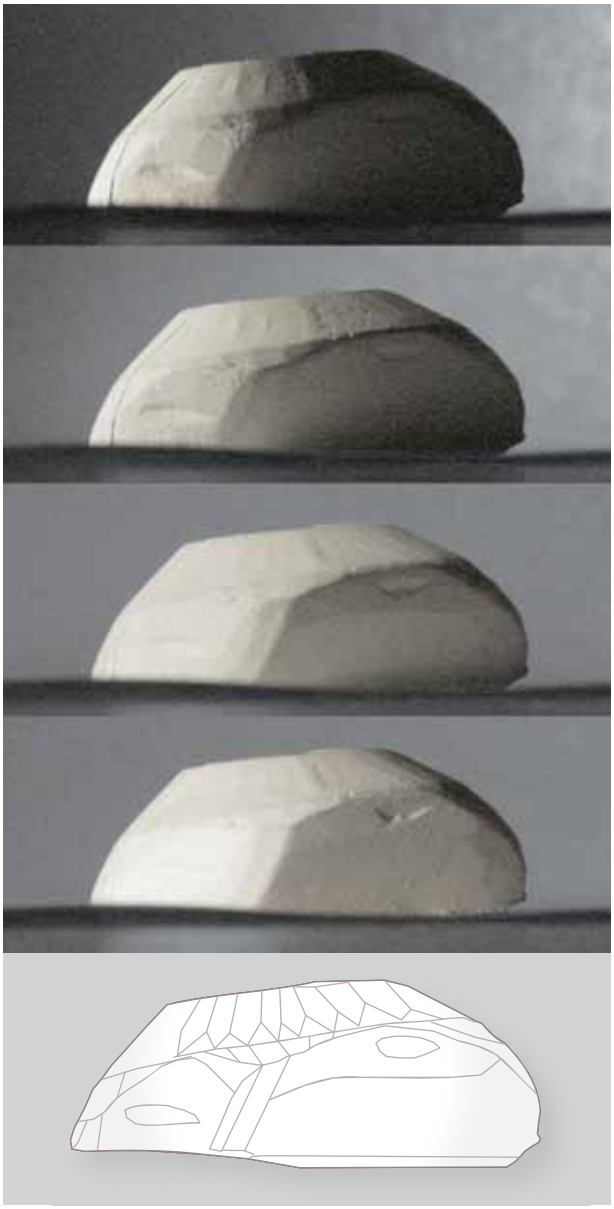

Figure 4. The four photos shown here produced this line drawing of the original Koh-i-Noor. The oval features are two of the cavities in the surface that were used for the prongs in the original mounting. Photos by S. Sucher.

Figure 5. The compass rose and model demonstrate how rotational alignment was maintained. The camera remained fixed as the diamond and compass rose were rotated. Photo by S. Sucher.

The Helium laser scanner has the following specifications: laser—635 nm; field of view—43.3 × 56.8 mm; rough capacity—5–500 ct; diamond holding—vacuum/glue assisted; 3-D model accuracy—better than 28 µm; a 1:4 lens; and CCD camera resolution—1920 × 1080 pixels.

The specifications of the X-ray scanner are: X-ray source—20–100 kV, 10 W, <5 µm spot size; X-ray detector—10 megapixel or 1.3 megapixel cooled CCD fiber-optically coupled to scintillator; detail detectability—<1 µm with 10 megapixel camera, <2 µm with 1.3 megapixel camera; size capacity—68 mm in diameter with 10 megapixel camera; reconstruction—single PC or cluster volumetric reconstruction (Feldkamp algorithm).

Although we used both tools to generate data, only the laser scan data were extensively analyzed once it was determined that the X-ray data closely matched them. The laser scan data generated 5,047 planar surfaces that defined the model's topography. Those planar surfaces were then reduced to the 169 facets shown on the line drawings. Thus, an average of 30 planes (5,047÷169) defined any given facet.

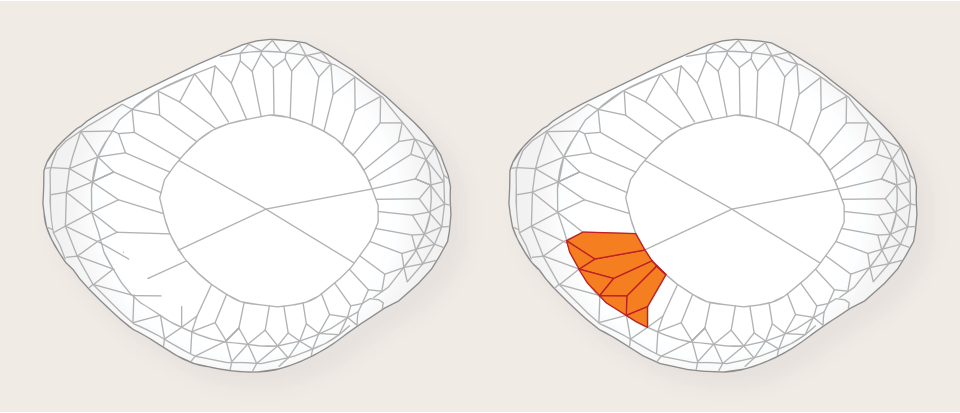

Figure 6. Some "missing" facets (left) could not be discerned in the photographs, but they were known to exist from analysis of the surrounding facets. The missing facets were filled in (right) by matching patterns on historic diamonds in the Crown Jewels of Iran with cuts similar to that of the Koh-i-Noor.

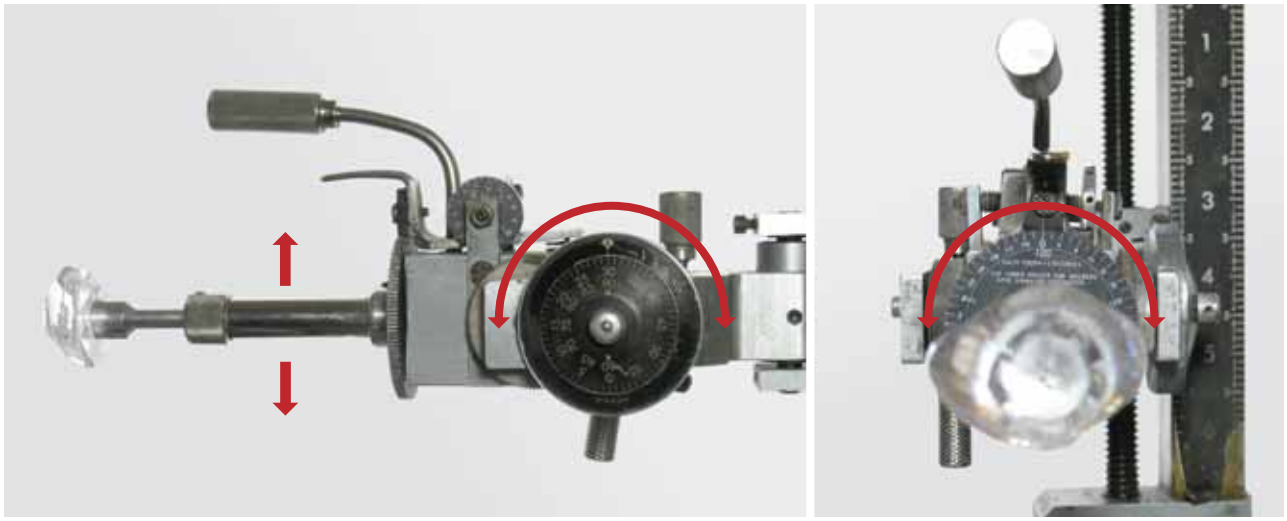

Figure 7. Each facet has a unique angle and index setting, as placement of the CZ model on this faceting machine illustrates. On the left: As the arm moves up and down, the angle dial rotates and displays the angle (0 reference is vertical). The arm position can be fixed at any angle setting to 0.25° accuracy. On the right: The arm is rotated about its longitudinal axis. Teeth on the gear behind the diamond allow any index setting to be fixed. A smaller wheel (the "index vernier" or "cheater," shown above and to the left of the index dial in the image on the left) allows finer settings to less than 0.10° accuracy. Photos by S. Sucher.

Computer Modeling. The line drawings created from the photos were used as design templates to virtually cut the diamond on the computer using GemCad, a software program for 3-D gem modeling. As noted above, the photographic process is a highly iterative one, where facet settings are derived primarily through trial and error. Because the original Koh-i-Noor was such a complex stone, we felt that placing the four large facets on the table in the computer model was a necessary first step in cutting (to both simplify the process and reduce the number of iterations needed). The appropriate line drawings were analyzed in Illustrator to determine the approximate settings needed to create these facets.

Cutting a facet, whether virtual or actual, requires the identification of two variables: the angle setting and the index setting (figure 7). These two settings are difficult to establish using the photographic technique, as they are determined through trial and error during computer modeling. Side photos showing the four crown facets were analyzed to determine the angle settings. Index settings were estimated using stonecutter judgment. These angle and index settings were entered in the modeling software to "cut" each virtual facet, and then they were iterated until facet size, shape, location, and intersections with neighboring facets matched the line drawing (figure 8). Dozens of iterations were required for just the first four facets, as the low crown angles had multiple index-setting solutions.

Once these four facets were placed on the model, the settings for adjacent facets were determined by resolving the intersections. Again, this process was highly iterative.

A limitation of both DiamCalc and GemCad is that they cannot model depressions such as the four cavities visible in the photos. To duplicate

Figure 8. This overlay of the modeling workspace with a preliminary computer model (gray) and line drawing (red) shows how real-time feedback is provided to ensure a virtual facet matches its counterpart in the line drawing. If the facet is not correct, its black outline will not match the red template.

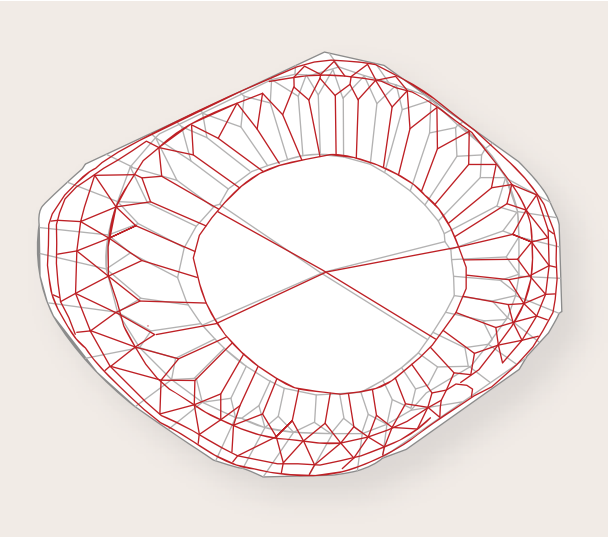

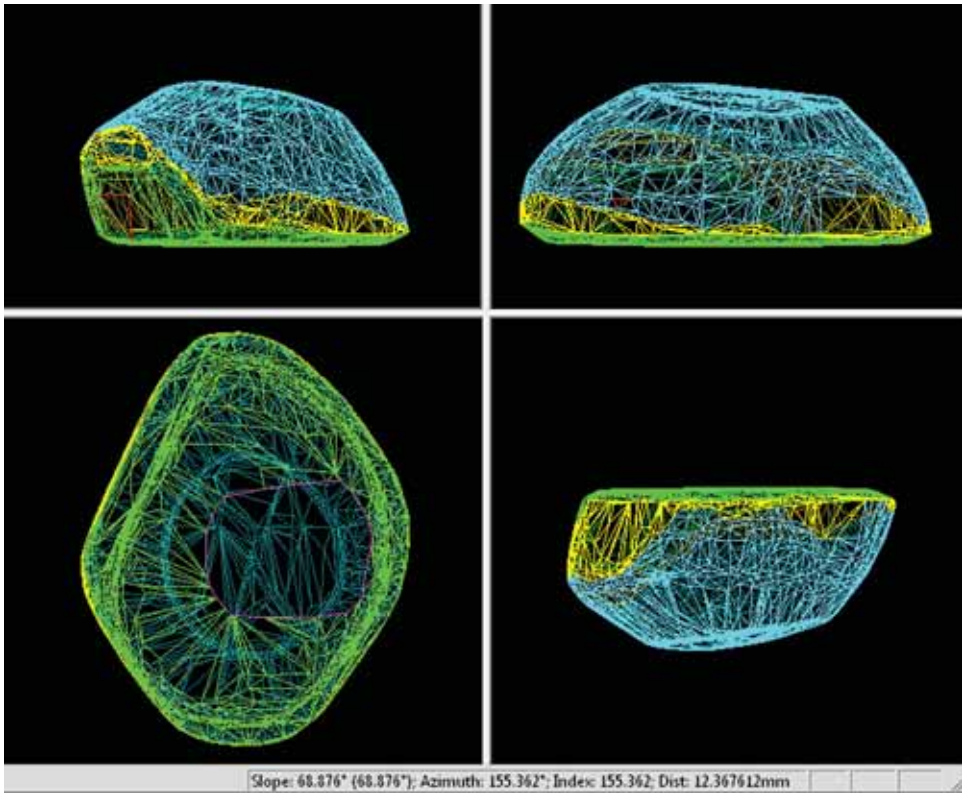

Figure 9. This graphical depiction of the scan data shows how the scan model can be rotated in all directions. Note the large triangular facet outlined in red in the upper left view, selected with a computer mouse. The angle (slope) and index (azimuth) of that facet (the facet settings) are displayed at the bottom of the screen. The distance value is the center-to-facet distance and was not used.

these cavities on the CZ replica, we used 10× magnification and a table gauge accurate to 0.1 mm to physically measure their dimensions during the cutting process.

The virtual solid generated by the scan data was displayed graphically in three dimensions with full rotation on the X, Y, and Z axes (figure 9). The settings for any particular plane could be found by positioning the cursor over that plane in the scan file. A readout provided facet settings to 0.001 in angle and index.

For the computer model, we overlaid each line drawing on the computer workspace and the scan picture (e.g., figure 10). We computed settings for each facet using the following procedure:

1. The facet of interest was identified in the line drawing.
2. The scan data were brought to the top, and the average of all facet settings in that area was determined.

Figure 10. In this overlay of a line drawing (red) on the scan data, the outlined yellow facet is the facet to be "cut" in GemCad. It shows the planes from the scan data that define that facet.

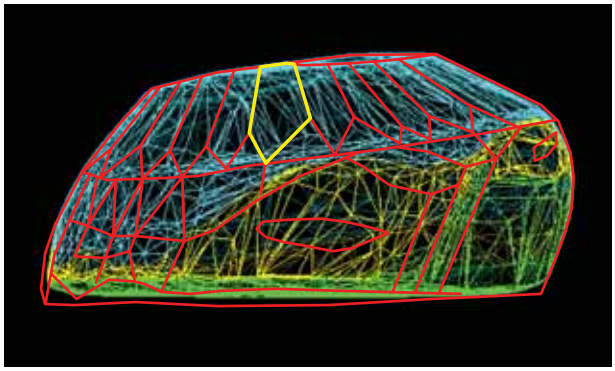

TABLE 1. Angles and indices of the planes outlined by the highlighted facet in figure 10.[a]

Angle	Index[b]
40.34°	227.91
41.83°	229.14
42.16°	230.04
42.31°	230.34
42.46°	230.92
43.82°	234.58
44.96°	238.03

[a] *Only planes 2–5 (highlighted here) were used to determine an average of facet settings, as the others have significantly different values.*
[b] *360 index wheel.*

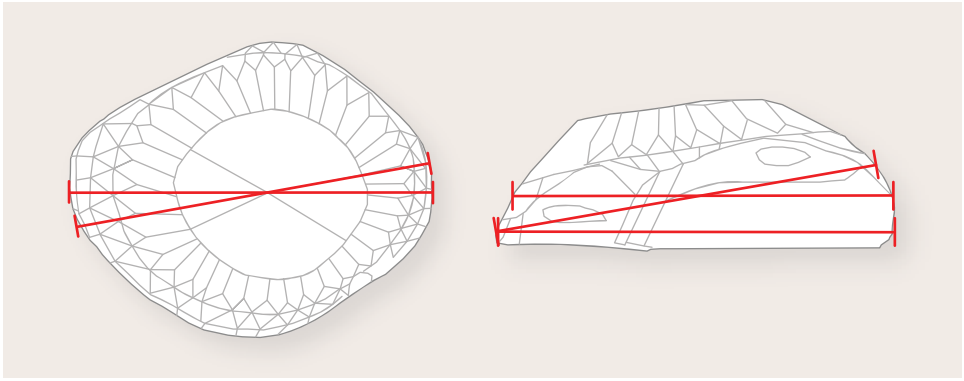

Figure 11. Sources of error that lead to inconsistent caliper measurements: (left) lack of girdle facets, combined with the ever-changing outline, makes reproducible positioning of calipers problematic (lines indicate axes of measurement); and (right) lack of a defined girdle makes it difficult to consistently position calipers so that they remain parallel to the model's base.

3. The workspace was placed on top, and the average of the settings was used to "cut" that facet in the computer model.

4. The new facet was compared to the line drawing to ensure it had the proper shape and size, and all facet intersections matched the drawing. If all three criteria were not met, then angle, index, and/or depth of cut were successively iterated within the range of angle- and index-setting values dictated by the scan data until the modeled facet matched the line drawing.

As an example of this process, table 1 lists the angles and indices of the larger planes for the facet described in figure 10. These were iterated in GemCad within the upper and lower values here until this facet matched the shape and size dictated by the line drawing.

Thus, the planar surfaces were reduced to the required 169 facets by using the line drawings to define the facet pattern and DiamCalc 3.0 to determine the angle and index settings of each facet from the laser scan data; both were then used to generate a computer model with GemCad.

The shape of the final GemCad model was then compared to the DiamCalc model from multiple perspectives to ensure the outlines matched. Any discrepancies were noted, and these areas were virtually "recut" until the model matched the scan data. At that point, the computer model was considered accurate.

This computer model could not be used directly to create a physical replica, as the model is dimensionless. The data alone could be used to cut a stone of 5 ct or 500 ct. GemCad has an algorithm for generating stone width, and hence length and depth, but any errors or assumptions during modeling would affect the result. Calipers could not be used to measure the plaster replica because its unusual shape and sidewall angles precluded reproducible measurement (figure 11). Values were in the vicinity of 41.7 × 33.9 × 16.7 mm, but they were highly variable depending on where the calipers were placed and whether the plane of measurement was parallel to the diamond's base. Even with utmost care, any measurement series had values that varied as much as 0.5 mm in length and width.

Replica dimensions were determined by exporting the .dmc format of the scan model as a .dxf file so it could be imported into TurboCad Pro 10 for measurement. The maximum dimension was determined by rotating the scan model one degree at a time until the longest measurement was achieved. Width was measured orthogonally to the length axis, and depth was provided by the scanning software. This resulted in dimensions of:

Length = 41.78 mm
Width = 33.63 mm
Depth = 16.56 mm

The dimensions were further adjusted after analysis revealed that these values caused a discrepancy with the historical Koh-i-noor's reported weight (see Weight Analysis below).

Physical Modeling. The CZ replica was created with the cutting instructions generated from the GemCad data. These instructions contained the angle and index setting of each facet, plus actual-size and magnified views from each viewing angle, and various templates for facet placement.

Two related factors that had to be considered during the computer and physical modeling processes were stone center and dop center. Stone center was critical for computer modeling, as facets are placed as a function of distance from this point. Since the computer data were being used to cut a physical replica, the axis of rotation during computer modeling (stone center) had to be aligned with the axis of

rotation on which the CZ replica was mounted during faceting (dop center, see figure 7, right).

Stone center (0,0) during computer modeling was achieved by creating a template of the outline from the top-down view and centering the virtual workspace in the X and Y directions within this outline. The computer model was then created around this 0,0 reference. Once the computer model was complete, a set of crosshairs was superimposed and centered in both the X and Y directions on the outline template. The template was then printed at actual size and glued to the rough CZ. A jig and specially built dop were used to align the dop axis with the crosshairs on the template on the rough at 10×. Stone center was now aligned with dop center, and cutting could begin.

The four largest facets were cut first using the angle and index settings generated by GemCad. Computer modeling showed that they had to be cut in a specific order to a specific depth. The depth issue was resolved by using templates and measurements to initially place these four facets in their approximate positions. Final placement did not occur until the first surrounding row of long facets was in place, whereupon another template was used to ensure each facet was the appropriate size, and the length of the facet junctions around these four facets were exactly those dictated by computer modeling (using a table gauge and 10× magnification).

The remaining facets were placed using the settings derived from computer modeling. The depth of cut (distance from stone center to facet), though readily available from the modeling data, could not be used during actual cutting, as there was no way to measure it.

However, this limitation could be overcome because each facet had a specific size, and this size could be directly measured during cutting. In practice, the facets were cut slightly under size, then gradually recut to the appropriate size. This was necessary, as material could always be removed, but if a facet was overcut (too much material removed), the mistake could not be undone. This continued until all facets were in place.

A limitation of such a process is that precise measurements are required for each facet. Yet absolute accuracy is not possible due to human error and the limits of the measuring tool. Consequently, after several facets, errors began to accumulate. These were manifested as facets that did not align properly or that deviated from the prescribed size. When such errors were encountered, the cutting of the preceding facets had to be reevaluated (size and shape) to determine where to recut the inaccurate facet(s). The entire stone was actually cut several times using smaller and smaller iterations until all facets were in place.

The four cavities that held the prongs were cut using a water-cooled dental drill with a superfine burr (3000 grit). Each cavity was placed by measuring the distance from the surrounding facets with a table gauge and then marking the surface with an indelible pen. Depth was gauged visually using a shadow technique with direct reference to the plaster replica.

DISCUSSION

Error Analysis. *Errors from Photography and Scanning.* The photographic method is useful for modeling diamonds to which we have limited access (such as those in various crown jewel collections), where data must be derived from just one or two photographs. This highly iterative method yields a model that is identical to the pictures, but it may still contain errors, as discussed above. As a result, it should only be used when other methods cannot.

Laser scanning is an objective and accurate process that eliminates the assumptions and iterations required with the photographic method for computer modeling. It also has its limitations, however, as evidenced by the number of planar surfaces comprising a single facet on this particular plaster replica, which became obvious when a line drawing was superimposed on its equivalent view from the laser scan (again, see figure 10). This demonstrated that the facets were not optically flat, but rather slightly rounded. This might have been due to the simple cutting equipment used to cut and polish the diamond centuries ago. It could also result from imperfections in the casting process, erosion of the model's surface, or slight deformation of the plaster model with age due to moisture absorption. We addressed this situation by using an average of the angle and index settings for every plane that defined a virtual facet. If the virtual facet's size and shape did not match its counterpart in the line drawing, we changed the angle and/or index (within the range limits defined by the scan planes) until the two matched. Thus, we basically "idealized" the facets to be flat and cut accordingly. However, this process of "iteration of averages" inevitably introduces error (see Error Mitigation below).

Errors Due to the Misaligned Mold for the Plaster Model. Another source of facet error was the fact

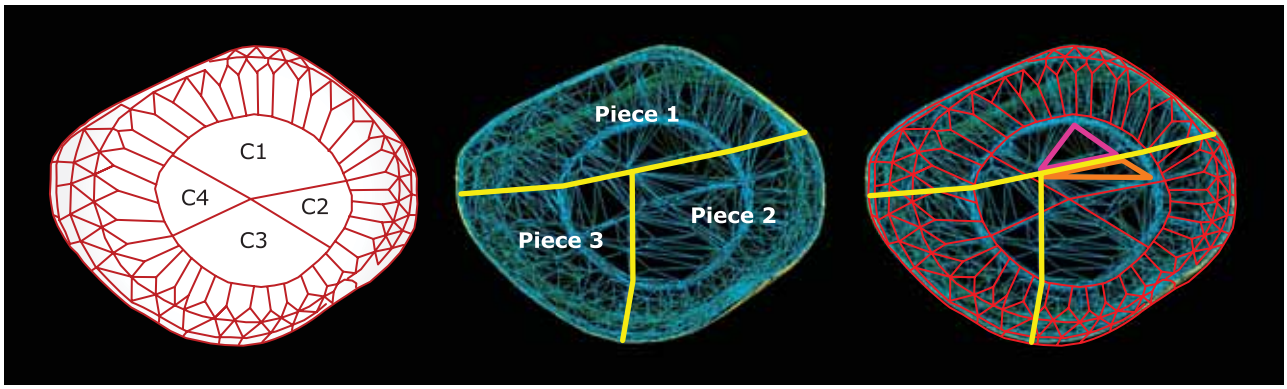

Figure 12. As shown in the line drawing (left), the original Koh-i-Noor had four main crown facets. These were reproduced by the top three pieces of the plaster model, as indicated by the seams shown in the scan data (center). An overlay of the line drawing on the scan data (right) reveals that the two planes defining facet C1 (pink and orange triangles) lie on separate pieces of the model—and that the upper and lower-right pieces of the model were slightly misaligned.

that the plaster replica was created from a mold that came in four sections, one for the bottom and three for the top (figure 12, center). The top three pieces were joined to form a single unit.

Although the seams from the mold pieces were difficult to discern in the scan data, they were clearly visible in the photographs (again, see figure 3). Overlaying the line drawing on the scan image distinctly showed their locations (figure 12, right). Analysis of the facet settings showed that pieces 2 and 3 were in alignment, as the planes on C3 (see figure 12, left) had similar settings regardless of whether the measurement was taken on piece 2 or piece 3. However, measurements on C1 had different settings depending on whether they were taken from pieces 1 and 2, or 1 and 3.

This is because when the model was created, piece 1 was slightly out of alignment, as shown by the angle and index settings of the planes described in figure 12, right: The index (based on a 360 index wheel) and angle settings for the orange portion of facet C1 were 240.21 and 5.57°, respectively, and for the pink portion they were 288.7 and 6.49°. Had piece 1 been properly aligned, these values should have been identical.

The settings for facet C2 were straightforward, as it resided solely on piece 2. For C1, we used the average of the two angles above (~6°) and the lines of intersection with C2 and C4 to calculate an index setting. An index of 250 satisfied all constraints. A similar process was used for C4, as it resides on non-aligned pieces (1 and 3), but the differences in facet settings were negligible.

This misalignment caused the spatial relationships between facets to change, affecting the angle and index settings recorded by the scanner. As a result, these settings could not be used unadjusted when virtually cutting these facets. This limitation was overcome by cutting the facets that overlapped these pieces with reference to the line drawing. Intermediate facets were cut using the relative differences between facet settings.

Error Mitigation. Creation of an accurate model requires accurate line drawings and facet settings. In both cases, however, the process used to maximize accuracy has been shown to introduce error. Additionally, one of the molds used to make the plaster replica was slightly out of alignment, so we had to use assumptions about the facet settings for this portion of the stone. Given these obstacles, how could we generate an accurate computer model?

To this end, we made two assumptions concerning these errors:

1. Any given facet intersection had multiple solutions. For instance, baseline settings for two adjacent facets could yield a satisfactory solution; that is, the virtual facet matched its counterpart on the line drawing. However, on some facets, changing the index by 0.1 and the angle by 0.25° yielded the same intersection, so a *satisfactory* solution might not be the *best* solution.

2. All errors are cumulative. This was borne out when the photographically derived model was compared to the model from the scan data. Although in general there was excellent correlation between the two models and the line drawings, a number of facet settings were considerably different (see figure 13 and table 2).

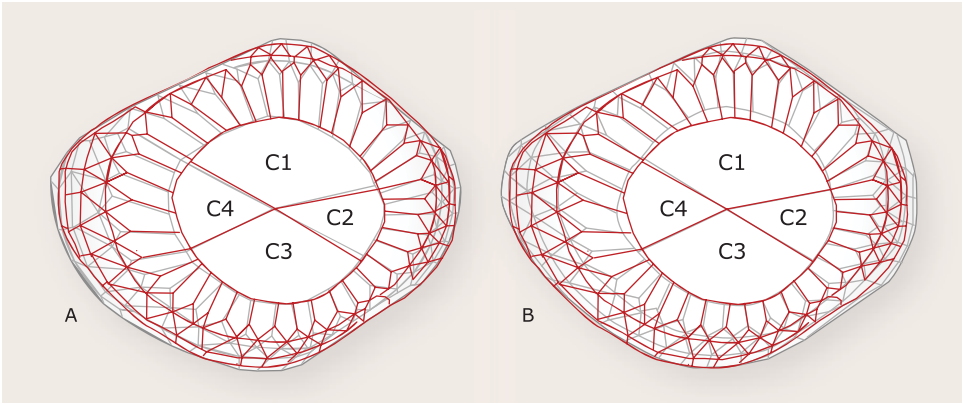

Figure 13. These two images compare angles and index solutions between the computer models (gray) overlaid with the line drawing (red) derived photographically (A) and from the scan data (B).

TABLE 2. Summary of angle and index settings of facets C1–C4 derived from photographic analysis only and using the scan data.

Crown facet	Photo data		Scan data	
	Angle	Index[a]	Angle	Index[a]
C1	9°	195	6°	249.9
C2	10°	325.5	12.5°	317.1
C3	14°	351	17°	347.1
C4	3°	72	7°	5.1

[a] *360 index wheel.*

To compensate for these errors, the "finished" GemCad model was divided into six 60° sectors for a comparison of sidewall angle with the laser-generated model. During computer modeling, eight side views were used and the sidewalls matched. Although there could have been errors in views intermediate to those used, division into six sectors was considered sufficient to verify the accuracy of those intermediate views.

The computer model's outline from each of the six side views was compared to its counterpart view in the scan data (figure 14). Two of the sectors deviated from the correct sidewall angle by around 3°, although their facet patterns matched the line drawings. This was corrected by changing individual facet settings (within the range of settings of the planar surfaces dictated in the scan data) until the sidewall angles matched. The computer model was considered accurate once the sidewall angles matched the scan data and the facet pattern matched all line drawings.

Accuracy can also be corroborated by the fixed rules of geometry that dictate how planar surfaces intersect:

1. The facet pattern on any diamond is a combination of planar intersections (facets), with each plane described by an angle and index setting, and a specified depth of cut. Change any variable for two adjacent facets and their shared edges change, which changes those for their neighbors, and so on throughout the diamond.

2. The irregular, curved surface of the Koh-i-Noor was more difficult to model than a more traditionally cut, symmetrical gem. However, the very complexity of the diamond helped ensure accuracy, as there are a limited number of combinations of 169 facets that can be used to describe a three-dimensional surface as complex as with this shape. The three cutting variables (depth of cut as well as angle and index) result in 507 dependent variables (169 × 3) that define the surface. Although there are many sources of error, we felt that a computer model satisfying 507 dependent variables within the accuracy of GemCad should be the best solution. (The accuracy of GemCad for this model was 40.22 units/mm, or 0.025 mm resolution. The model was magnified approximately 3× onscreen, so nominal resolution was approximately 0.008 mm. However, the program only measures at four-unit intervals, so the actual resolution was closer to 0.03 mm.)

Weight Analysis. The dimensions obtained by computer modeling were derived from the scan data, but there was a 13.17 ct discrepancy between the weight calculated from the scan data and the diamond's reported weight based on these dimensions. Given the known volume, and a density of 3.522 g/cm^3, the scanning software calculated a diamond weight of 204.20 modern carats. However, multiple historical records report a weight of 186.1 old carats (0.2053 g per carat), or 191.03 modern carats (0.2 g per carat). A reduction in weight due to the cavities was considered, but from direct measurement all

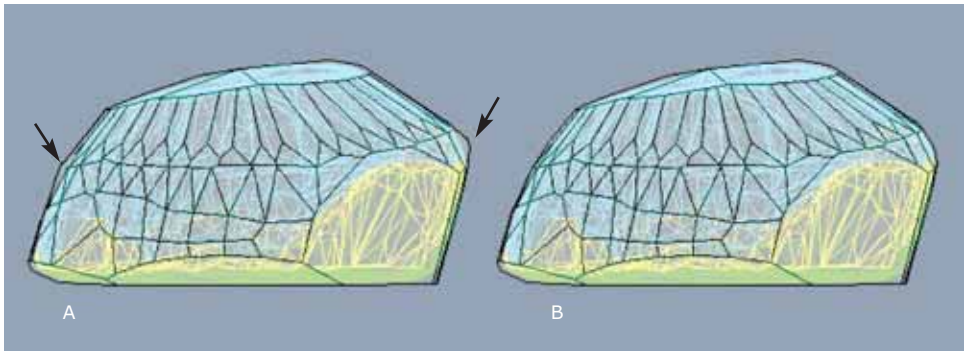

Figure 14. This is a comparison of sidewall angles between the computer model (black) and scan data. In A, the outlines do not correlate (arrows), indicating that errors in the line drawings and computer model exist below the detection threshold. In B, the affected areas have been recut (changing individual facet settings) so the sidewall angles do match.

four encompassed an approximate volume equivalent to just 8 points of diamond weight. How could the latest in 21st century technology be at such large variance with a well-documented weight?

The scanned model was made of 155-year-old plaster and had been stored in the damp environment of England. It is possible that the plaster had swollen in the intervening years or during the casting process to attain the volume indicated by the heavier weight. Unfortunately, confirmation of either theory was outside the scope of this experiment. What is known is that a 204.2 ct computer model of the Koh-i-Noor measures 41.78 × 33.63 × 16.56 mm, and if corrected to 191.03 carats (performed through the scanning software and measured in TurboCad), its dimensions become 40.85 × 32.57 × 16.18 mm. This indicates that the plaster expanded 0.97 mm in length (2.3%), 1.06 mm in width (3.3%), and 0.27 mm in depth (2.3%), changing the volume by 7%. Any explanation as to why it would swell more in width than in length or depth would be pure speculation.

Crystallographic Analysis. Once the diamond was modeled on the computer, we used it to test claims by Tennant (1851) and Streeter (1882) that the larger "facets" were cleavages. Tennant studied the original diamond prior to recutting and concluded that the base (figure 15, yellow facet) was a cleavage face and the largest facet (green) was an unpolished cleavage (both being {111}, or octahedral crystal faces). We tested this by merging our computer model with the model of a perfect diamond octahedron featuring small dodecahedral crystal faces. Rotating the Koh-i-Noor within the octahedron confirmed that both the yellow and the green unpolished facets were indeed aligned with {111} faces. The computer model also showed that the blue facet was very close to the index of another octahedral face, but the angle differed by approximately 17°. When the green (unpolished) facet is assumed to be a cleavage (i.e., index 0.0 and angle 0.0°), calculations yield index and angle results of 0.1 and 1.52° for the base (yellow) and 0.4 and 16.69° for the blue facet, respectively. Perfect alignment between a cleavage and a polished facet is not to be expected, as diamond is hardest parallel to a cleavage plane. Grinding or polishing parallel to a cleavage is impossible. If a facet needed to be placed in this approximate configuration, it would have to be offset from perfect alignment.

Ball (1925, p. 342) and Streeter (1882, page 83) speculated that the green unpolished facet was the result of intentional cleaving to damage the diamond prior to handing it over to the British or during some earlier forcible transfer of ownership. The plaster replica and scan data do not support this, as this

Figure 15. This study also investigated historical claims that some of the Koh-i-Noor's original facets were actually cleavages: The area shaded in green, an unpolished cleavage; the base (yellow), a polished face very close to a cleavage; and the blue facet, aligned with the index of a cleavage. When the computer model is merged with the model of a perfect diamond octahedron, the alignment of the green "facet" with one of the cleavage planes suggests that it is an unpolished cleavage plane and the blue facet is close to another cleavage plane, but the angle differs by about 17°.

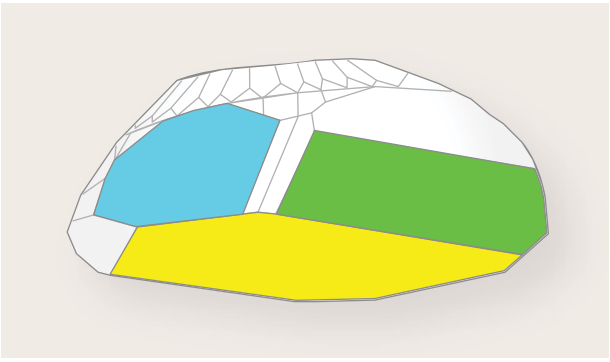

facet has significantly rounded edges. If the damage was from cleavage performed after the diamond had been polished, someone would have had to regrind the edges to round them and place facets on these surfaces, a somewhat arduous task. Also, the facets surrounding this plane suggest the cutter "blended" them into a preexisting surface; he did not end them abruptly as one would expect if any face were cleaved later. Blending the facets would also be expected to give the diamond a finished appearance while conserving weight. Because of these factors, and a lack of evidence to the contrary, this facet is more than likely the result of natural processes (and subsequent working) rather than intentional damage. Thus, it seems that no damage was inflicted after the Koh-i-Noor was originally cut unless it was disguised by further cutting prior to receipt of the diamond by the British.

This does not explain the unpolished nature of the green facet as described by Tennant. The model indicates it is an octahedral face (111), which would make it physically impossible to polish (although changing the grinding angle by just a few degrees could have permitted this). Perhaps it was a clean cleavage, shiny enough that the cutter felt it needed no further working. Unfortunately, any explanation of why this one facet remained unpolished would be purely conjecture.

Relationship to the Great Mogul Diamond. Ball and Streeter also theorized that the cleavage facets were the result of several diamonds, including the Koh-i-Noor, having been cut from a much larger diamond called the Great Mogul (Ball, 1925, p. 343). According to Tavernier (1676, p. 97), the Great Mogul weighed 279 9/16 ct (286.97 modern ct) and was shaped like half an egg (figure 16). This is the only known historical reference to this diamond's existence. Unfortunately, this diamond subsequently disappeared, negating any truly definitive study.

Streeter and Ball went on to suggest that the Great Mogul disappeared when the Koh-i-Noor was cut from it (figure 17). We tested this hypothesis by comparing computer models of the two diamonds.

The Great Mogul was computer-modeled by superimposing the computer workspace over Tavernier's line drawing of it, similar to the modeling already described. Since Tavernier described the stone as half an egg, a circular cross-section was assumed. We used a photogrammetric process to simultaneously model the diamond in two views, top down (to maintain the circular shape) and from the side (to match the shape and sidewall angles shown in the drawing.) An analysis of the drawing showed changes in the symmetry of each row of facets, but the pattern appeared to be trapezoidal facets alternating with triangles. Different symmetries were tested to see which could generate this facet pattern and still create sidewall angles to match the drawing. A 32-fold symmetry satisfied

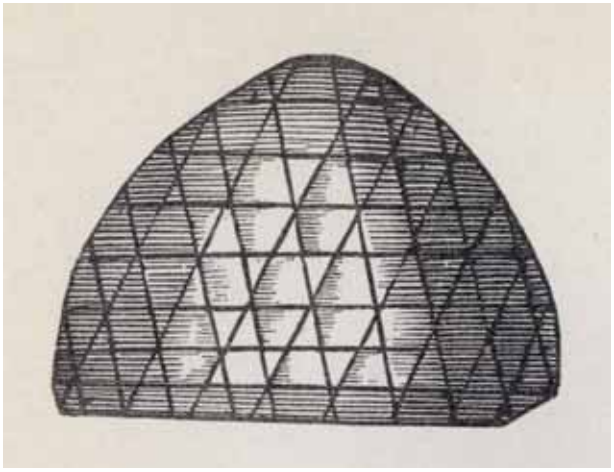

Figure 16. This 17th century drawing published by French gem trader Jean Baptiste Tavernier (1676) is the only known illustration of the Great Mogul diamond.

Figure 17. Streeter (1882) and Ball (1925) hypothesized that the Koh-i-Noor (black area) would have fit inside the Great Mogul diamond (circle). From Ball (1925), p. 342.

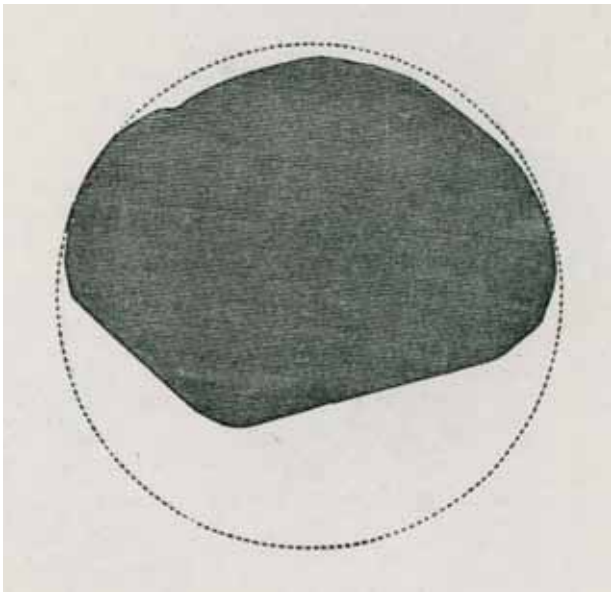

these constraints and was used for modeling. Once the computer model was complete, it was sized to encapsulate a volume equivalent to Tavernier's reported weight. This resulted in a diamond 34.85 mm in diameter and 25.61 mm in depth. The Koh-i-Noor was 40.85 × 32.57 × 16.18 mm. The result of superimposing one model on the other is shown in figure 18. Unless Tavernier's reported weight was too low by a large degree, it is clear that there can be no connection between the Great Mogul and the Koh-i-Noor as suggested by Streeter and Ball.

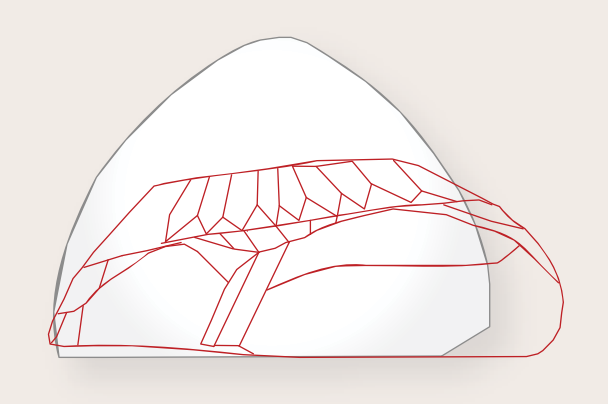

Figure 18. Computer models showed that the Koh-i-Noor (red) could not have been cut from the Great Mogul (black).

Recutting of the Historical Koh-i-Noor to the Modern Diamond. The orientation of the modern Koh-i-Noor within the original version was performed solely as an academic exercise. The modern stone was modeled with a photo from the top-down view and the published dimensions of 36.00 × 31.90 × 13.04 mm. Facet angles were determined by successively iterating pavilion and crown main facets to meet the reported weight of 105.60 ct (Bari, 2001, p. 178).

Once the computer models of both diamonds were merged in GemCad, the orientation of the historical Koh-i-Noor was maintained while the modern version was rotated through various configurations. The number of possible configurations was limited, as the modern diamond was asymmetrically cut. From a top-down view, there are four areas of the girdle that are much flatter than a perfect oval would dictate. These correspond to similar surfaces

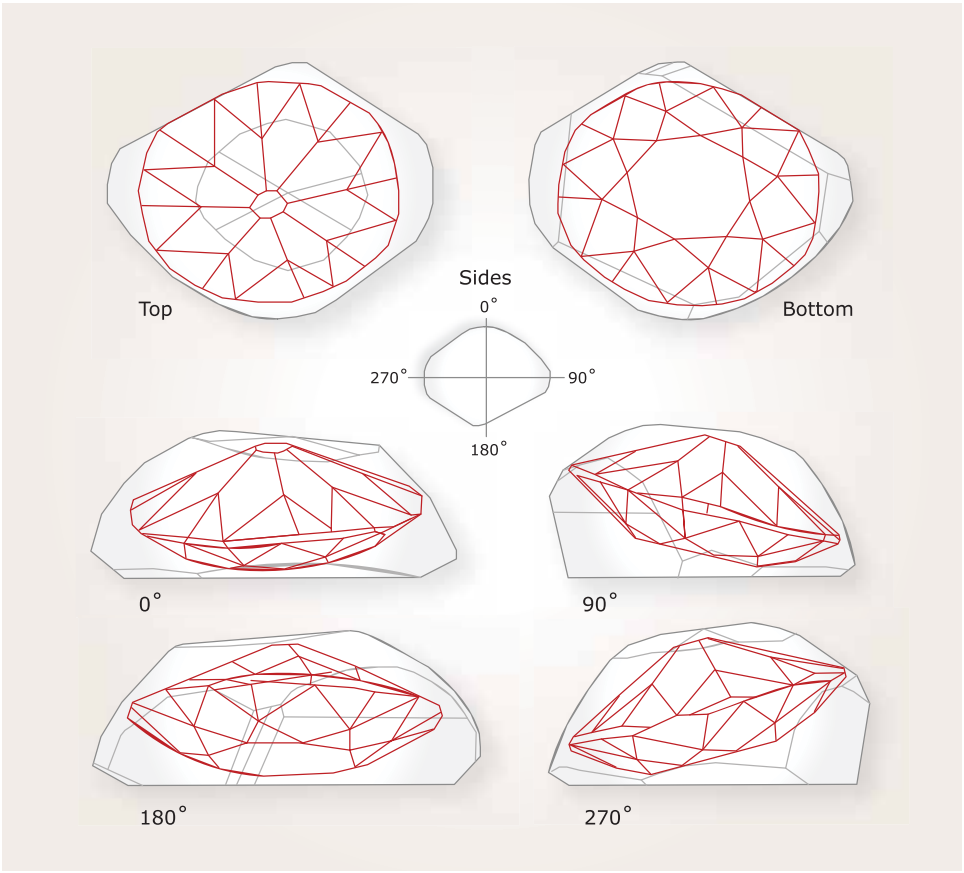

Figure 19. These six illustrations show the most likely orientation of the modern Koh-i-Noor inside the original cut, according to computer modeling. Tennant (1852) stated that it was necessary to turn the stone on its side to remove a flaw where the yellow and the green facets in figure 15 intersect, and to accommodate the removal of an inclusion and fracture in creating the future girdle.

Figure 20. This photo of the CZ replica demonstrates the optical effects that may have been displayed by the original Koh-i-Noor. A 6.5 mm CZ equivalent to a 1 ct diamond is shown for scale. Photo by S. Sucher.

on the historic diamond. Once these were aligned, orientation was a function of tilting the modern model to determine the best fit. Figure 19 shows the approximate orientation of the modern Koh-i-Noor to its original version.

The modern Koh-i-Noor has been described as asymmetrical and lacking brilliance—not an improvement over the original (Streeter, 1882; Balfour, 2000). However, an analysis of the two computer models showed the cutter's limitations. It is obvious that the cutter attempted to create a stone as large and symmetrical as possible, with the former constraint the more important one. Tennant (1852) mentioned no less than five flaws that needed to be removed, imposing additional cutting constraints. Rotating the modern model within the historical model shows that the final orientation removed the existing flaws and maximized both length and width—a larger stone could not have been cut. This also explains the flat spots on the girdle: They were retained to conserve weight, as the cutter knew they would not be quite so apparent when the stone was set.

The lack of brilliance can be attributed to the rather shallow angles on the pavilion main facets, in the vicinity of 27°, about 2.5° above the critical angle of 24.4° for diamond. Crown main angles range from 24–30°. These are a function of girdle placement within the historical stone and the properties dictated by its shape.

Tolkowsky (1919) suggested angles of 40.75° for the pavilion, and 34.5° for the crown for maximum brilliance for a round brilliant cut. Although these values can vary somewhat depending on other factors (size of the table, presence of a culet facet, the facet pattern used), those used on the modern Koh-i-Noor still vary significantly from those that would produce a diamond of, in Tolkowsky's words, "magnificent brilliancy." Unfortunately, the lower angles were necessary to maintain maximum apparent size from a face-up view. Although the stone is not as brilliant or symmetrical as it could be, modeling indicates that the cutter maximized the yield given all known constraints. This was indeed the typical standard for cutting in those days—diamond cutters could be penalized in their pay for not retaining the maximum weight, and beauty was rarely a consideration (Dieulafait, 1874.)

As the CZ replica suggests, the original Koh-i-Noor diamond was brilliant and a unique cut (figure 20). The curved surface seems to magnify reflection, refraction, and dispersion. If this model displays the original optical properties, then it is unfortunate that this diamond was recut.

The replica was subsequently donated to the Natural History Museum in London and is currently on display in their "The Vault" exhibit.

SUMMARY

The photographic and laser scan analysis of the plaster model of the historic Koh-i-Noor diamond shows that the original diamond had 169 facets, with

dimensions of 40.85 × 32.57 × 16.18 mm. It had a high-domed crown, flat base, and predominantly triangular and rectangular facets covering its surface, reminiscent of other Mogul-cut diamonds in the Iranian Crown Jewels. Although the scan data suggested a 204.20 ct stone, rather than the reported 191.03 ct, the authors surmise that this was due to expansion of the plaster model by 7%, either as a result of water absorption over the past 150+ years or as an artifact of the casting process.

A crystallographic analysis confirmed earlier reports that the base and largest facet are aligned with cleavage faces. A third facet was close to the index of another cleavage face, but deviated by 17°. This information also was used to determine that no intentional damage was inflicted on the original stone during any previous transfer of ownership, as suggested by earlier reports. It also showed that the Koh-i-Noor could not have been cut from the Great Mogul diamond, as the latter was too small, discounting another theory.

An analysis of the recutting of the original Koh-i-Noor to its modern version showed that the cutter was operating under tight constraints. Maximum apparent size was paramount, but this came at the expense of symmetry and brilliance. However, the cutter did a superlative job within the constraints, as a stone of larger dimensions would not have been physically possible.

Creation of a cubic zirconia replica offers the best approximation of the brilliance and optics of the original stone to date. It is the opinion of the authors that this was a magnificent example of ancient cutting technique, with optics unusual for a faceted diamond, and that something of historic value was lost when it was recut.

ABOUT THE AUTHORS
Mr. Sucher (scottsucher@museumdiamonds.com), a retired Air Force instructor pilot who has been creating replicas of famous diamonds since 1980, is the principal of The Stonecutter in Tijeras, New Mexico. Mr. Carriere is a colored gemstone faceter in Prescott, Arizona.

ACKNOWLEDGMENTS
The authors thank Alan Hart and Magdalena Witczyk (Natural History Museum, London) for their assistance in arranging the loan of the 1851 plaster replica of the Koh-i-Noor. They are also grateful to Sergey Sivovolenko (OctoNus Finland Oy, Lansi, Finland) for volunteering scanning services. Drs. Paul Van Der Steen (Matrix Diamond Technologies, Antwerp) and Alexander Sassov (SkyScan, Kontich, Belgium) coordinated the laser and X-ray scanning, respectively. Garry Holloway (Garry Holloway Diamonds, Melbourne, Australia) offered invaluable advice in using the DiamCalc 3.0 software, and Robert Strickland (GemSoft Enterprises, Austin, Texas) provided technical support with GemCad. The authors also thank Drs. Mark Yarbrough and Gaylina Reachi (ABQ Dentists, Albuquerque, New Mexico) for the loan of grinding tools to create the four cavities on the replica, and Al Gilbertson (GIA, Carlsbad) for helpful comments on the manuscript and suggestions for improvement.

REFERENCES

Attaway N. (2005) The French connection. *Lapidary Journal*, Vol. 59, No. 3, pp. 24–28.

Balfour I. (2000) *Famous Diamonds*. Christie, Manson & Woods, London.

Ball V. (1925) *Appendix to Tavernier's Travels in India, Volume II*. Oxford University Press, London.

Bari H. (2001) *Diamonds, in the Heart of the Earth, in the Heart of Stars, at the Heart of Power*. Industrie Grafiche Editoriali Musumeci S.p.A., Val d'Aosta, Italy.

Bauer M. (1968) *Precious Stones*, Vol. 1. Dover Publications, New York.

Blair C., Bury S., Grimwade A., Harding R., Jobbins E.A., King D., Scarratt K. (1998) *The Crown Jewels, the History of the Coronation Regalia in the Jewel House of the Tower of London*. Stationery Office Books, London.

Copeland L.L. (1974) *Diamonds—Famous, Notable and Unique*. Rev. by R. A. P. Gaal and J. Taylor, Gemological Institute of America, Los Angeles, CA.

Diamond teaser: Indian ire at glittering royal funeral (2002) *The Guardian*, April 27, 2002, p. 2.

Dieulafait L. (1874) *Diamonds and Precious Stones*. Scribner, Armstrong, and Co., New York.

Fritsch E. (1998) The nature of color in diamonds. In G. E. Harlow, Ed., *The Nature of Diamonds*, Cambridge University Press, Cambridge, UK, pp. 23–47.

Hatleberg J.N. An exact replica of the original Mogul cut Koh-i-Noor diamond. *Gems & Gemology*, Vol. 42, No. 3, pp. 158–159.

Mawe J. (1815) *A Treatise on Diamonds, and Precious Stones: Including Their History—Natural and Commercial*. Printed for Longman, Hurst, Rees, Orme, and Brown, London.

Meen V. (1968) *The Crown Jewels of Iran*. University of Toronto Press, Toronto.

Streeter E. (1882) *Great Diamonds of the World*. G. Bell and Sons, London.

Tavernier J. B. (1676) *Les Six Voyages de Jean Baptiste Tavernier, Ecuyer Baron d'Aubonne qu'il a fait en Turquie, en Perse, et aux Indes* [*The Six Voyages of Jean Baptiste Tavernier, Baron d' Aubonne, that he made to Turkey, Persia, and the Indies*]. Gervais Clouzier et Claude Barbin, Paris.

Tennant J. (1852) *Lecture on Gems and Precious Diamonds*. London.

Tolkowsky M. (1919) *A Study of the Reflection and Refraction of Light in a Diamond*. Spon & Chamberlain, New York.

COATED TANZANITE

Shane F. McClure and Andy H. Shen

Examination of 23 tanzanites coated by an apparently new technique revealed that the smaller stones (4–5 mm) could be identified as coated based on a combination of the unusually intense color and microscopic examination, which revealed surface iridescence as well as wear on facet junctions (small areas where the coating was abraded away). The two larger (3+ ct) stones did not show iridescence or wear, only small clues with high magnification, and therefore were much more difficult to identify. EDXRF and LA-ICP-MS analyses showed the presence of Co, Zn, Sn, and Pb in the coating.

The practice of coating gemstones to improve their color has existed for thousands of years (see, e.g., Ball, 1950; Nassau, 1984). None of these coatings is permanent, but they range in durability from being difficult to scratch with a metal point to being easily wiped off with a cleaning cloth. As a result, the treatment is impractical at best and fraudulent at worst (Overton, 2004). Last year, GIA researchers reported on the emergence of a new generation of coatings—created using technology from other industries—that are much more durable than those studied previously (Shen et al., 2007). Although we are aware that a number of companies are using this treatment on diamonds, the *Gems & Gemology* report focused on colored coatings on diamonds by a company called Serenity Technologies.

See end of article for About the Authors and Acknowledgments.
GEMS & GEMOLOGY, Vol. 44, No. 2, pp. 142–147.

While we were studying the diamond coatings, we learned that some of these same companies were also applying coatings to colored stones and pearls, as well as to various gem simulants. In many cases, the treaters maintained that the coatings were diamond-like carbon (DLC) and were being applied to improve durability (see, e.g., Serenity Technologies, 2008; Zolastar, 2008). There appeared to be some basis for these claims, since for some gem materials the addition of color either was undesirable (e.g., white pearls) or unnecessary because the stone already had plenty of color (e.g., garnet).

During our investigation of these new coating operations in 2006, we also examined a tanzanite that purportedly was coated to enhance its durability. We noted some coating material on the surface of the stone, but it covered only a very small portion of the pavilion near the girdle and could be removed with a mere cleaning cloth. Chemical analysis of the coating revealed a large concentration of cobalt (together with Zn, Sn, Ta, Ag, Au, and Pb). The client also supplied an uncoated control sample of tanzanite that was similar to the one he had coated, and there was no significant difference between the colors of the two face-up. The nonpermanence and ineffectiveness of this coating did not distinguish it from most of the coatings that have been reported in the past. (For reviews of coatings in the marketplace since the 1980s, see Kammerling et al., 1990; McClure and Smith, 2000; Overton and Shigley, 2008.)

In April of this year, however, Los Angeles colored stone dealer Evan Caplan of Omi Gems contacted us about a parcel of tanzanite his company had just received from New York. Mr. Caplan said the color did not look right, and when his company had one stone repolished, the color became significantly lighter (figure 1). This indicated the material might

be coated, so we asked Mr. Caplan if we could examine some of the stones. Initially, his company sent two 3+ ct octagonal step cuts and four 4–5 mm rounds (figure 2). Examination of the step cuts at about 10× magnification did not reveal anything obvious. Coatings are usually visible in reflected light or by looking through the table of the stone toward the pavilion in transmitted light. The features we typically look for—surface iridescence in reflected light, or gaps or worn-off areas in the coating—were not immediately evident. In fact, polishing lines were plainly visible on most of the facets.

On closer inspection at higher magnification, however, clues began to appear. Subsequently, at our request, Omi Gems sent us 18 more samples of 4–5 mm round brilliant cuts. All these samples had a depth of color that would be considered very unusual for tanzanite in such small sizes (again, see figure 2). Similar samples were supplied to the American Gem Trade Association Gem Testing Center (AGTA GTC) and American Gemological Laboratories; their observations were outlined in a press release issued on May 23 (see, e.g., "AGTA GTC. . .," 2008). Many of their findings parallel our own, but we discovered some additional identification features (McClure, 2008) and were able to more thoroughly characterize the coating material through laser ablation–inductively coupled plasma–mass spectrometry (LA-ICP-MS).

Figure 1. These two 5 mm stones were originally the same color. Repolishing of the one on the right resulted in a significant loss of color. Photo by C. D. Mengason.

MATERIALS AND METHODS

As indicated above, we examined a total of 23 coated tanzanites. Two weighed 3.01 and 3.21 ct, respectively, while the remainder were between 0.27 and 0.62 ct (4–5 mm; again, see figure 2).

All stones were examined with a gemological microscope at various magnifications and with several lighting conditions. A polarizing filter was employed to check the pleochroism of 10 stones. To test the durability of the coatings, we used a standard steel straight pin on three samples and a hardened chrome-steel knife blade on one of them.

Qualitative chemical analysis was conducted on 20 stones, table and pavilion, using a Thermo-Noran Spectrace QuanX energy-dispersive X-ray fluorescence (EDXRF) spectrometer. Quantitative chemical analysis using a Thermo X Series II ICP-MS, combined with a New Wave UP-213 laser-ablation system, was performed on three of the smaller samples: (1) one set of three spots on the girdle and a second

Figure 2. Omi Gems brought these tanzanites to the lab's attention because they suspected some form of treatment. Even the 4–5 mm stones were strongly colored. All proved to be coated, but it was very difficult to detect the coatings on the two larger tanzanites (3.01 and 3.21 ct). Photo by C. D. Mengason.

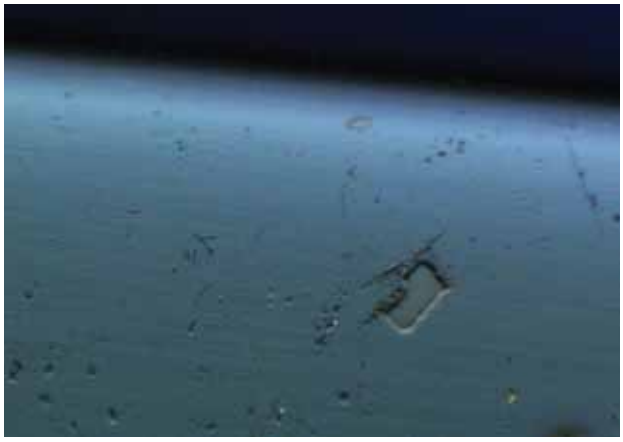

Figure 3. Examination with magnification as high as 60× and reflected light revealed numerous tiny holes in the coatings on the two 3+ ct tanzanites. Photomicrograph by S. F. McClure; image width 0.64 mm.

set on the pavilion, (2) one set of three spots on the girdle, and (3) three spots on the girdle and one spot on the table. The laser setting was 40 µm spot diameter, 10 J/cm^2 fluence, and a 7 Hz repetition rate using National Institute of Standards and Technology (NIST) 610 and 612 glasses for calibration. The laser-ablation time for each spot was 40 seconds; as the laser was ablating into the surface over this period, the signal recorded by the ICP-MS was in fact a depth profile of the material being analyzed. A chemically homogeneous material will yield a smooth and consistent signal throughout the analysis, but a thin layer of foreign material will show up in the time trace as a spike or peak in one or more of the elements being analyzed. The relative position in the time trace is a good indication of the relative position of this foreign chemical layer. If the spike in the element signal is at the beginning of the laser ablation, it is clear the layer is at the surface of the material.

Figure 4. Some facets on the larger step-cut coated tanzanites did not show any holes or breaks in the coating. They also did not show any iridescence. Photomicrograph by S. F. McClure; image width 2.48 mm.

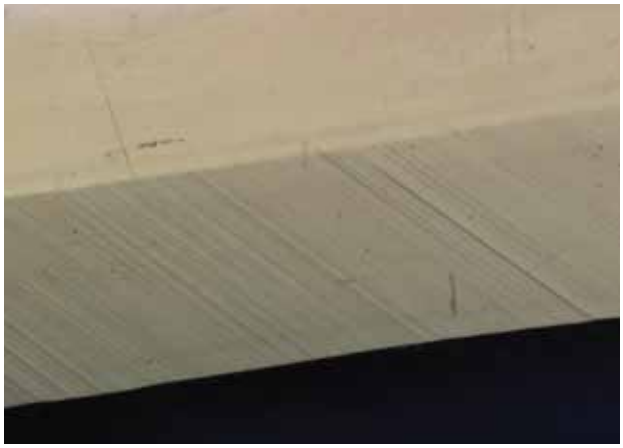

RESULTS AND DISCUSSION

Appearance. Face-up, with the unaided eye, the color of these stones—violetish blue to bluish violet—did not appear unusual for tanzanite. The one exception was the depth of color in the 4–5 mm stones (again, see figure 2). It is very uncommon to see such intense color in tanzanites this small.

Microscopic Examination. We examined the two large step cuts first. The coating on these stones was not obvious at 10× magnification. As noted above, there was no surface iridescence in reflected light and no easily visible gaps in the coating or abraded areas on the surface of the crown or pavilion. With reflected light at higher magnification (up to 60×), however, we saw numerous tiny holes in the coating on some of the facets (figure 3). These holes seemed relatively

Figure 5. Numerous whitish marks that resembled dirt (but could not be wiped off) were visible on most of the coated tanzanites with fiber-optic illumination, which also revealed orange iridescent lines crossing facet junctions on some stones (see inset). Photomicrographs by S. F. McClure; image widths 4.04 mm and (inset) 0.56 mm.

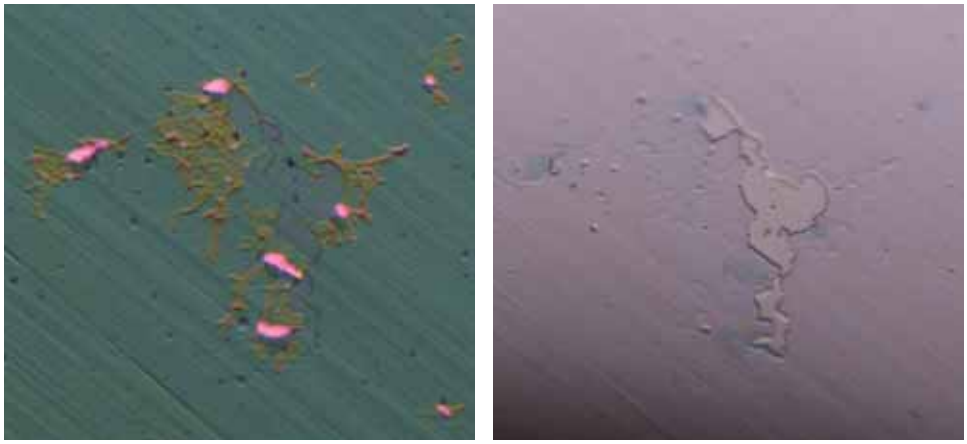

Figure 6. Tiny bright pink to orange flashes were visible on some of the coated tanzanites with fiber-optic illumination (left). These flashes are related to minute areas of damage to the coating that could be seen with transmitted light (right). Photomicrographs by S. F. McClure; image widths 0.52 mm (left) and 0.44 mm (right).

sharp-edged, and the coating looked thicker than we typically see. However, several of the facets showed no holes or other evidence of a coating (figure 4).

Fiber-optic illumination revealed whitish marks on the surface that looked like dirt but could not be wiped off (figure 5). It also revealed several orange iridescent lines that crossed facet junctions; these were similar in appearance to lines that might be left by a liquid drying on the surface (again, see figure 5). In addition, there were tiny bright pink to orange flashes of light that turned out to be related to minute areas of damage on the coating (figure 6). Although sometimes difficult to see on our coated samples, none of these surface features would be observed on an uncoated tanzanite.

The color coating Shen et al. (2007) described was present only on the pavilion of the diamonds, and a difference in luster between the coated pavilion and the uncoated crown was readily apparent. No such easily distinguishable difference was visible in these two larger coated tanzanites. Immersion in water also showed very little evidence of a coating. Tiny areas of lighter color could be seen, but they were not obvious. In general, these two larger tanzanites lacked many of the features we expect to see in coated stones, and the treatment would be particularly difficult to detect on them.

However, all the smaller samples showed some characteristics that would be associated with a coating. Examination with magnification and reflected light revealed a pale iridescence on the surface of all the smaller coated tanzanites (figure 7). In addition, the coating was worn off along some facet junctions or at the culet on all of those stones; such abrasion is typical of the "paper wear" often present on gems that are stored in stone papers as lots instead of individually (again, see figure 7). The worn facet junctions and culets were readily apparent when the tanzanites were examined with immersion in water, since they appeared lighter in color than the rest of the stone (figure 8). These features made the smaller stones easier to detect.

The 10 samples we examined using a polarizing filter showed the typical strong pleochroism that one would expect for tanzanite. This clearly indicates that these stones have some intrinsic color, if not the depth of color seen with the coating (again, see figure 1).

We were unable to scratch the coating with a pin, which is consistent with the Serenity coatings we examined earlier. However, we did scratch it without difficulty using the hardened chrome-steel knife blade.

Figure 7. All the smaller tanzanites examined for this study showed a weak iridescence in reflected light and areas along facet junctions or the culet where the coating had worn off. Photomicrograph by S. F. McClure; image width 0.66 mm.

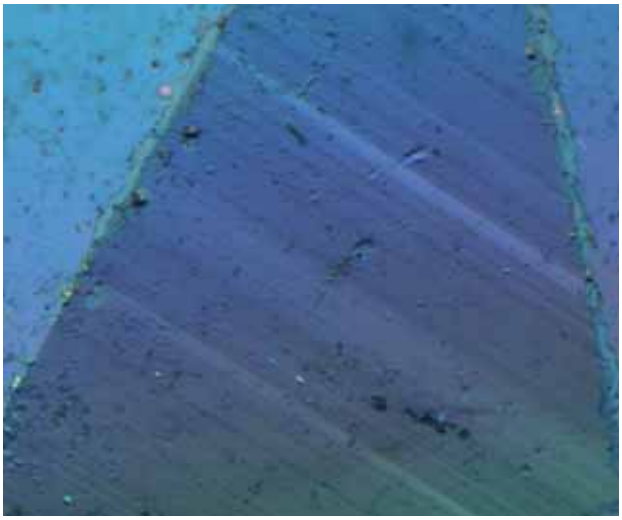

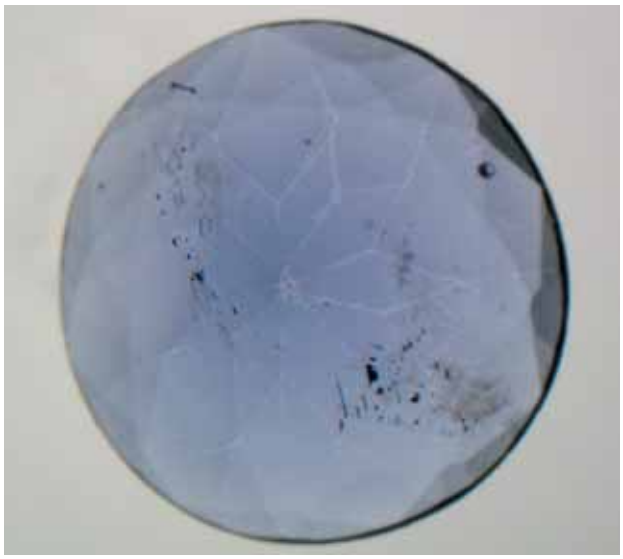

Figure 8. Abrasion of the coating at facet junctions was plainly visible when the smaller tanzanites were immersed in water over diffused transmitted light. Photomicrograph by S. F. McClure; image width 4.93 mm.

Chemical Analysis. EDXRF analysis showed cobalt as a major constituent of the coatings on all the samples we examined. This is consistent with the composition of the coating on tanzanite we documented in the laboratory in 2006 and very different from the Serenity diamond coatings we examined (i.e., no silver or gold; again, see Shen et al., 2007). In all 20 samples tested, significant amounts of cobalt were found only on the pavilion and girdle facets. The crown facets typically showed only minute amounts of cobalt, a small fraction of that recorded on the pavilion.

The LA-ICP-MS results on the girdle and pavilion were very consistent: In the time traces of Co, Zn, Sn, and Pb, all spots showed spikes in the element signals at the surface that were not seen deeper in the stone (see, e.g., figure 9 for Co; the analyses for Zn, Sn, and Pb are available in the *G&G* Data Depository at www.gia.edu/gemsandgemology). This is a clear indication that there is a surface layer on these tanzanite samples. The spot on the table showed only minute (sometimes below the detection limit of the instrument) but nearly constant concentrations of Co, Zn, Sn, and Pb (i.e., no spikes), which confirms that the coating was only on the girdle and pavilion facets of the stone. These ICP-MS results are somewhat similar to those for the tanzanite sample we examined in 2006 that was allegedly coated to improve its durability. In that sample, sharp surface spikes of Co, Zn, Sn, Ta, Ag, Au, and Pb were seen on both pavilion and girdle facets. No analysis was done on the table facet.

CONCLUSION

To summarize, the 4–5 mm tanzanites were immediately suspect because of their great depth of color, which is very uncommon for uncoated tanzanites in

Figure 9. The relative positions of peaks in these LA-ICP-MS time traces (taken from a spot on the pavilion facet) provide a good indication of a surface layer with a foreign chemical composition on this tanzanite. The horizontal axis indicates the time (in milliseconds, which translates to depth within the stone) and the vertical axis is the count rate. During the first 40 seconds, the laser is not firing and the system background level is evaluated. Because silicon (^{29}Si, the top trace) is in the chemical formula for tanzanite, it is present throughout the time period when the laser is firing. Cobalt, on the other hand (here ^{59}Co, the bottom trace), appears only as a spike at the surface of the stone and then disappears; it is not intrinsic to tanzanite and clearly is present in a very thin layer on the surface of the stone.

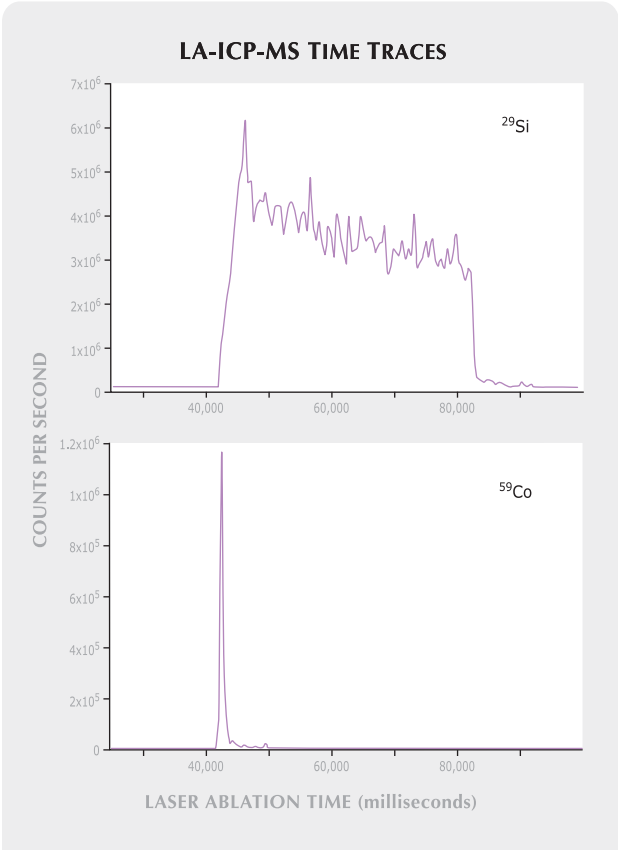

these sizes. These smaller stones also exhibited a weak iridescence as well as abrasion of the coating on the facet junctions and/or culet, probably from paper wear, which makes the coating somewhat easier to detect (provided the gems are stored in this fashion). However, larger stones that are likely to be stored individually may not show these features, and we know that at least some do not show iridescence in reflected light. Detection of a coating on these larger stones requires careful observation with a gemological microscope or, where available, chemical analysis. One might think the pleochroism, which is so strong in tanzanite, would give a useful clue to the coated nature of these stones. In this case, though, because the starting material already possessed some color, pleochroism was not helpful.

It is important to emphasize that these coated tanzanites were sold undisclosed on the market in New York. We do not know at this time how far down the pipeline they passed from the treater, or who originally decided to sell them without disclosing the treatment, but unfortunately it is inevitable that this will happen at some level. As with all treatments that have a substantial effect on value, this coating must be disclosed when present. In addition, sales of gems with nonpermanent treatments such as coatings must include instructions on any special care necessary to prevent damage; failure to do so in the United States is a violation of the guidelines set out by the Federal Trade Commission.

It is also clear that we are witnessing a new era of coatings on gemstones, which are both much more durable and much more difficult to detect. It is very possible—no, likely—that this treatment will be applied commercially to other gem materials. Gemologists must be more vigilant in their search for coatings than ever before. In the case of tanzanites in particular, every stone—regardless of size—should be checked carefully (keeping in mind that the coating may appear on only part of the stone) with a gemological microscope or sent to a well-equipped laboratory for advanced testing.

ABOUT THE AUTHORS

Mr. McClure (smcclure@gia.edu) is director of Identification Services, and Dr. Shen is a research scientist, at the GIA Laboratory in Carlsbad, California.

ACKNOWLEDGMENTS

The authors thank Karen Chadwick, staff gemologist at the GIA Laboratory in Carlsbad, for performing the EDXRF analyses.

REFERENCES

AGTA GTC and AGL identify coated tanzanite (2008) Press release, May 23, www.agta-gtc.org/coated-tanzanite.htm.

Ball S.H. (1950) *A Roman Book of Precious Stones*. Gemological Institute of America, Los Angeles.

Kammerling R.C., Koivula J.I., Kane R.E. (1990) Gemstone enhancement and detection in the 1980s. *Gems & Gemology*, Vol. 26, No. 1, pp. 32–49.

McClure S.F. (2008) From GIA Research: Large coated tanzanites lack typical identifying features. *GIA Insider*, Vol. 10, No. 10, June 6, http://app.e2ma.net/campaign/35e913c2819a961cf9503f041f293eb6#article2.

McClure S.F., Smith C.P. (2000) Gemstone enhancement and detection in the 1990s. *Gems & Gemology*, Vol. 36, No. 4, pp. 336–359.

Nassau K. (1984) The early history of gemstone treatments. *Gems & Gemology*, Vol. 20, No. 1, pp. 22–33.

Overton T.W. (2004) Gem treatment disclosure and U.S. law. *Gems & Gemology*, Vol. 40, No. 2, pp. 106–127.

Overton T.W., Shigley J.E. (2008) A history of diamond treatments. *Gems & Gemology*, Vol. 44, No. 1, pp. 32–55.

Serenity Technologies (2008) Gem enhancement—vibrant living color. www.serenitytechnology.com/gemstoneenhancement.htm [date accessed: 06/25/08].

Shen A.H., Wang W., Hall M.S., Novak S., McClure S.F., Shigley J.E., Moses T.M. (2007) Serenity coated colored diamonds: Detection and durability. *Gems & Gemology*, Vol. 43, No. 1, pp. 16–34.

Zolastar (2008) University letter. www.zolastar.com/technical-data/university-letter [date accessed: 06/25/08].

COLORING OF TOPAZ BY COATING AND DIFFUSION PROCESSES: AN X-RAY PHOTOEMISSION STUDY OF WHAT HAPPENS BENEATH THE SURFACE

Harald Gabasch, Frederik Klauser, Erminald Bertel, and Thomas Rauch

Surface-treated topaz has become a viable alternative to topaz colored by irradiation. Unlike irradiation, which modifies the entire gemstone, coloration by chemical modification is limited to the near-surface region. The treatment techniques are well established, but less is known about how the processes involved create the desired appearance. In this study, X-ray photoemission spectroscopy in combination with sputter depth profiling proved successful in characterizing two fundamentally different coloration mechanisms of chemically treated topaz: colored coatings and diffusion-induced coloration.

Topaz [$Al_2SiO_4(F,OH)_2$] occurs as an accessory mineral in some granites and associated hydrothermally altered rocks, as well as in pegmatites, rhyolites, and other aluminous rocks. The crystallographic, optical, and chemical properties of topaz can vary with chemical composition, which reflects the petrogenesis of the rocks in which the individual crystal formed (Christiansen et al., 1983). However, most topaz is colorless as mined, so it is often color enhanced for use in jewelry.

See end of article for About the Authors and Acknowledgments.
GEMS & GEMOLOGY, Vol. 44, No. 2, pp. 148–154.

One common method used to produce color centers in topaz consists of irradiating the gem with gamma rays, neutrons, or electrons, followed by low-temperature annealing (Nassau et al., 1978, 1985). Unfortunately, this procedure may induce radioactivity, thus requiring that the gems be stored safely until their activity has decayed below the legal limits. In some cases, depending on the procedure and the nature of the starting material, the decay process requires more than a year of storage, a costly delay for the owner of the topaz. In other cases, material has been released into the market prematurely (see, e.g., Ashbaugh and Shigley, 1993). Although no health impairments arising from treated gems with radioactivity below the legal limit have been reported, government, industry, and consumer groups alike are concerned about the potential risk should radioactive topaz inadvertently enter the gem market (see, e.g., Yonick, 2007; Kremkow, 2008).

In response to these concerns, two color enhancement processes that do not involve irradiation have been successfully developed. One is a coating, and the other is a diffusion-driven layer near the surface of the host gem. The main difference between these two treatments, as will be explained in more detail in the following sections, lies in the interaction of the added elements with the gemstone's surface.

While both of these techniques are well established and detailed descriptions of the procedures involved are available (Starcke et al., 1996; Pollack, 1997), less is known about the atomic-scale processes that occur during the color treatment. This article focuses on the principal mechanisms giving rise to

Figure 1. These three color-treated topazes were analyzed for this study: coated pink (left), diffusion-treated "Summer Blue" (middle), and diffusion-treated "Ice Blue" (right). All stones weigh 0.42 ct; photos by Tiroler Repro Druck.

coloration in topaz treated by these techniques. Not only is this information important from a scientific standpoint, but it may also help predict some relevant gemological properties.

For coated stones, the chemical and thermal durability of the color is determined by the composition of the coating and is independent of the substrate. Therefore, besides imparting color to a gem, the coating may also act as a protective layer. However, as with all coated gemstones, the differences in the physical properties between the stone and the color layer are also responsible for the main drawbacks of this technique. The difference in the thermal expansion coefficient may lead to severe stress at the interface when the gem is exposed to rapid temperature changes, so the coating could delaminate. Furthermore, the abrupt change in optical density (i.e., refractive index) between the coating and the gem causes angle-dependent interference effects in the wavelength of visible light (400–700 nm), which may give the gem an artificial appearance.

For diffusion-treated gems, the color treatment is more stable. Although the surface region is modified by the introduced ions, the relevant properties more closely resemble those of the topaz. Heat-induced stress or interference effects are no longer significant. The gem is unlikely to delaminate and has a more normal appearance to the unaided eye.

BACKGROUND

Coloration of some gemstones can be achieved without irradiation by introducing transition metal ions into the crystal lattice (see, e.g., Nassau, 1978). The resulting color (see, e.g., figure 1) is not only a function of the element(s) introduced, but it also depends very strongly on the valence state of that element and the symmetry of the neighboring host atoms, as well as on the chemical composition of the topaz (Nassau, 1978).

As noted above, two possibilities are available for coloring a gemstone with transition metals. In the coating process (figure 2, left), a thin film is deposited on the surface of the gem and has a well-defined interface of only a few nanometers thickness, which is much less than the wavelength of visible light. Chemical reactions as well as atomic exchange between the coating and the gem's surface, which are responsible for adhesion, are limited to this narrow interface. Therefore, the color effect produced by the coating arises solely from the coating itself; it is independent of the substrate's composition. The same coating would lead to the same color, whether the colorless substrate was topaz or any other material.

In the diffusion-driven process (figure 2, right), the coloring agent permeates the gem's surface. This may be accomplished either by depositing a precursor material on the surface or by embedding the stone in the desired matrix (Pollack, 1997), followed by heat treatment. As a result, various components migrate into deeper atomic layers and the elemental composition of the surface changes. This diffusion process results in substantial broadening of the interface. In fact, depending on the process parameters, it might be difficult to identify the interface. Instead, a complicated and sometimes oscillatory concentration gradient is established from the surface into the body of the gem. The material placed on the gem's surface (in the case of topaz, e.g., cobalt, chromium, or copper) does not in and of itself produce the resulting color; rather, it interacts with the chemical components of the host gem to produce the desired color.

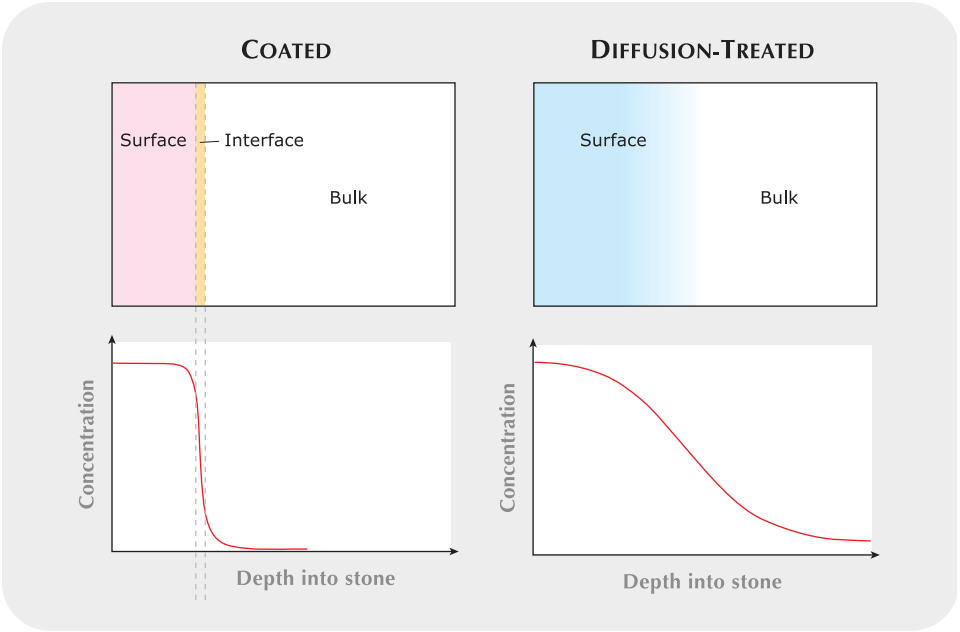

Figure 2. The diagram on the left represents a concentration profile typical of a coated stone, whereas the figure at right resembles that for a diffusion-treated gem. In both diagrams, the left side represents the gem's surface and the horizontal axis represents the depth into the stone.

MATERIALS AND METHODS

To investigate whether these two different procedures can be discriminated in commercially available gemstones, we analyzed three color-treated princess-cut examples, each weighing 0.42 ct, by X-ray photoelectron spectroscopy (XPS; see box A): a pink topaz, a "Summer Blue" topaz, and an "Ice Blue" topaz (again, see figure 1). All three gemstones were originally colorless and were selected as representative of each of these categories in the product line of D. Swarovski & Co.

The color of the pink treated topaz was achieved through the embedding of gold into SiO_2. The color of the Summer Blue topaz was achieved by exposing a colorless topaz to a cobalt-containing environment (cobalt oxide powder) accompanied by annealing under well-defined conditions at around 1000°C for more than three hours (Pollack, 1997). These same procedures were used to treat the Ice Blue topaz, with the addition of chromium.

XPS allows a detailed, quantitative analysis of elemental composition on and just below the surface of a gem. Compared to commonly used analytical techniques such as energy-dispersive X-ray (EDX) spectroscopy, XPS has the advantage of extreme surface sensitivity (providing information to a depth of up to 5 nm, compared to 1 µm for EDX) and the capability of reporting the concentration of elements down to 0.1 at.% (Hofland, 1998). When combined with argon ion etching, the surface sensitivity of XPS can create concentration profiles with high depth resolution.

XPS not only detects the concentration of elements, but it can also monitor changes in valence state (e.g., the oxidation state as a function of depth). In addition, it lacks undesirable matrix effects such as those encountered with SIMS (secondary ion mass spectrometry; Watts and Wolstenholme, 2003). Since the chemical state of the coloring elements (i.e., the exact oxidation state and the phases present after treatment) is not well known, quantification and therefore a subsequent analysis by SIMS or similar techniques is very difficult.

All XPS measurements were conducted at the Institute of Physical Chemistry at the University of Innsbruck with a Thermo Electron Corp. MultiLab 2000 XPS probe that features a double-focusing hemispherical electron energy analyzer with an electrostatic entrance lens. Depth profiling was conducted using a scanning argon ion sputter gun.

The analyses were done under ultra-high vacuum at a background pressure of 1×10^{-9} mbar. The specimens were first cleaned in an ultrasonic bath of acetone and water before they were introduced into the instrument. Survey spectra monitoring all elements present were taken initially and then after every sputter erosion cycle, to determine the actual surface composition and to avoid artifacts caused by impurities. The sputter spot size was 1×1 mm^2, whereas the focused spot size of the analyzing X-ray beam was kept below 0.4×0.4 mm^2. Ten scans per cycle were made to improve the signal-to-noise ratio.

Two additional samples of each color variety of treated topaz were analyzed with the same instru-

BOX A: XPS ANALYSIS

X-ray photoelectron spectroscopy is a very powerful surface science tool for investigating the composition of various solids. In gemology, it can be used in a variety of applications, such as investigating the origin of heat-induced color changes in rubies (Achiwawanich et al., 2006). A complete system costs approximately US$550,000.

In XPS, the sample is irradiated with X-rays of energy, hν, which are produced in an X-ray tube (Hofland, 1998). The X-rays are absorbed in an atom (e.g., atom A in figure A-1) and transfer their energy to a core electron. The core electron then has enough energy to overcome the binding energy, E_{bind}, and leaves the solid with a kinetic energy of $E_{kin} = h\nu - E_{bind}$. The kinetic energy, E_{kin}, is determined by an energy analyzer. Using the known X-ray energy, hν, and the determined kinetic energy, the binding energy can be calculated. The binding energy is specific to each element in the periodic table (compare magnitudes of the different binding energies between atoms A and B in figure A-1). Therefore, the observation of electrons at specific energies indicates the presence of the associated element in the sample. The number of such electrons detected is proportional to the concentration of the element within the probing depth.

The probing depth is limited by the mean free path of the ejected electrons in the sample (i.e., the average distance that electrons can travel before they get scattered and do not reach the analyzer). This distance is typically ~5 nm or less. Hence the technique is very surface sensitive. To obtain a concentration profile as a function of depth into the sample, one has to combine this technique with argon ion etching. Here the surface is eroded (sputtered) layer by layer using an ion beam with typical energies of 1–5 keV. The rate of erosion can be calibrated for topaz using films of known thickness, and spectra recorded after predetermined time intervals yield the element concentrations at the respective sputter depth.

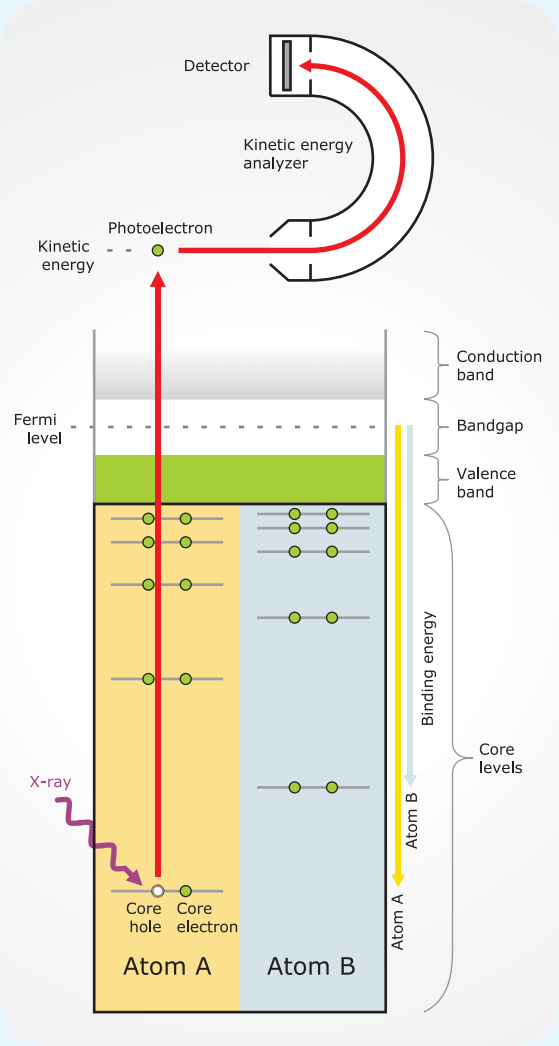

Figure A-1. In XPS, the X-ray photons are absorbed by an atom in a molecule or solid, leading to the emission of core (inner shell) electrons (green circles). The kinetic energy of the ejected electron (photoelectron) is characteristic for each element and detected by the energy analyzer.

ment using procedures that yield less accurate results (i.e., longer ablation time between analysis points) to evaluate the reproducibility of the measurements. To minimize edge effects and sputter-induced mixing, we scanned the ion beam over the analyzed area, thus eroding the sample almost layer by layer. After predetermined erosion periods (approximately one hour per cycle), we recorded the XPS spectra and monitored the change in chemical composition as a function of eroded depth. The sputter efficiency was calibrated using sputter targets of similar material (Al_2O_3 and SiO_2) and known thickness, so that the

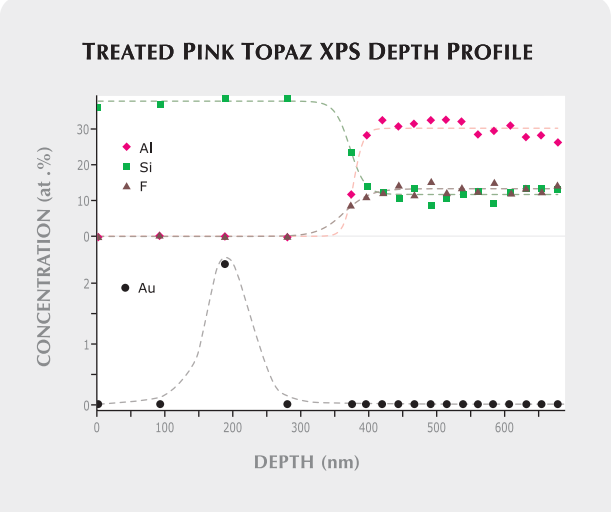

Figure 3. The distribution of elements in the pink treated topaz as a function of sputter depth is shown. The elements of the topaz lattice are plotted in the top graph, while the color-causing element, gold, is plotted in the lower diagram. The chemical patterns are consistent with a coated stone, and a comparatively sharp step in the individual components can be seen.

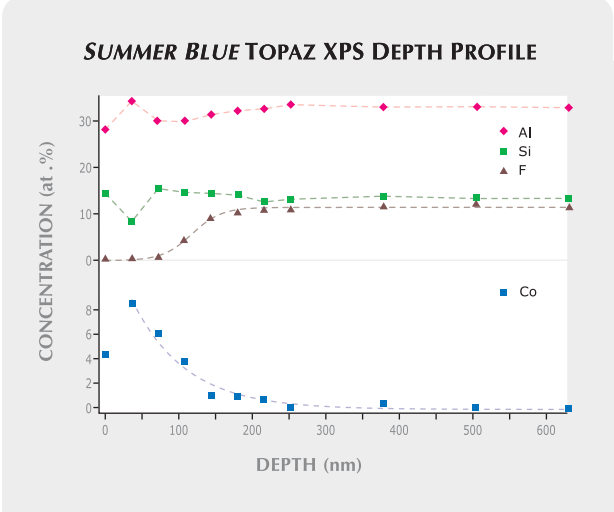

Figure 4. The lower graph in this elemental depth profile of the "Summer Blue" topaz shows the distribution of the color-causing component, Co. The trends in the graph follow the pattern expected for a diffusion-treated stone; no sharp step in the concentrations can be detected.

erosion time could be converted into a depth scale. Although the calibration has an estimated uncertainty of about 20%, the reproducibility of the experiments was excellent.

RESULTS AND DISCUSSION

Pink Coated Topaz. For the pink sample (figure 3), only SiO_2 was detected in the outermost surface region. At a depth of approximately 200 nm, a sharp gold component joined the Si signal in the spectrum, but it vanished after the next sputter cycle (280 nm). At approximately 350 nm, the composition changed dramatically: The Si signal decreased, Al became dominant, and fluorine rose from zero to 12 at.%.

From about 400 nm onwards, the composition remained constant—resembling that of pure colorless topaz. Within the limits of our experimental accuracy, we can state that no interdiffusion took place between the gold-bearing SiO_2 layer (present at a depth of ~200 nm) and the topaz (the component belonging to the topaz first appeared at 350 nm). The XPS signal of the gold did not overlap with any of the bulk components (Al, F), and we detected no significant diffusion of Al into the SiO_2 layer.

This treated stone showed no evidence of appreciable diffusion apart from the defined interface, which is limited to depths between 350 and 400 nm. This finding was supported by the angle-dependent reflection that was readily apparent when the stone was examined with the unaided eye; this results from the interference of the light with the coating.

"Summer Blue" Diffused Topaz. If there is no interdiffusion of the various elements, as we observed in the pink coated topaz, then one would expect a surface covered predominantly by "olive" green cobalt oxide or metallic cobalt in the Summer Blue topaz, depending on the oxidizing or reducing atmosphere in which it was annealed (Pollack, 1997). In addition, all the elements intrinsic to the topaz (Al, Si, F) should only be detectable once this surface layer has been eroded. However, the Summer Blue topaz revealed a completely different elemental distribution (see figure 4).

Unlike the coating on the pink treated topaz, the near-surface region (0–70 nm) of this blue treated topaz exhibited an alternating enrichment in Si and Al. Due to thermodynamic considerations, the surface tends to maximize its stability, so that a thin layer of the most stable components forms there. In the present case, this was a Si-rich layer. Therefore, the layer immediately beneath the surface was somewhat depleted of Si and exhibited a corresponding enrichment of Al and Co. In this sample, Co reached a concentration of about 8 at.%. This composition

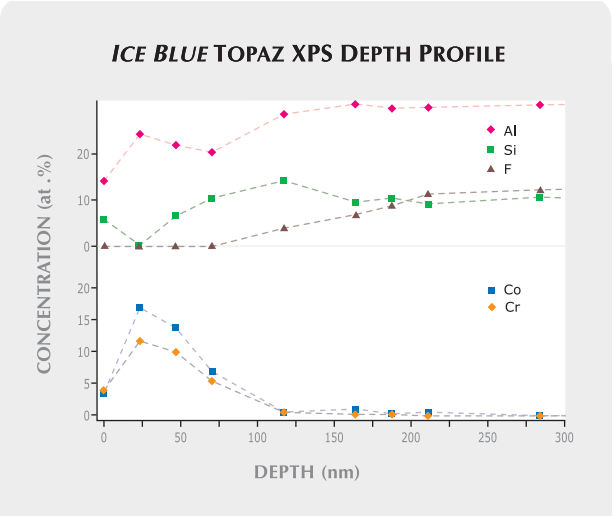

Figure 5. The elemental depth profile of the "Ice Blue" topaz reveals chemical trends that are consistent with coloration caused by diffusion of Co and Cr into the topaz.

prevailed to a depth of about 80 nm.

From depths of ~80 to ~200 nm, the Co concentration decreased exponentially (which is characteristic of diffusion profiles according to Fick's law; Kittel, 2005), while the Al and Si concentrations approached those present in the bulk of the gemstone. F showed a steady, continuous rise in concentration throughout this depth region. As previously observed (Marques et al., 2002), fluorine is very sensitive to the destabilization of the crystal lattice, and can become volatile above 600°C if the crystal lattice is damaged; these temperatures were reached during the annealing step.

Therefore, F may be used as a tracer element indicative of the topaz bulk. Figure 4 shows a broad transition region where Co and F were detected simultaneously; measurable amounts of Co are visible in the spectra down to a depth of 380 nm. No sharp step in the concentration profile was observed in this treated topaz.

From these observations, we conclude that cobalt diffusion into the topaz is a prerequisite for the desired coloration. We did not detect any concentration threshold that would allow us to identify an interface between the surface coating and the gemstone. These findings are further supported by the optical properties of the stone. No interference effects were observed; the reflectance resembles that of natural topaz, indicating the lack of a well-defined phase boundary such as was observed in the pink treated topaz.

"Ice Blue" Diffused Topaz. For the Ice Blue topaz, we observed a concentration profile (figure 5) that was slightly different from that of the Summer Blue sample, probably due to the addition of chromium. Although the outermost layer down to ~50 nm depth also exhibited an oscillatory concentration profile with Si enrichment at the surface, just below the surface the Si concentration decreased below the detection limit. Cobalt and chromium reached their maximum in this strongly Al-enriched region at 10–50 nm depth. However, unlike the chemical profile of the Summer Blue topaz, the concentration of F remained low until the Co and Cr levels had fallen to ~5 at.%, at about 80 nm depth. Only then did the fluorine concentration start to rise. After another ~40 nm, the Si and Al concentrations were close to those in the bulk of the topaz, but still varied slightly. The F signal attained its bulk value at 200 nm depth.

Because the Ice Blue topaz was treated in a procedure similar to that patented by Pollack (1997), we know that Al and Si were not components of the initial coloring agent. In a process similar to that observed with the Summer Blue topaz, Co and Cr likely diffuse into the gemstone and form a colored near-surface layer. We observed, however, a few significant differences. Co and Cr interdiffuse massively with the alumina component of the topaz, reaching a combined concentration maximum of almost 30 at.% at a depth of ~20 nm. Si and F were not present in this range. These findings suggest the formation of a new phase—one that may not be present in the Summer Blue topaz. The phase transformation could perhaps preclude F from incorporation into the newly formed phase or lead to a complete release of the fluorine into the atmosphere. The phase transformation leads to a Co-, Cr-, and Al-rich phase, perhaps a Co-Cr-aluminate spinel phase, which incorporates the transition metal into the lattice, thus preventing their further diffusion into the topaz.

In a sense, the new phase could be considered a coating on the topaz. However, the coating phase is produced by strong diffusion and is probably followed by a chemical reaction establishing a new phase in the near-surface region. Furthermore, although the decay of the Co and Cr concentrations creates a region that may be considered an interface, this interface is much broader than that observed in a typical coating process, as can be seen from comparison with the pink coated topaz. Additionally, traces of the transition metals are still present in

deeper regions (200 nm). Thus we classify the color treatment of the Ice Blue topaz as a diffusion-induced process probably accompanied by phase transformation in the near-surface region.

This model is in good agreement with the empirical observations of the stone's appearance. Although the thickness of the color-bearing layer is in the range of the visible-light wavelength, no angle-dependent interference effects were observed, indicating the lack of a sharp change in refractive index.

SUMMARY AND CONCLUSION

Three color-treated (without irradiation) topazes from the product line of D. Swarovski & Co. were examined by XPS to determine the concentration profile of the colored surface. The resulting spectra revealed the mechanisms involved in the formation of the coating or layers responsible for the desired color. In the case of the pink treated topaz, a defined color layer with a sharp interface was detected. No evidence of any significant interaction between the gemstone and the gold-bearing SiO_2 surface layer was found. Color layers such as this can therefore be described as a coating.

The blue colors of treated topaz behaved differently. A considerable alteration of the outer surface of the topaz was detected. In the Summer Blue topaz, a diffusion profile of the cobalt into the topaz was clearly visible and no sharp interfaces were present. The situation becomes more complex when chromium is combined with cobalt in the surface treatment, as for the Ice Blue topaz. A stronger interdiffusion between the bulk elements (Si, Al) and the transition metals was observed.

The XPS results are in good agreement with some optical observations of the analyzed gemstones. As mentioned in the introduction, a sharp change in refractive index on a nanometer scale could cause interference effects. Indeed, the pink coated topaz showed such effects, in contrast to the blue diffusion-treated ones.

Additionally, we have shown that XPS analysis is an appropriate tool to investigate the mechanisms taking place near the surface during the coloration process. Simpler tests, such as etching the surface by hydrofluoric acid (Befi et al., 2006), may give a rough estimate of the thickness of the colored layer. However, such techniques (which are also destructive) cannot be used to establish whether diffusion of the various elements is occurring.

ABOUT THE AUTHORS

Dr. Gabasch and Mr. Rauch are research scientists at D. Swarovski & Co. in Wattens, Austria. Mr. Klauser is a PhD candidate and Dr. Bertel is a professor and head of the Institute of Physical Chemistry, University of Innsbruck, Austria.

ACKNOWLEDGMENTS

The authors would like to thank Signity AG of Horgen, Switzerland, for the samples analyzed and Dr. Michael Schlamadinger of D. Swarovski & Co. for fruitful discussions.

REFERENCES

Achiwawanich S., Brack N., James B.D., Liesegang J. (2006) Surface analysis of heat-treated Mong Hsu rubies. *Applied Surface Science*, Vol. 252, pp. 8646–8650.

Ashbaugh C.E., Shigley J.E. (1993) Reactor-irradiated green topaz. *Gems & Gemology*, Vol. 29, No. 2, pp. 116–121.

Befi R., Kiefert L., Htut M. (2006) Coated topaz. *Gems & Gemology*, Vol. 42, No. 3, pp. 128–129.

Christiansen E.H., Burt D.M., Sheridan M.F., Wilson R.T. (1983) The petrogenesis of topaz rhyolites from the western United States. *Contributions to Mineralogy and Petrology*, Vol. 83, pp. 16–30.

Hofland G. B. (1998) Spectroscopic techniques: X-ray photoelectron spectroscopy, auger electron spectroscopy, and ion scattering spectroscopy. In J. C. Rivière and S. Myhra, Eds., *Handbook of Surface and Interface Analysis*, Marcel Dekker, New York, pp. 57–151.

Kittel C. (2005) *Introduction to Solid State Physics*, 8th ed. John Wiley & Sons, New York, 588 pp.

Kremkow C. (2008) Kimberley process for blue topaz? *Modern Jeweler*, Vol. 107, No. 3, pp. 16, 18.

Marques C., Falcão A., da Silva R.C., Alves E. (2002) Structural and optical characterization of topaz implanted with Fe and Co. *Nuclear Instruments and Methods in Physics Research B*, Vol. 191, pp. 312–316.

Nassau K. (1978) The origins of colors in minerals. *American Mineralogist*, Vol. 63, pp. 219–229.

Nassau K. (1985) Altering the color of topaz. *Gems & Gemology*, Vol. 21, No. 1, pp. 26–34.

Pollack R. (1997) Method for enhancing the color of minerals useful as gemstones. U.S. Patent No. 5,888,918.

Starcke S.F., Kearnes R.H., Bennet K.E., Edmonson D.A. (1996) Method of improving the color of transparent materials. U.S. Patent No. US5853826.

Watts J.F., Wolstenholme J. (2003) *An Introduction to Surface Analysis by XPS and AES*. Wiley Publishing, New York.

Yonick D.A. (2007) A blue Christmas? Industry awaits word from NRC. *MJSA Journal*, Vol. 30, No. 46, pp. 24–25.

LAB NOTES 2008

EDITORS
Thomas M. Moses and
Shane F. McClure
GIA Laboratory

DIAMOND

With Color Contributed by the 594 nm Center?

The 594 nm center is commonly observed in the absorption spectra of irradiated and annealed diamonds and also is detected occasionally in some naturally colored diamonds (see, e.g., T. W. Overton and J. E. Shigley, "A history of diamond treatments," Spring 2008 *Gems & Gemology*, pp. 32–55). Its occurrence is widely used as an identification feature for colored diamonds; however, its contribution to the bodycolor of a diamond is not well recognized. Recently, in the New York laboratory, we examined a diamond with a strong orange color that was believed to be partially caused by the 594 nm absorption.

This 0.90 ct marquise-cut stone (9.12 × 5.19 × 3.43 mm) was color graded Fancy Deep brownish yellowish orange (figure 1). With magnification, the color distribution appeared very slightly patchy, but we saw no other internal features (the clarity grade was VVS_2). When exposed to long-wave ultraviolet (UV) radiation, it displayed a moderately strong green fluorescence, with a weak yellow reaction to short-wave UV; no phosphorescence was observed. The DiamondView instrument revealed blue and greenish yellow fluorescing growth zones.

Figure 1. The deep orange color of this 0.90 ct treated diamond was likely influenced by a very strong 594 nm absorption.

Figure 2. The 594 nm absorption center, seen here in the Vis-NIR spectrum of the diamond in figure 1, is a common result of irradiation and annealing treatment. The very strong absorption in this diamond is likely a significant contributor to the orange bodycolor.

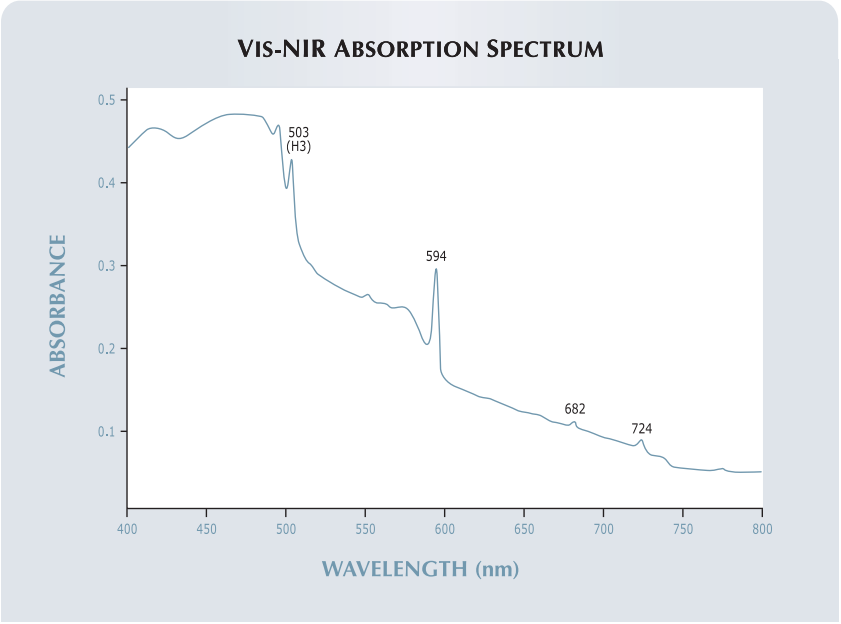

The absorption spectrum in the mid-infrared (IR) region revealed that this diamond contained a high concentration of nitrogen, as is typical of a type Ia stone. Moderately strong H1a, H1b, and H1c absorptions were also observed. The Vis-NIR spectrum showed a gradual increase in absorption toward the blue end of the spectrum (figure 2). In addition to weak N3 (415 nm) and very strong H3 (503 nm) absorptions, moderately strong absorptions were also observed at 682 and 724 nm. An outstanding feature was the extremely strong absorption at 594 nm and its possible side band at ~575 nm. All of these spectral features established that the color of this diamond was the result of irradiation and subsequent annealing.

The intensity of the 594 nm absorption is normally far less than that of the N3 or H3. This stone's strong selective absorption in the 550–600 nm region efficiently blocked yellow and some green light, making it very likely that the 594 nm absorption contributed significantly to the observed orange color. It is very rare to encounter a colored diamond in which the bodycolor has been influenced by this defect.

Wuyi Wang

Subtle Flash-Effect Colors in a Filled Diamond

Glass filling is often easily observed due to obvious flash-effect colors in a large feather or feathers. In some diamonds, though, the effect is not so easy to detect.

Earlier this year, a 5.01 ct pear-shaped brilliant was submitted to the New York laboratory for a full grading report. A few large feathers were noted, but none exhibited any flash-effect colors. However, closer scrutiny through the pavilion of the diamond revealed a small feather that had very subtle blue and pale purple colors (figure 3). Only one other small feather exhibited similar colors.

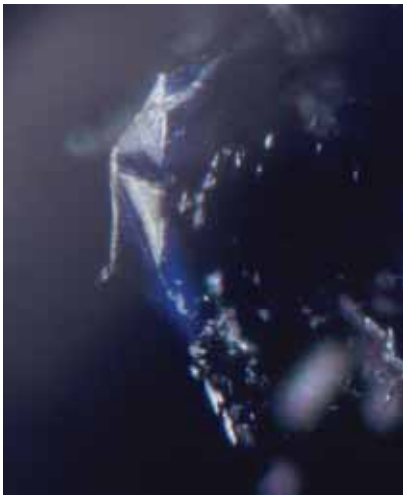

Figure 3. These subtle blue and pale purple flash-effect colors are indications that this diamond has been glass filled. Magnified 60×.

When a grader observes what is thought to be potential glass filling, the diamond is sent to the Gem Identification Department for further testing. Fractures that exhibit flash-effect colors are tested for the presence of lead, a major component of the filling material. This stone was tested by energy-dispersive X-ray fluorescence (EDXRF) spectroscopy, which confirmed the presence of lead.

It is GIA's policy not to grade diamonds treated by glass filling, even when only a small amount is noted.

Vincent Cracco and Paul Johnson

"Unidentified Clarity Characteristic" in Diamond

Professional diamond graders are taught to classify internal characteristics in diamonds using such dry descriptive terms as *crystal*, *pinpoint*, and *feather*. Due to time constraints, solid inclusions are rarely fully identified unless it is necessary for scientific reasons. Depending on their size, solids are generally described as either *pinpoints* or *crystals* for the purpose of assigning clarity grades. That said, from time to time we have reported on features in diamonds that captured our imaginations because they resembled familiar objects from our daily lives (e.g., Winter 2007 Lab Notes, pp. 363–364).

Occasionally, brightly colored mineral inclusions such as red and orange garnets and green diopside crystals will catch a diamond grader's attention simply because of their intense hues. More commonly, however, solid inclusions are essentially transparent and colorless, or opaque and black, and thus command little interest beyond their impact on the clarity grade.

Since diamond is composed of carbon, it stands to reason that one of the most commonly encountered dark inclusions in diamond is graphite, the hexagonal polymorph of carbon. True "carbon spots," most graphite inclusions appear as nondescript smudges in cleavage cracks or within the gaps between solid inclusions and the host diamond. Typically, these are considered undesirable features; occasionally, however, even opaque black graphite can create an interesting internal scene that captures the viewer's imagination.

One example of this was a tiny hexagonal platelet that appeared to be graphite, although it could not be analyzed because of its depth in the diamond. The platelet had formed aligned along an octahedral plane as graphite hexagons in diamonds commonly do, and it was skirted by a small cleavage disk caused by the expansion strain that occurred when the diamond in this spot was converted to graphite. Normally, graphite platelets are so thin as to be virtually invisible when viewed edge-on, but this particular inclusion had a very distinct depth to it, as it was made up of a stack of graphite plates of different diameters (figure 4). This assemblage caused it to resemble a tiny "flying saucer" of the type seen in 1950s science fiction movies. The fact that it was so small it appeared grainy even with the sharpest possible focus also enhanced the imagery. While diamond grading can

Editors' note: All items are written by staff members of the GIA Laboratory.

GEMS & GEMOLOGY, *Vol. 44, No. 2, pp. 156–163.*

Figure 4. Aligned along an octahedral plane in its diamond host, and measuring only 0.36 mm across, this minute crystal formation (probably graphite) is reminiscent of the "flying saucers" often featured in early science fiction movies and grainy photos purported to be of such phenomena.

become routine, inclusions are occasionally fun, and this "unidentified clarity characteristic" provides an excellent example of an inclusion that stimulates the imagination.

John I. Koivula and Karla F. Onstott

Gem-quality CVD SYNTHETIC DIAMOND with Traces of Boron

Several years after it was first announced, gem-quality chemical vapor deposition (CVD)-grown synthetic diamond is still encountered only rarely among the stones submitted for a GIA diamond report (e.g., Spring 2008 Lab Notes, pp. 67–69). Recently, a brown round cut submitted to the New York laboratory was identified as a CVD synthetic diamond with some unusual spectroscopic features.

This 1.25 ct sample (6.82 × 6.97 × 4.20 mm) was color graded Fancy brown (figure 5). It showed very slightly patchy color distribution and strong graining with magnification. Several fractures were present along the girdle region. It fluoresced very weak yellow to long-wave UV radiation and weak orange to short-wave UV; no phosphorescence was observed. The DiamondView reaction was dominated by moderately strong orangy red fluorescence with a notable irregular blue region (figure 6); a moderately strong blue phosphorescence was also observed. These luminescence features are typical for CVD-grown diamonds (see W. Wang et al., "Latest-generation CVD-grown synthetic diamonds from Apollo Diamond Inc.," Winter 2007 *Gems & Gemology*, pp. 294–312).

The infrared absorption spectrum revealed that this diamond contained no detectable nitrogen, which is not unexpected for CVD synthetic diamonds (most of which are nominally type IIa), but we did observe weak absorptions at 2925 and 2800 cm^{-1} from trace amounts of boron. This is the first type IIb CVD diamond we have identified in the lab. Unlike the latest CVD-grown diamonds from Apollo Diamond with strong brown color (again, see Wang et al., 2007), this synthetic diamond showed no absorption in the 1500–1300 cm^{-1} region. We did observe weak absorptions at 7353, 6856, 6425, and 5564 cm^{-1} in the near-infrared region. The Vis-NIR spectrum, collected at liquid-nitrogen temperature, showed a gradual increase in absorption toward the low-wavelength side (figure 7). In addition to a very strong absorption from the Si-V defect (737.0 nm)—an outstanding feature of this diamond—a weak peak at 596.5 nm and a broad band centered at ~520 nm were also observed. The assignment of these peaks is not clear, but it is obvious that the trace boron in this diamond does not contribute much to the bodycolor of this stone. Si-V is a common defect in CVD synthetic diamond; however, its concentration is usually extremely low and only rarely can it be detected with absorption spectroscopy. The photoluminescence spectrum (514 nm excitation), collected at liquid-nitrogen temperature, displayed strong emissions from N-V centers (zero-phonon lines [ZPL] at 575 and 637 nm) and from the Si-V defect (doublet at 736.6 and 736.9 nm). Weak but clear emissions at 596.5 and 597.1 nm were also recorded.

Figure 5. This 1.25 ct Fancy brown synthetic diamond proved to be CVD grown, but it had some unusual spectroscopic features.

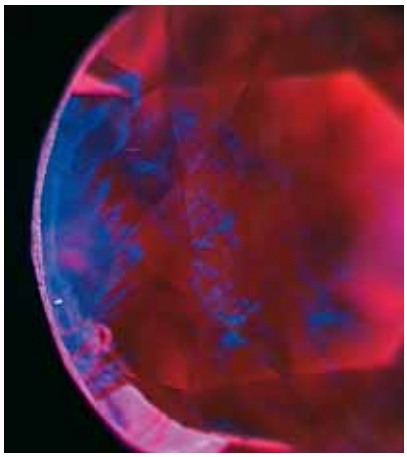

Figure 6. In the DiamondView, the synthetic diamond in figure 5 is dominated by moderately strong orangy red fluorescence with a large irregular blue region. This luminescence is similar to that seen in products from Apollo Diamond Inc.

P. M. Martineau et al. ("Identification of synthetic diamond grown using chemical vapor deposition [CVD]," Spring 2004 *Gems & Gemology*, pp. 2–25) described gem-quality boron-doped type IIb CVD synthetic diamonds, but the gemological and spectroscopic features of their (blue) samples were very different from those of the 1.25 ct brown CVD synthetic we examined. Whether the boron in this diamond was doped intentionally or

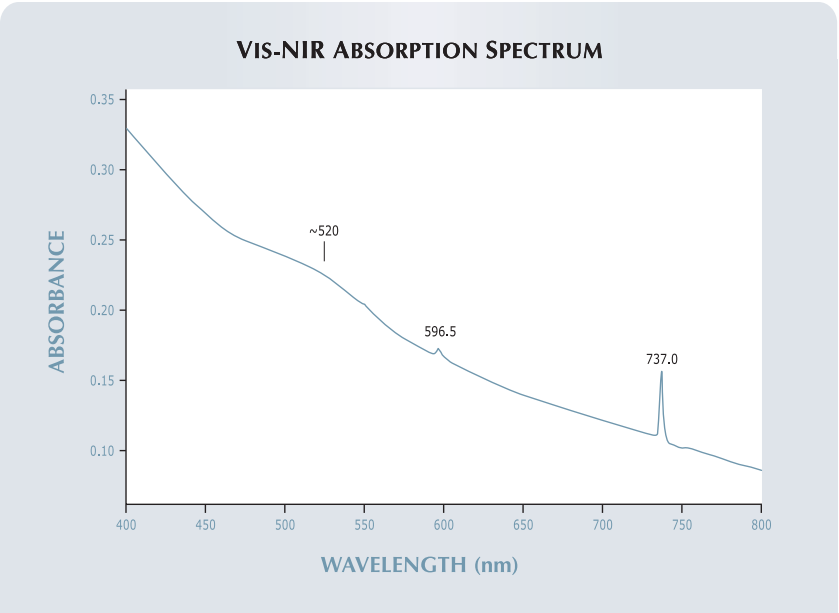

Figure 7. An outstanding feature of the brown CVD synthetic diamond is a very strong absorption from the Si-V defect (ZPL at 737.0 nm) in the Vis-NIR spectrum. This defect has only rarely been detected in the absorption spectra of CVD-grown diamonds.

incorporated accidentally is unclear.

All these absorption and luminescence features established that this was an as-grown CVD synthetic diamond, though with some unusual features compared to previously reported material. These include its relatively large size (1.25 ct), its normal cutting proportions, the fact that it contained trace boron, and its extremely high concentration of Si-V defects.

Wuyi Wang and Thomas M. Moses

Bleached *Pinctada Margaritifera* CULTURED PEARLS in Non-"Chocolate" Colors

The bleaching of *P. margaritifera* cultured pearls to achieve a brown color has become a popular and widely disclosed treatment (see W. Wang et al., "Identification of 'chocolate pearls' treated by Ballerina Pearl Co.," Winter 2006 *Gems & Gemology*, pp. 222–235). Over the last year, however, the New York laboratory received for identification two strands of cultured pearls (which proved to be from the *P. margaritifera* mollusk) that featured colors other than brown that showed evidence of bleaching.

The cultured pearls in the first strand (figure 8) had good luster, moderately spotted surfaces, and good matching. Those in the second strand (figure 9) had very good luster, lightly spotted surfaces, and very good matching. The color variation in the second strand was broader and more pronounced. In addition to "chocolate pearls," both strands contained cultured pearls in an assortment of atypical colors. Many of the grays and greens were uncharacteristically muted in tone and saturation, and there were a number of unusual light-toned yellow-browns or brown-yellows. Overall, these cultured pearls were lighter in tone and warmer in hue than most *P. margaritifera* pearls, but darker and cooler than most of those from the *Pinctada maxima* mollusk. In most of the cultured pearls, magnification revealed evidence of bleaching, including slightly desiccated patches and color distribution (color concentrations and streaks) typical of Tahitian cultured pearls that have been bleached brown, with similar though subtler color variegation in some colors.

Exposure of the second strand to long-wave UV radiation also produced some unusual results. The tone and intensity of the reaction was directly related to the tone and saturation of the color in the cultured pearls:

Figure 8. The cultured pearls (10.50–13.50 mm) in this variously colored strand are from the Pinctada margaritifera *mollusk. All except the greenish ones showed evidence of bleaching.*

Figure 9. All but two of the cultured pearls (11.00–13.50 mm) in this second strand from P. margaritifera *also showed evidence of bleaching.*

Lighter samples fluoresced weak-to-moderate yellow, and dark neutrals produced weak dark or inert reactions. Additionally, the reactions varied in hue throughout the strand, and they differed significantly from the inert to weak reddish brown reaction normally produced by naturally colored *P. margaritifera* pearls. A number of samples showed yellow, orange, or reddish orange reactions, and one fluoresced a distinct green-yellow.

EDXRF analysis of all the cultured pearls in the second strand detected calcium and strontium but no silver, which indicated that they were not dyed. UV-Vis reflectance spectroscopy revealed evidence of bleaching in the browns and all but two of the other colors. The background tilted toward the high-energy side, and the organic peaks were weak and broad (see, e.g., figure 9 of Wang et al., 2006, p. 228). While the level of treatment applied to the other colors visually appeared less pronounced than what is often found in "chocolate pearls," UV-Vis reflectance spectroscopy did not produce any results to corroborate this.

The popularity of "chocolate pearls" seems to have led manufacturers to extend a similar bleaching treatment to cultured pearls of other colors.

Akira Hyatt

Blue-Green PLAGIOCLASE FELDSPAR, Possibly Colored by Copper

Blue-to-green potassium feldspar, known in the trade as *amazonite*, owes its color to a combination of natural irradiation and trace concentrations of lead and water (A. M. Hofmeister, and G. R. Rossman "A spectroscopic study of irradiation coloring of amazonite: Structurally hydrous, Pb-bearing feldspar," *American Mineralogist*, Vol. 70, 1985, pp. 794–804). The Carlsbad lab recently received for identification two opaque bluish green rocks (figure 10) measuring 46.90 × 35.18 × 21.38 mm and 45.38 × 24.05 × 21.69 mm that, on initial observation, appeared to be amazonite. On closer inspection, however, the rocks lacked the mottled grid-like color patterns (exsolution lamellae, caused by the intergrowth of microcline and albite) that characterize amazonite. Instead, the structure was massive and fairly uniform.

On the exterior of the rocks was a brownish crust, beneath which were layers and veins of a darker bluish green material. A rough RI measurement of 1.54 suggested a plagioclase feldspar (oligoclase). Laser ablation–inductively coupled plasma–mass spectrometry (LA-ICP-MS) and electron microprobe analyses confirmed that the composition fell within the albite-oligoclase range. Very little potassium was detected; nor was lead present in significant concentrations (<4 ppm). Instead, the

Figure 10. Chemical analysis of these two samples of bluish green plagioclase feldspar (45.38 and 46.90 mm in longest dimension) suggested that they were colored by copper.

analyses showed high levels of copper (up to ~12,000 ppm). Great care was taken during analysis to make sure that none of the surface minerals were mixed with the feldspar.

The client, Daniel Anderson, was kind enough to loan us several additional pieces of rough for testing, and these samples reinforced our earlier observations and analyses. Mr. Anderson plans to polish this plagioclase feldspar and introduce it to the market in the near future. He reports that it occurs in altered pegmatites of Jurassic age (~150–200 million years) in northern Nevada. Further testing is currently being performed to determine the extent to which copper might be responsible for the color.

It is quite unusual to come across feldspar with such a distinct bluish green color that is not an alkali (potassium) feldspar colored by lead.

Alethea Inns and Christopher M. Breeding

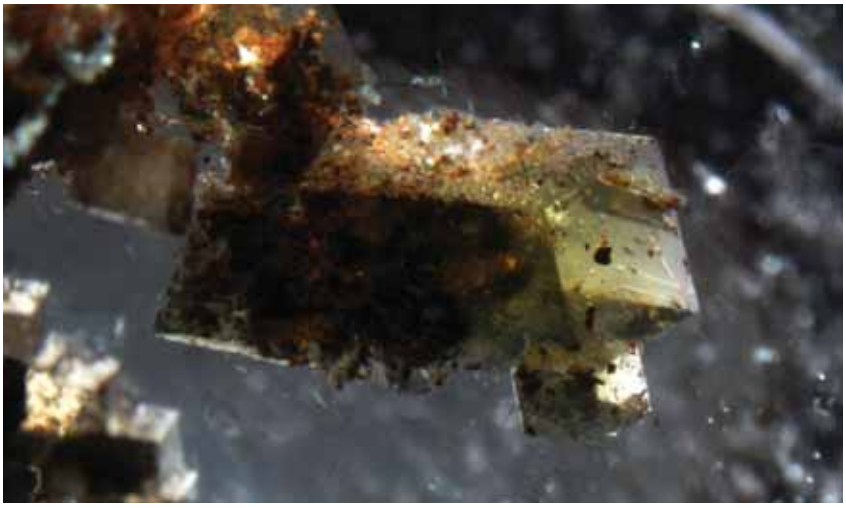

Figure 11. The primary petroleum fluid inclusions in the trigonal cavities of this quartz had an unusual green color that was not the result of either visible-light luminescence or UV fluorescence. Field of view 4.4 mm.

Unusual Green Fluid Inclusions in QUARTZ

Petroleum is one of the most important substances on Earth. Civilization as we know it would cease to exist without natural petroleum and the products derived from it. Because of this, fluid inclusions containing natural petroleum have fascinated geologists, gemologists, and other earth scientists for decades.

Hydrocarbons usually form primary fluid inclusions composed of liquid natural petroleum and methane gas, with water sometimes also present as an immiscible secondary liquid phase (see, e.g., Spring 2004 Gem News International, pp. 79–81). Opaque black to dark brown translucent bituminous material, identified under the general heading *asphaltite*, may also be present as a solid daughter phase. The liquid petroleum portion is generally yellow in color, but it may range from nearly colorless to deep golden brown to pinkish orange (similar to the color of gasoline). If present, water will be forced to the outermost edges of the void, and the vapor bubble (again, usually methane) will always be in the liquid petroleum portion and not in the water.

An interesting identifying characteristic of petroleum in fluid inclusions is that when it is illuminated from the side with an incandescent fiber-optic light source, it displays a slight bluish green to green luminescence. This reaction is different from the long-wave UV fluorescence it also displays—commonly a chalky blue to yellow, or very rarely orange.

Recently, Kevin Lane Smith, a jeweler and lapidary from Tucson, Arizona, showed this contributor a polished quartz specimen that, without magnification, appeared to contain a few small light green angular crystals. On closer inspection, however, it was determined that the green material was actually a liquid filling small trigonal cavities (figure 11). Detailed micro-examination showed that the inclusions were intact with no surface-reaching cracks. Exposure to UV radiation caused the liquid to fluoresce a chalky blue, and light transmitted through the side of the stone caused the fluid inclusions to luminesce a chalky bluish green, both as would be expected of natural petroleum (again, see Spring 2004 GNI entry). This behavior strongly suggested that these fluid inclusions were composed of natural petroleum. The unusual green color did not appear to be caused by luminescence or UV radiation, however, since it was clearly visible in dark-field illumination without any overshadowing chalkiness.

John I. Koivula

Inclusions within Inclusions in RUBY

The New York laboratory recently had the opportunity to examine an attractive 2.06 ct red oval mixed-cut ruby (figure 12) with a highly interesting inclusion scene. Standard gemological testing identified the stone as a natural ruby. With magnification, we saw numerous transparent near-colorless crystals. The pristine state of the inclusions indicated that the stone had not been heat treated. What was most interesting was that several of the crystals clearly had inclusions of their own.

The crystal in figure 13 contained a rod-shaped inclusion that appeared to break through another crystal, both showing a multistepped surface. All the elements in this inclusion exhibited birefringence between crossed

Figure 12. This untreated natural ruby (7.76 × 6.32 × 4.94 mm) contained some unusual crystal inclusions.

Figure 13. Hosted within this pristine crystal in the ruby in figure 12 were rod-shaped crystals that still retained their original crystal faces. Field of view 0.76 mm.

Figure 14. Another included crystal (identified as corundum) in the ruby contained a fan-shaped spray of needles. Field of view 0.63 mm.

polarizers. Unfortunately, we were not able to obtain sufficiently clear Raman spectra to identify them.

Other attractive inclusions were discovered within a crystal that was visible through the pavilion. Located between two cavities in the host ruby, the crystal displayed a nicely formed fan-shaped spray of needles (figure 14). The transparent-to-translucent needles appeared unaltered and also exhibited birefringence. We were able to identify the host crystal as corundum, but the Raman laser could not reach the needles. According to GIA chief gemologist John Koivula, these needles were probably boehmite or diaspore, both of which are alteration products of corundum.

Their complete enclosure in the crystal inclusions indicates that the unaltered rod-shaped crystals and the fan-shaped spray of needles could have formed before the growth of the host ruby. Thus, these inclusions could be defined as both protogenetic (pre-existing inclusions) and idiomorphic (still retaining their original crystal faces).

Even though mineral inclusions in corundum have been studied extensively, none of us at the New York lab had previously seen such well-formed "inclusions within inclusions."

Wai L. Win and Riccardo Befi

Blue SAPPHIRE, With Unusually High Concentration of Rare-Earth Elements

Common chemical impurities in natural corundum include Mg, Ti, V, Cr, Fe, and Ga. A number of colors can be induced by these elements through various mechanisms as they integrate into the corundum lattice (see, e.g., E. Fritsch and G. R. Rossman, "An update on color in gems, part 2: Colors involving multiple atoms and color centers," Spring 1988 *Gems & Gemology*, pp. 3–15). Be has also been found in natural corundum from several geographic sources in trace amounts ranging from less than 1 ppm to over 10 ppm; other trace elements (e.g., Nb, Ta, U, Pb, Th, Zr, or W) are almost always present with naturally occur-

Figure 15. This blue sapphire (5.95 × 5.91 × 3.52 mm) has an unusual trace-element composition: relatively high concentrations of light rare-earth elements.

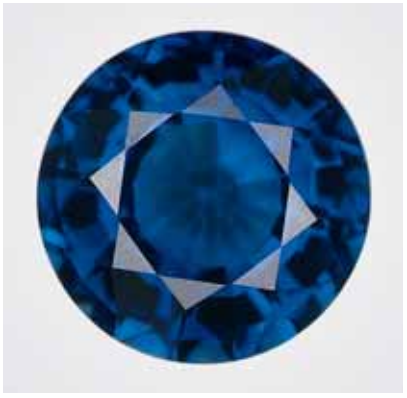

Figure 16. Three spots on both blue and near-colorless zones in the girdle region of the blue sapphire in figure 15 were analyzed using LA-ICP-MS, but no substantial variation in trace-element composition was detected. Field of view 3.5 mm.

TABLE 1. Trace-element composition of the unusual 1.02 ct blue sapphire.[a]

Element	Mg	Ti	V	Cr	Fe	Ga	Zr	Nb	La	Ce	Nd	Sm	Ta	W	Pb	Th	U
Concentration (ppm)	19.11	195.4	3.15	2.87	3887	59.95	0.05	0.11	0.66	1.55	0.29	0.02	0.26	0.12	0.37	4.96	0.01

[a]*Average of three spots, as recorded with LA-ICP-MS. Rare-earth elements are highlighted in blue.*

ring Be (A. H. Shen et al., "From the GIA Laboratory: Beryllium in corundum—The consequences for blue sapphire," *GIA Insider*, Vol. 9, No. 2, January 26, 2007). However, these elements—in contrast to the substitution impurities noted earlier—are believed to occur within clouds of submicroscopic particulate inclusions, not as part of the crystal lattice. In the New York laboratory, we recently examined a sapphire that displayed atypical trace-element composition—specifically, relatively high concentrations of other rare-earth elements (REEs) that appear to be independent of submicroscopic "clouds" or inclusions.

This intense blue 1.02 ct round-cut stone (figure 15) was identified as natural sapphire by standard gemological testing. With magnification, it exhibited sharply defined blue and near-colorless parallel bands (figure 16). Small melted inclusions with altered or melted radial expansion fractures were also observed, indicating the stone was heat treated. No clouds or bands of particles were visible at 80× magnification, and there was no detectable chalky yellow fluorescence to short-wave UV radiation, as is sometimes seen in heated blue sapphire.

Three spots along the girdle region (again, see figure 16) were analyzed using LA-ICP-MS, calibrated against corundum standards for Be, Mg, Ti, V, Cr, Fe, and Ga, and against National Institute of Standards and Technology (NIST) glasses for other elements. The blue and near-colorless zones showed similar trace-element composition. Consistent with blue sapphire from many different sources, this stone had a high concentration of Fe, moderate amounts of Ga and Ti, and very low concentrations of Mg, V, and Cr (table 1). An outstanding feature was the relatively high concentration of light REEs (La, Ce, Nd, Sm), which we have observed only rarely in the thousands of natural corundum samples we have examined from various geographic sources. In addition, despite significant amounts of Zr, Nb, Ta, W, Pb, Th, and U, no Be was detected (our instrument detection limit for Be is 0.01 ppm).

Observations from this unusual stone strongly indicate that microinclusions in corundum may have large variations in composition, including (to the best of our knowledge) previously undocumented rare-earth elements. This stone also confirms that Nb and Ta may occur independently of Be in sapphire.

Donna Beaton and Wuyi Wang

PHOTO CREDITS
Jian Xin (Jae) Liao—1, 5, 8, 12, and 15; Vincent Cracco—3; John I. Koivula—4 and 11; Wuyi Wang—6 and 16; Sood Oil (Judy) Chia—9; Robinson McMurtry—10; Wai L. Win—13; Riccardo Befi—14.

DIAMONDS

Bird-like inclusion in diamond. In March 2008, jewelry appraiser Lori Provo Coogan (Cohasset Jewelers, Cohasset, Massachusetts) was appraising a 2.41 ct diamond set in a ring when she noticed an interesting internal feature. Centered just under the table, it was comprised of a brownish orange mineral inclusion that was surrounded by tension fractures (figure 1). The distribution and shape of the fractures—which are apparently following two cleavage directions in the diamond—show a strong resemblance to a bird in flight. There are even patterns resembling feathers and a curved "beak." The color and form of the mineral inclusion suggest that it is an eclogitic garnet (John I. Koivula, pers. comm., 2008).

Brendan M. Laurs

Figure 1. The internal feature centered under the table facet of this diamond is composed of a mineral (probably garnet) that is surrounded by tension fractures. The overall inclusion scene (~1 mm long) shows a striking resemblance to a bird in flight. Photomicrograph by Lori Provo Coogan.

A colorless diamond showing strong phosphorescence. Unlike fluorescence to UV radiation, which is commonly observed in natural diamonds, phosphorescence is quite rare, and is mainly observed in type IIb blue diamonds, "color-change" (i.e., chameleon) diamonds, and some other colored diamonds (see J. E. Field, Ed., *The Properties of Natural and Synthetic Diamond*, Academic Press, London, 1992; S. Eaton-Magaña et al., "Fluorescence spectra of colored diamonds using a rapid, mobile spectrometer," Winter 2007 *Gems & Gemology*, pp. 332–351). In the case of blue type IIb diamonds, red, orange, and blue phosphorescence with an average duration of 18 seconds has been reported (J. M. King et al., "Characterizing natural-color type IIb blue diamonds," Winter 1998 *Gems & Gemology*, pp. 246–268). The phosphorescence behavior of these type IIb diamonds has been explained by a model of electron transition from the unknown donor to the boron acceptors, which display long decay times due to the low concentration of boron (K. Watanabe et al., "Phosphorescence in high-pressure synthetic diamond," *Diamond and Related Materials*, Vol. 6, 1997, pp. 99–106). Phosphorescence is rarer in other diamond types, and when seen it is both less intense and of shorter duration (again, see Eaton-Magaña et al., 2007).

Editor's note: Interested contributors should send information and illustrations to Brendan Laurs at blaurs@gia.edu or GIA, The Robert Mouawad Campus, 5345 Armada Drive, Carlsbad, CA 92008. Original photos can be returned after consideration or publication.

GEMS & GEMOLOGY, Vol. 44, No. 2, pp. 164–190

Figure 2. This 0.54 ct colorless type IIa diamond showed strong phosphorescence. Photo by H. Ito.

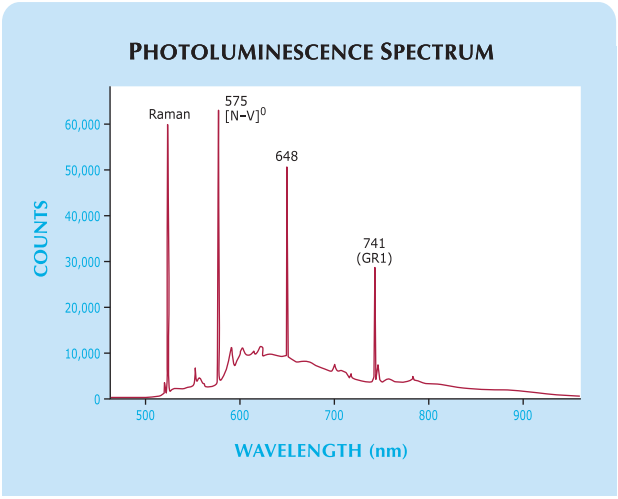

Figure 4. The photoluminescence spectrum of the type IIa diamond (here, recorded with a 488 nm laser) shows a sharp emission peak at 648 nm that may be related to its phosphorescence.

Recently, a 0.54 ct colorless diamond (figure 2) was submitted to the AGT Gem Laboratory for a diamond grading and identification report. Gemological examination and Fourier-transform infrared (FTIR) spectroscopy proved that the D-color, VVS_1 diamond was type IIa. There was no reaction to long-wave UV radiation. However, when the diamond was examined with high-energy short-wave (<230 nm) UV radiation in the DiamondView instrument, it displayed a weak dark blue fluorescence and a very strong blue phosphorescence (figure 3). No distinct growth bands or other internal features were seen with either type of luminescence. Long-lived blue phosphorescence was also seen after exposure to a short-wave UV lamp (254 nm) in a dark room; it took about four minutes for the phosphorescence to fade entirely.

To explore possible mechanisms for the phosphorescence, photoluminescence spectra excited by both 488 and 514.5 nm lasers were recorded at liquid-nitrogen temperature. The PL spectra did not show the 776.5 nm peak that has been associated with phosphorescence in natural blue diamond (Fall 2005 Lab Notes, pp. 258–259). Instead, they showed a strong and sharp emission peak of unknown origin at 648 nm, in addition to a GR1 peak at 741 nm and the $[N\text{-}V]^0$ center at 575 nm (figure 4).

Figure 3. These DiamondView images of the 0.54 ct diamond illustrate the weak dark blue UV fluorescence (left) and strong blue phosphorescence (right).

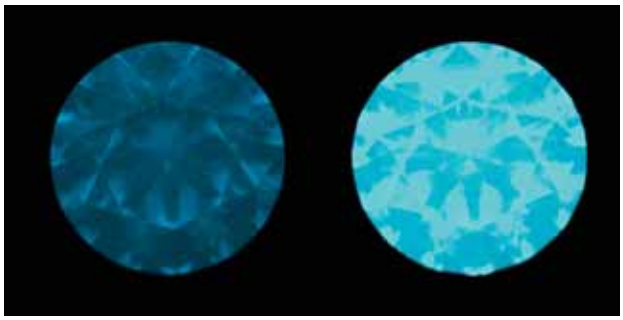

The optical center(s) for the phosphorescence in this type IIa diamond are apparently different from those in type IIb diamonds. The detailed mechanism is unclear, but the 648 nm peak may be related to the phosphorescence in this diamond.

Taijin Lu (taijinlu@hotmail.com), Tatsuya Odaki, Kazuyoshi Yasunaga, and Hajime Uesugi
AGT Gem Laboratory, GIA Japan, Tokyo

COLORED STONES AND ORGANIC MATERIALS

Almandine-spessartine from Lindi, Tanzania. At the 2008 Tucson gem shows, Steve Ulatowski (New Era Gems, Grass Valley, California) had some attractive euhedral crystals of a new orange-red garnet from Tanzania. The crystals reportedly were mined from an area in Lindi Province, not far from the source of the pink "Imperial" pyrope-spessartine described in the Spring 2006 Gem News International (GNI) section (pp. 66–67). Mr. Ulatowski first obtained the material in January 2007, and estimates that about 1–3 kg of mixed-quality rough has been produced each month. The crystals are well-formed but typically rather small, yielding cut stones averaging <0.50 ct.

One crystal and a 1.35 ct modified round brilliant garnet (figure 5) were donated to GIA by Mr. Ulatowski, and the cut stone yielded the following properties: color—orange-red; diaphaneity—transparent; RI—1.800; SG—4.17; Chelsea filter reaction—red; and fluorescence—inert to both long- and short-wave UV radiation. The desk-model spectroscope showed weak absorption lines at 480 and 520 nm, stronger lines at 460, 505, and 565 nm, and general absorption to 440 nm. Microscopic examination

Figure 5. Lindi, Tanzania, is reportedly the source of these samples of almandine-spessartine. GIA Collection nos. 37613 (cut stone, 1.35 ct) and 37612 (crystal, 0.5 g); photo by Robert Weldon.

revealed pinpoint inclusions, short needles, and straight transparent growth lines. Energy-dispersive X-ray fluorescence (EDXRF) spectroscopy indicated major amounts of Si, Al, Mn, and Fe, and minor Mg and Ca.

The physical and chemical properties identify the garnet as almandine-spessartine, with minor pyrope and grossular components. Its refractive index and specific gravity are slightly lower than those reported for almandine-spessartine by C. M. Stockton and D. V. Manson ("A proposed new classification for gem-quality garnets," Winter 1985 *Gems & Gemology*, pp. 205–218). These differences are most likely attributable to the minor pyrope and/or grossular components.

Elizabeth Quinn Darenius
(eqdarenius@aglgemlab.com)
American Gemological Laboratories, New York

Brendan M. Laurs

"Red andesine" from China: Possible indication of diffusion treatment. At the June 2007 Sainte Marie aux Mines show in France, we acquired a 1.30 ct oval-cut, orangy red stone that was sold as andesine from China (figure 6). The stone was obtained to supplement our reference gemology collection, and because it was sold for a much lower price than similar andesine-labradorite that has been represented as being from the Democratic Republic of the Congo or other localities (see, e.g., Winter 2005 GNI, pp. 356–357, and references therein).

The sample was birefringent and biaxial negative, with RIs of 1.550–1.559 and a hydrostatic SG of 2.70. These properties were consistent with plagioclase feldspar, and were closer to those of labradorite than andesine. We observed a weak orange-red/light red-orange pleochroism, and the stone was inert to both long- and short-wave UV radiation. A fairly broad absorption in the yellow region was seen with the handheld spectroscope. Next, we measured the sample's chemical composition using a JEOL 5800 scanning electron microscope (SEM) equipped with a high-resolution Princeton Gamma Tech IMIX-PTS germanium energy-dispersive detector. The stone had the following composition (atomic percent): 19.31% Si, 11.16% Al, 4.18% Ca, 3.34% Na, 0.29% K, 0.17% Fe, and 61.5% O. These values are also consistent with a feldspar. The anorthite content of $An_{55.5}$ [Ca/(Ca+Na) = 0.555] corresponds to the range for labradorite ($An_{50–70}$), but is close to that for andesine ($An_{30–50}$).

Figure 6. This 1.30 ct orangy red feldspar, sold as andesine from China, proved to be labradorite with unusual color concentrations. Note the pale-colored zones in the upper portion of the stone. Photo by B. Mocquet.

Even with the unaided eye, it was evident that the sample had uneven coloration (again, see figure 6), particularly when viewed from the pavilion side. Microscopic examination revealed abundant parallel empty tubes or channels, as well as a few twin planes. Also seen were orangy red color concentrations around some of the channels, particularly at the terminations of those that were surface-reaching on their opposite ends (figure 7, left). It appeared as if the chromophore had diffused an equal distance in all directions from the terminations of the channels into the surrounding near-colorless areas. In addition, black pinpoint inclusions (as yet unidentified) were visible in and around the orangy red areas, but they were not present in the near-colorless zones. Hence, the stone's appearance under the microscope was very different from that of typical red andesine, which is usually almost free of inclusions and homogeneous in color. The unusual color distribution suggests a diffusion process, presumably of copper, which is a red chromophore in feldspar. Although no copper was detected in the stone, Cu in red or green feldspar is typically below the detection limit of our instrument.

With magnification, we also observed thin orange patches on the surface of some facets (figure 7, right). Because of the presence of significant red areas inside the stone, we do not believe this film contributed to the color. When these areas were analyzed with the SEM, we detected the presence of Fe in addition to the feldspar composition; the iron is probably responsible for the rust-like color of the patches. The presence of this film indicates that the stone was exposed to some type of process or treatment after faceting.

The combination of the peculiar red color distribution and the surface film residue offers evidence that the stone

Figure 7. With magnification, the labradorite shows red color concentrations around surface-reaching channels, particularly at their terminations (left; photomicrograph by B. Rondeau, magnified 40×). Some of the facets on the stone were coated with patches of a thin film containing traces of iron (right; photomicrograph by B. Mocquet, magnified ~30×).

was initially pale colored and possibly underwent diffusion treatment to acquire the orangy red color.

Emmanuel Fritsch

Benjamin Rondeau
CNRS, Team 6112, Laboratoire de Planétologie et Géodynamique, University of Nantes, France

Blanca Mocquet and Yves Lulzac
Centre de Recherches Gemmologiques (CRG)
Nantes, France

Orange beryl from India. At the 2008 Tucson gem shows, Cameron McGowan and Willie Neilson (Crystalline Dream, Lake Ohau, New Zealand, and San Francisco, California) showed the *Gems & Gemology* editors some deep orange beryl. They obtained several faceted samples of this beryl (e.g., figure 8) from a local gem dealer while traveling in India in 2007. The coloration was represented as natural, and the dealer said he had collected the stones from central India over an unspecified period of time.

To investigate the origin of color in these stones, a representative 4.47 ct modified cushion step cut was loaned to American Gemological Laboratories for examination, and the following properties were determined: color—brownish orange, with weak brownish yellow and yellow-orange dichroism; diaphaneity—semitransparent to translucent; RI—n_o = 1.587 and n_e = 1.580; birefringence—0.007; SG—2.72; Chelsea filter reaction—none; fluorescence—inert to long- and short-wave UV radiation; and general absorption to 450 nm and a cutoff at 670 nm visible with a desk-model spectroscope. These properties are consistent with those reported for beryl by M. O'Donoghue, Ed. (*Gems*, 6th ed., Butterworth-Heinemann, Oxford, UK, 2006, pp. 162–166).

Microscopic examination revealed numerous small needles and platelets (possibly hematite) that appeared brownish reddish orange when they occurred in larger sizes (figure 9, left), numerous two-phase (liquid and gas) inclusions, three-phase inclusions containing dark solids (figure 9, right), "fingerprints," and fine growth tubes oriented parallel to the c-axis. Several of the two- and three-phase inclusions were surrounded by whitish film-like halos. The stone also showed evidence of clarity enhancement (fractures containing flattened gas bubbles, indicating the presence of a filler).

UV-Vis-NIR spectroscopy showed total absorption to 450 nm, a sharp peak at 455 nm, a weak shoulder at the foot of the absorption continuum at ~505 nm, and a weak broad band centered at ~835 nm. The stone's unusually deep brownish orange coloration was probably due to a combination of its orange-yellow bodycolor (most likely the result of $O^{2-} \rightarrow Fe^{3+}$ charge transfer; see p. 94 of E. F. Fritsch and G. R. Rossman, "An update on color in gems. Part 3," Summer 1988 *Gems & Gemology*, pp. 81–102), evidenced in the visible spectrum by the 455 nm band, and the abundant brownish reddish orange inclusions.

Elizabeth Quinn Darenius

Figure 8. These yellowish orange to brownish orange beryls (10.31–11.47 ct) are reportedly from central India. Photo by Robert Weldon.

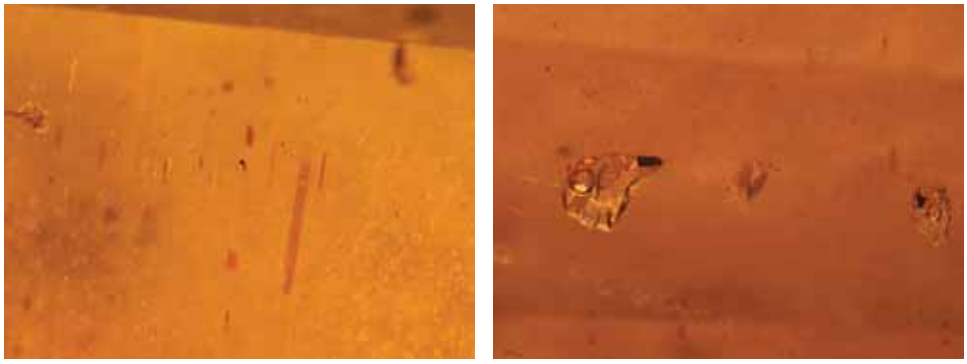

Figure 9. Brownish reddish orange needles and platelets (possibly hematite) were partially responsible for this beryl's apparent color (left). The stone contained two- and three-phase inclusions; the latter consisted of a gas bubble, a liquid, and a dark solid (right). Photomicrographs by E. Q. Darenius; magnified 65× (left) and 75× (right).

Chromium-rich clinochlore (kämmererite) from Turkey. Clinochlore—$(Mg,Fe^{2+})_5Al(Si_3Al)O_{10}(OH)_8$—is a member of the chlorite group. Its name is derived from a combination of the Greek words *klino* ("incline"), in allusion to its monoclinic habit, and *chloros* ("green"), in reference to its most common color (J. W. Anthony et al., *Handbook of Mineralogy*, Vol. 2, Mineral Data Publishing, Tucson, AZ, 1995, p. 143). Other documented colors of clinochlore include yellow, white, and a red to purple-red Cr-rich variety that is commonly referred to as *kämmererite*. Since clinochlore has a low hardness (Mohs 2–2.5) and perfect cleavage, it is not suitable for jewelry use but is typically sold as crystal specimens or, rarely, as a collector's stone.

Alexandra Woodmansee of Rock Logic (Glencoe, Minnesota) recently loaned GIA two faceted samples (a 0.92 ct oval and a 0.52 ct cut-cornered rectangular mixed cut; figure 10) of Cr-rich clinochlore obtained from Turkey. While Cr-rich clinochlore has been reported from, among other locations, the U.S. (California, North Carolina, and Pennsylvania) and Russia (Ural Mountains), the most famous source is the Kop Mountains in eastern Turkey (see, e.g., R. Dietrich and O. Medenbach, "Kämmererite from the Kop Krom mine, Kop Dağlari, Turkey," *Mineralogical Record*, Vol. 9, No. 5, 1978, pp. 277–287).

Examination of the two stones gave the following properties (with those for the oval cut listed first for RI and SG): color—medium-dark purplish red; RI—1.580, 1.588; hydrostatic SG—2.65, 2.67; fluorescence—inert to both long- and short-wave UV radiation; Chelsea filter reaction—positive (pink); and absorption below 440 nm and from 500–590 nm seen with a desk-model spectroscope. Microscopic examination revealed numerous fractures and cleavages, as well as crystals, needles, and clouds of tiny pinpoint inclusions. The surface of both stones showed a poor polish and many scratches and gouges, consistent with the low hardness.

The physical properties we recorded are comparable to those reported for Cr-rich clinochlore by M. O'Donoghue, Ed. (*Gems*, 6th ed., Butterworth-Heinemann, Oxford, UK, 2006, p. 420) with the exception of the SG, which O'Donoghue stated as 2.60–2.64. There are also some differences from the data presented by W. Wight ("Check-list for rare gemstones—Kämmererite," *Canadian Gemmologist*, Vol. 17, No. 1, 1996, pp. 14–17); that article cited an absorption band at ~510–620 nm and lines at ~650 and 690 nm, as well as RIs of n_α = 1.597, n_β = 1.598, and n_γ = 1.599–1.600—but also listed other reported RI values of 1.585–1.594. Wight (1996, p. 17) further indicated that the

Figure 10. Commonly referred to as kämmererite, *Cr-rich clinochlore is rarely seen in faceted form (here, 0.92 and 0.52 ct). Photo by Robert Weldon.*

Figure 11. The UV-Vis-NIR absorption spectra for the two samples in figure 10 show absorption peaks near 400 and 550 nm, corresponding to Cr^{3+}, and two smaller peaks at ~680 and 685 nm.

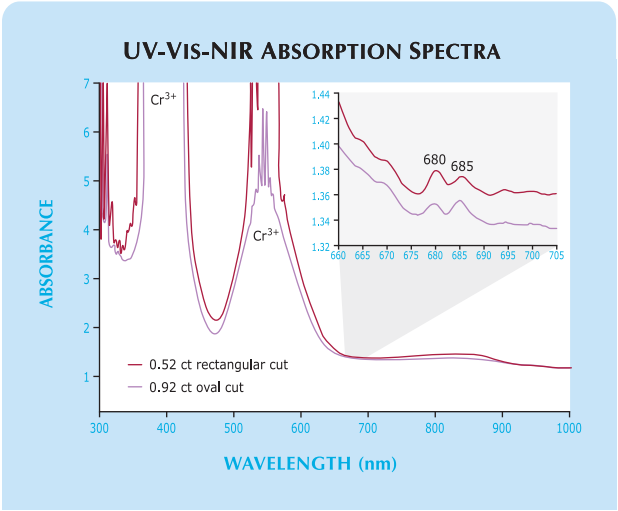

low birefringence (0.003) of Cr-rich clinochlore "might result in only one line being seen in the refractometer." This observation, coupled with the poor polish of the two stones we examined, could explain the single RI readings on our samples.

Raman analysis of these two specimens confirmed that the material was, indeed, "kämmererite." The UV-Vis-NIR absorption spectra (figure 11) showed transmission windows in the blue and red portions of the spectrum, which are consistent with the purplish red color of the samples. The strong absorption peaks near 400 and 550 nm correlate to the features seen in the desk-model spectroscope, and are attributed to Cr^{3+} (R. G. Burns, *Mineralogical Applications of Crystal Field Theory*, 2nd ed., Cambridge University Press, Cambridge, UK, 1993, p. 200). Also noted were two smaller peaks at ~680 and 685 nm that may correspond to the ~690 nm line cited by Wight (1996). EDXRF analysis verified the presence of Cr as a major element in the samples, as well as Mg, Al, and Fe in major amounts, which would be expected in Cr-rich clinochlore; Ca, V, Ni, and Zn were detected in trace amounts.

According to Mrs. Woodmansee, the stones were cut from old stock. The 0.92 ct stone is one of the largest faceted specimens known to her; in general, most of the rough material is small and not suitable for cutting. Since the Turkish mine closed in 1991 due to low prices for chromium, faceted Cr-rich clinochlore will most likely continue to be extremely rare.

Karen M. Chadwick (karen.chadwick@gia.edu)
GIA Laboratory, Carlsbad

Yellow danburite from Tanzania. For years, gem-quality yellow danburite was known from Myanmar and Madagascar (e.g., W. Wight, "Danburite," *Canadian Gemmologist*, Vol. 6, No. 4, 1985, pp. 110–113), and also reported from Sri Lanka (see, e.g., Spring 1986 Lab Notes, p. 47) and California (e.g., Fall 1998 Gem News, p. 220). Most recently, yellow danburite gemstones were described from a new locality in Tanzania ("Nuovi ritrovamenti: Danburite gialla di qualità gemma e gatteggiante dal Madagascar e dalla Tanzania," *Rivista Gemmologica Italiana*, Vol. 2, No. 3, 2007, pp. 228–229).

In January 2008, we learned more about this new Tanzanian danburite from Mark Kaufman (Kaufman Enterprises, San Diego, California) and Werner Radl (Mawingu Gems, Niederwörresbach, Germany). Mr. Radl subsequently visited the deposit, which is located in the Morogoro region, in April 2008. The danburite is mined from at least two steeply dipping granitic pegmatites (e.g., figure 12) using hand tools and explosives. The pegmatites are hosted by marble, and locally contain coarse-grained pale blue-green K-feldspar (amazonite) and black tourmaline (identified as dravite-schorl by Dr. William "Skip" Simmons at the University of New Orleans by electron-microprobe analysis). The same pegmatites have reportedly produced smoky quartz and a translucent bluish violet quartz that appears to be colored by abundant micro-inclusions.

Figure 12. This granitic pegmatite in the Morogoro region of Tanzania recently produced significant quantities of yellow danburite. Courtesy of W. Radl.

Mr. Kaufman loaned GIA, for examination, two rough specimens (a 1.61 g fragment and a 12.68 g crystal) as well as two faceted (1.88 and 7.14 ct) and two cabochon-cut (8.22 and 19.41 ct) examples of the yellow danburite (e.g., figure 13). Mr. Radl showed one of us (BML) some additional faceted stones (e.g., figure 14) at the February 2008 Tucson gem shows, including a 22.48 ct oval cut, and donated a 4.37 g crystal to the Institute. Both of the crystals were tabular and twinned, resulting in a leaf-like appearance (again, see figure 13).

Examination of the cut stones gave the following properties (where they differed, values for the cabochons are noted in parentheses): color—light-to-medium yellow to orangy yellow; pleochroism—none; RI—n_α = 1.629–1.631 and n_γ = 1.638 (spot reading of 1.62); birefringence—0.007–0.009; hydrostatic SG—3.01 (2.97 and 3.00); inert to both long- and

Figure 13. Yellow danburite from Tanzania commonly contains abundant growth tubes, as shown by this chatoyant cabochon (8.22 ct) and twinned crystal (12.68 g). Photo by Robert Weldon.

Figure 14. Transparent yellow danburite from Tanzania has been faceted into attractive gemstones (here, 9.92 and 8.67 ct). The pear shape shows distinct color zoning (yellow and near colorless). Courtesy of Mawingu Gems; photo by Robert Weldon.

short-wave UV radiation; and no spectrum observed with the desk-model spectroscope. Most of these properties are consistent with those given by M. O'Donoghue, Ed. (*Gems*, 6th ed., Butterworth-Heinemann, Oxford, UK, 2006, p. 403): n_α = 1.627–1.633 and n_γ = 1.633–1.639, birefringence—0.006–0.008, and SG—3.00. However, O'Donoghue reports blue to blue-green fluorescence to long-wave UV radiation, and in some stones an absorption spectrum consisting of fine lines that correspond to rare-earth elements (REEs). Wight (1985) also noted blue (and violet-blue) to blue-green fluorescence in danburite. The absence of fluorescence in the Tanzanian samples we examined—which were confirmed as danburite by Raman spectroscopy—is therefore somewhat unusual, though consistent with the Sri Lankan stones described in the Spring 1986 Lab Note.

Microscopic examination of the two faceted samples revealed long, thin, curved growth tubes (figure 15, left), as well as "fingerprints" containing angular liquid inclusions and some two-phase (liquid and gas) inclusions. The presence of growth tubes and fingerprints is consistent with internal features reported in yellow danburite from Mogok, Myanmar (Summer 2007 GNI, pp. 167–168). While the two cabochons contained similar inclusions, plus a few fractures, a much denser concentration of parallel growth tubes in some stones (figure 15, right) resulted in chatoyancy (again, see figure 13).

The cause of color in yellow danburite is as yet undetermined. EDXRF analysis of five samples detected the presence of Si and Ca in major amounts, minor Sr, and traces of Fe and REEs (Ce and possibly La or Pr). Laser ablation–inductively coupled plasma–mass spectrometry (LA-ICP-MS)—performed on the two cabochons and the larger twinned crystal by GIA Laboratory research scientist Dr. Andy H. Shen—verified the presence of Sr (~450 ppm), Fe (~30 ppm), and the light rare-earth elements La (~350 ppm), Ce (~500 ppm), Pr (~30 ppm), and Nd (~60 ppm). Heavier REEs (Sm through Lu) were present in very low concentrations (<5 ppm) or were below the detection limit of the instrument. A UV-Vis-NIR spectrum collected from the larger faceted stone showed (in addition to a transmission window encompassing the yellow region) a minor absorption feature extending from ~564 to 589 nm. This feature peaked at 585 nm, which correlates with an absorption line attributed to REEs in yellow danburites from Sri Lanka (again, see the Spring 1986 Lab Note).

Figure 15. Growth tubes in the Tanzanian danburite may exhibit a curved, almost hooked, appearance (left). Chatoyant material contains dense concentrations of parallel growth tubes (right). Photomicrographs by K. M. Chadwick; image width approximately 4.4 mm.

According to Mr. Radl, the Tanzanian danburite was first discovered in late 2006, but only small amounts were produced until late 2007. As of the February 2008 Tucson shows, he had obtained approximately 1 tonne of mixed-grade material, but less than 5 kg was of gem quality. From this small amount he had faceted ~200 carats, in clean stones weighing up to 27.8 ct (but typically <10 ct). In late February 2008, gem dealer Syed Iftikhar Hussain (Syed Trading Co., Peshawar, Pakistan) reported seeing a parcel of rough Tanzanian danburite in Bangkok consisting of 2.4 kg of chatoyant material and 1.6 kg of faceted rough, as well as an attractive cat's-eye stone weighing about 52 ct. He estimated that larger cabochons could be cut.

Karen M. Chadwick and Brendan M. Laurs

Figure 16. These faceted lawsonites (0.09–0.18 ct) from Marin County, California, were selected to show the range of color of the faceted material. Photo by Kevin Schumacher.

Lawsonite from Marin County, California. The mineral lawsonite [$CaAl_2Si_2O_7(OH)_2 \cdot (H_2O)$] was first discovered in 1895, on the Tiburon Peninsula in Marin County, California. It was named in honor of Professor Andrew C. Lawson of the University of California at Berkeley (L. F. Ransome, "On lawsonite, a new rock-forming mineral from the Tiburon Peninsula," *Bulletin of the Department of Geology*, University of California Publications, Vol. 1, No. 10, 1895, pp. 301–312). Lawsonite is found in low-temperature, high-pressure metamorphic rocks formed in subduction zones, and is typically opaque, brittle, and highly included. Therefore it was a gemological treat when Steve Perry of Steve Perry Gems (Davis, California) showed us numerous samples of translucent-to-semitransparent lawsonite at the 2008 Tucson gem shows. He obtained the material from an old mineral collection that he had recently purchased, consisting of about 320 kg of lawsonite specimens collected by a road construction mechanic on the Tiburon Peninsula. Although the time in which the specimens were collected is unknown, newspapers used for wrapping them were dated 1953.

According to Mr. Perry, the specimens consist of a matrix of glaucophane schist with small cavities containing crystals of lawsonite, pyrite, and rutile needles. Also present in the matrix of some pieces were brown garnet, chlorite, and opaque sphene. From a selection of broken lawsonite crystals, Mr. Perry arranged to cut 11 carats of faceted stones and 110 carats of cabochons. Of these, approximately 80% were "peachy" pink, 15% were grayish blue, and 5% were near colorless; less than 5% of the cabochons showed chatoyancy. Overall, less than 0.1% of the rough material was facet grade, and the vast majority ranged from translucent to opaque. The largest transparent faceted stone weighed 0.40 ct.

Mr. Perry loaned several rough and cut samples to GIA for examination, including five faceted stones and a cabochon showing chatoyancy (0.09–0.43 ct; figures 16 and 17). The following gemological properties were recorded on the faceted lawsonites: color—light pink, or near colorless to grayish blue; pleochroism—strong, in light pink and near colorless, or blue and near colorless; RI—1.664–1.687; birefringence—0.023; SG—3.08–3.30; and fluorescence—inert to both long- and short-wave UV radiation. These properties are comparable to those reported for lawsonite by R. Webster (*Gems*, 5th ed., revised by P. G. Read, Butterworth-Heinemann, Oxford, UK, 1994, p. 349). Microscopic examination revealed numerous crystals, clouds, feathers, and "fingerprints" in all the samples. Perfect incipient cleavage planes were also present. A few samples showed areas of chips and cavities, a result of the material's brittleness. UV-Vis absorption spectroscopy revealed only a broad band centered at 450 nm. Further spectroscopic and chemical analysis would be needed to understand the cause of the various colors shown by these gems.

This is the first time cut and polished lawsonite has been seen in the GIA Laboratory.

Kevin G. Nagle (kevin.nagle@gia.edu)
GIA Laboratory, Carlsbad
Brendan M. Laurs

Figure 17. This 0.43 ct lawsonite cabochon shows chatoyancy. Photo by Robert Weldon.

Figure 18. These Cr/V-bearing mica samples (3.33 g and 16.54 ct) from northern Pakistan were identified as consisting predominantly of paragonite. Photo by Robert Weldon.

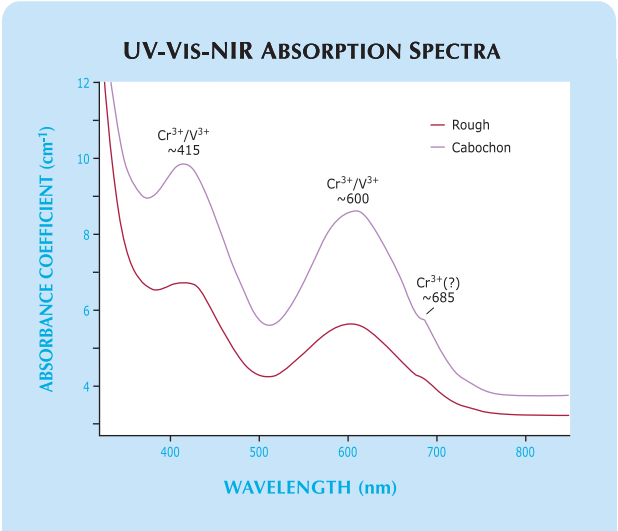

Figure 19. The unoriented UV-Vis-NIR absorption spectra of the paragonite show strong absorption peaks at ~415 and ~600 nm, corresponding to Cr^{3+} and/or V^{3+}, and a small peak at ~685 nm, probably attributable to Cr^{3+}.

Green mica (paragonite) from Pakistan. The term *green mica* usually calls to mind phlogopite or Cr-bearing muscovite ("fuchsite"), or possibly celadonite or margarite. However, Makhmout Douman (Arzawa Mineralogical Inc., New York) recently loaned GIA two samples of green mica from Pakistan—one polished stone and one piece of rough weighing 16.54 ct and 3.33 g, respectively (figure 18)—that proved to be none of these. Mr. Douman reported that the material is hosted by mica schist in a remote area about 160 km northeast of the town of Mingora (famous for producing emeralds).

Examination of the cabochon gave the following properties: color—medium bluish green; pleochroism—none; RI—1.59 (flat facet reading from base and spot reading from top); hydrostatic SG—2.89; fluorescence—faint green to long-wave and inert to short-wave UV radiation; Chelsea filter reaction—positive (pink); and a band at ~600 nm and cutoff at ~410 nm observed with a desk-model spectroscope. The physical properties (RI and SG) were consistent with those given for phlogopite and Cr-bearing muscovite, but not for celadonite or margarite, by M. E. Fleet (*Rock-Forming Minerals—Sheet Silicates: Micas*, Vol. 3A, 2nd ed., Geological Society, London, UK, 2003). The properties were also consistent with those cited by Fleet for paragonite—$NaAl_2[AlSi_3O_{10}](OH)_2$. That material is generally colorless to light yellow, but purplish red paragonite has also been reported (e.g., Fall 1993 Gem News, p. 212). Microscopic examination of the two samples revealed a granular texture, while the piece of rough was intergrown with some off-white material (again, see figure 18).

Raman spectra collected from both the cabochon and the rough specimen gave excellent matches for the paragonite spectrum in the RRUFF database (http://rruff.info; sample no. R050447), and were also consistent with a spectrum for paragonite published by A. Tlili et al. ("A Raman microprobe study of natural micas," *Mineralogical Magazine*, Vol. 53, 1989, pp. 165–179). The spectra were not consistent with phlogopite, muscovite, margarite, or celadonite. Raman spectroscopy also identified the off-white material on the rough sample as sodic plagioclase.

EDXRF analysis of both samples revealed major amounts of Na, Al, Si, and K; minor amounts of Ca, Fe, and Sr; and minor or trace amounts of Ti, V, Cr, Ga, Rb, Ba, and Pb. LA-ICP-MS analysis of the rough confirmed the presence of each of those elements, and also detected Li (not detectable by EDXRF), Mg (present in quantities too low to

Figure 20. This attractive 14.04 ct opal (left) displayed interesting and unusual lizard skin–like growth features, but it proved to be of natural origin. It exhibited bright green fluorescence to UV radiation (right). Photos by G. Choudhary.

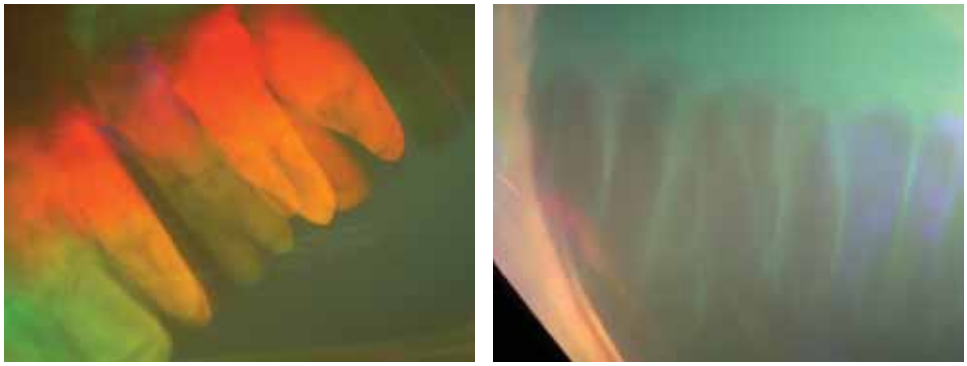

Figure 21. Distinct columnar flashes of color were seen when the opal was illuminated with a fiber-optic light (left). The columns took on a grayish appearance when the light source was placed in certain orientations (right). Note the transparent areas between the grayish zones. Photomicrographs by G. Choudhary; magnified 70× (left), 50× (right).

detect with our EDXRF instrument), and traces of several additional elements. While the elemental concentrations of the samples indicated that paragonite could be the major component, it is possible that micro-inclusions of feldspar might contribute to the excess K and Al that we detected. X-ray diffraction (XRD) analysis of the rough sample was performed by Dr. Anthony Kampf at the Natural History Museum of Los Angeles County. His results were also consistent with paragonite. We concluded on the basis of the structural and compositional evidence that the samples were indeed predominantly paragonite.

The visible region of unoriented UV-Vis-NIR spectra (figure 19) of both samples showed a transmission window at about 505–510 nm, consistent with their blue-green to bluish green color. The spectra also exhibited two areas of strong absorption at approximately 415 and 600 nm, which correspond to Cr^{3+} and/or V^{3+} in muscovite (see, e.g., R. G. Burns, *Mineralogical Applications of Crystal Field Theory*, 2nd ed., Cambridge University Press, Cambridge, UK, 1993). Concentrations of V and Cr obtained from our LA-ICP-MS analysis were ~280 and 580 ppm, respectively. A small peak at ~685 nm was also recorded in the absorption spectra; a similar feature at about 676 nm in Cr-bearing muscovite was attributed to Cr^{3+} by G. H. Faye ("The optical absorption spectra of certain transition metal ions in muscovite, lepidolite, and fuchsite," *Canadian Journal of Earth Sciences*, Vol. 5, No. 1, 1968, pp. 31–38).

According to Mr. Douman, this green mica is from an isolated discovery, from which approximately 20–30 kg/month of mixed-quality rough have been produced seasonally; production is limited by the harsh conditions and remoteness of the area. Gem-quality pieces typically range from 3 to 20 g.

Karen M. Chadwick and Andy H. Shen
GIA Laboratory, Carlsbad

An interesting opal. Recently, staff members at the Gem Testing Laboratory, Jaipur, India, examined an opal that exhibited an interesting and unusual growth pattern. The 14.04 ct oval cabochon (figure 20, left) had a semitransparent, colorless to milky white appearance with distinct play-of-color.

A spot RI of 1.46 and a hydrostatic SG of 2.03 were consistent with opal—natural as well as synthetic. The specimen fluoresced a striking bright green to UV radiation (figure 20, right), with a stronger reaction to short-wave than to long-wave UV.

With magnification and a fiber-optic light, the play-of-color patches appeared to be restricted to zones or planes (figure 21, left), which gave the impression of columns rising from a common base. When the light source was moved, the colors of these zones changed dramatically; in some orientations they appeared grayish (figure 21, right) and revealed the growth structure of this opal. With careful examination, some milky zones were evident between the boundaries of the columns. Viewing along the column direction, we observed a cellular growth pattern (figure 22, left). When the stone was examined while immersed in water, the cellular growth structure showed unexpected whitish zones in a net-like pattern with pseudo-hexagonal

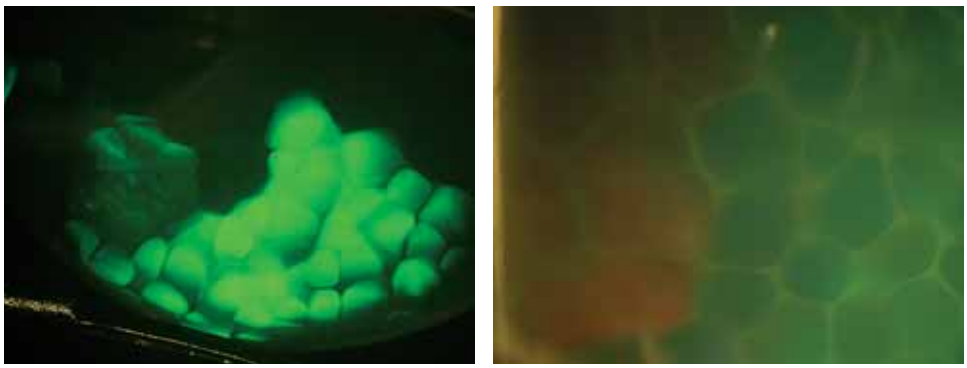

Figure 22. When the opal was viewed down the length of its columnar structure, a cellular pattern became evident in reflected light (left), and a lizard skin–like structure with pseudo-hexagonal whitish boundaries was visible when using transmitted light (right). Photomicrographs by G. Choudhary; magnified 50× (left), 80× (right).

Figure 23. A special engraving technique was used to fashion this single-strand Islamic rosary of black cultured pearls. The round ones range from 11 to 14 mm in diameter. Photo by S. Singbamroong, © Dubai Gemstone Laboratory.

boundaries (figure 22, right), which is very similar to the "lizard skin" effect observed in synthetic or imitation opals.

E. J. Gübelin and J. I. Koivula (*Photoatlas of Inclusions in Gemstones*, Vol. 2, Opinio Publishers, Basel, Switzerland, 2005, pp. 500–501) illustrated similar columnar and cellular patterns in natural opal from Nevada. However, no reports of a cellular structure with whitish boundaries were found during a literature search.

The overall features of this opal indicated natural origin, but FTIR spectroscopy was performed for confirmation. The spectrum was similar to those reported for natural material, with an absorption band in the 5350–5000 cm^{-1} region, a hump ranging from 4600 to 4300 cm^{-1}, and strong absorption from approximately 4000 to 400 cm^{-1}. EDXRF analysis revealed Si and traces of Ca and Fe.

This is another illustration of the importance of careful observation. Misinterpreting the lizard skin–like growth features in this opal could have resulted in a misidentification as synthetic.

Gagan Choudhary (gtl@gjepcindia.com)
Gem Testing Laboratory, Jaipur, India

Figure 24. When examined closely, the engraved cultured pearls showed a glassy appearance. Photo by S. Singbamroong, © Dubai Gemstone Laboratory.

Engraved black cultured pearls. Several fashioning and manufacturing techniques for cultured pearls have been developed in the past decade. These include Komatsu faceted "Flower Pearls" (Summer 1997 Gem News, pp. 146–147) and "Magic Pearls" with gem inlays (Spring 2002 GNI, pp. 97–98). Recently, the Dubai Gemstone Laboratory had the opportunity to see an interesting engraving technique applied to black cultured pearls.

Umit Koruturk of Australian Pure Pearl (Sydney) submitted an attractive single strand of engraved black cultured pearls (figure 23) to the Dubai Gemstone Laboratory

Figure 25. With reflected light, it was obvious that the cultured pearls had been coated with a transparent, colorless substance (left, magnified 20×). Small fissures and exposure of the white shell bead nucleus were seen in areas with thin nacre (right, magnified 12×). Photomicrographs by S. Singbamroong, © Dubai Gemstone Laboratory.

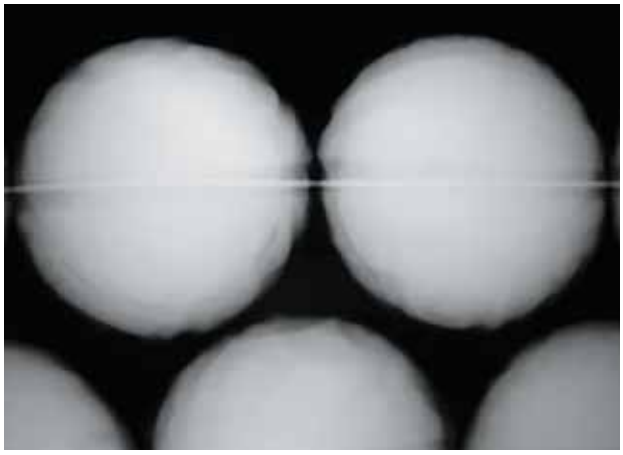

Figure 26. X-radiography revealed nacre thicknesses of only 0.3–0.6 mm in some of the engraved cultured pearls. Image by S. Singbamroong, © Dubai Gemstone Laboratory.

for an identification report. A traditional Islamic rosary, the strand consisted of 33 engraved round pearls (11–14 mm in diameter), two button-shaped pearls used as separators, and an engraved drop-shaped pearl for joining the strand. The cultured pearls had gray, brown, and black bodycolors with overtones varying from rosé to green.

On closer visual examination, the cultured pearls showed a glassy appearance (figure 24). When examined with magnification and reflected light, it was evident that they had been coated with a transparent, colorless substance (figure 25, left), possibly to improve the durability and apparent luster. Some of those with thin nacre showed small fissures and areas in the engraved patterns where the white bead nucleus was exposed (figure 25, right).

The cultured pearls were inert to long- and short-wave UV radiation. X-radiography revealed that the nacre varied from 0.3 to 1.3 mm thick, with a few having nacre in the 0.3–0.6 mm range (figure 26). UV-Vis reflectance spectra consistently revealed absorption maxima at 700 nm, which is characteristic of natural-color black cultured pearls from the *Pinctada margaritifera* oyster. EDXRF analysis also confirmed the absence of manganese and metals such as silver, proving the pearls were of saltwater origin and natural color.

According to Umit Koruturk, the design was drawn on the cultured pearls' surface before the hand-engraving work, which utilized special tools and a unique method that requires an experienced fashioner. The fashioner can engrave from 3 to 10 pearls per day. The company has reserved about 9,000 cultured pearls for this engraving process, mainly consisting of South Sea (Indonesian) material in nearly the entire range of bodycolors and overtones. As of mid-June 2008, approximately 2,000 cultured pearls had been engraved by this technique.

Sutas Singbamroong (sssutas@dm.gov.ae)
and Ayesha Rashid Ahmed
Dubai Gemstone Laboratory
Dubai, United Arab Emirates

***Pinctada maxima* cultured pearls grown beadless in the mantle.** Several lots of oddly shaped silvery white pearls (see, e.g., figure 27) arrived at the SSEF laboratory in March 2008. They were rather flat on one side, with the largest being 19 mm long. Many appeared to be intergrown, and the multiple structures were clearly visible with X-radiography (figure 28). The appearance and growth structure were strongly reminiscent of some beadless freshwater cultured pearls from China. Natural saltwater pearls only very rarely contain two centers and commonly display a more complex growth pattern.

When considering the various methods for culturing pearls, we can postulate a few options for these samples. Both freshwater (e.g., *Hyriopsis, Anadonta, Cristaria*) and saltwater (e.g., *P. maxima, P. margaritifera*) mollusks can be used as hosts for pearl culturing. Growth can be stimulated with a piece of mantle tissue grafted into either the gonad or the mantle. In addition, the tissue piece can be implanted with or without a bead. Thus far, a number of

Figure 27. The five white beadless cultured pearls shown here (up to 19 mm long) were likely mantle grown in a P. maxima *oyster. A pink Chinese freshwater cultured pearl is shown for comparison. Photo by H. A. Hänni, © SSEF.*

Figure 28. X-radiography of the cultured pearls in figure 27 shows their composite nature with multiple centers. The dark lines mark the intergrowths. Image by H. A. Hänni, © SSEF.

combinations have been seen: Freshwater mussel + mantle grown + beadless = a Japanese Biwa cultured pearl or the classic Chinese freshwater cultured pearl. Saltwater oyster + gonad grown + bead = a product such as Akoya or South Sea cultured pearls. Less well known are South Sea "keshi" cultured pearls (saltwater oyster + gonad grown + beadless; see H. A. Hänni, "A short review of the use of 'keshi' as a term to describe pearls," *Journal of Gemmology*, Vol. 30, 2006, pp. 51–58). A more recent development consists of freshwater mussels with coin-shaped beads (freshwater mussel + mantle grown + bead; see D. Fiske and J. Shepherd, "Continuity and change in Chinese freshwater pearl culture," Summer 2007 *Gems & Gemology*, pp. 138–145).

The cultured pearls we examined appeared to be a new variation: saltwater oyster + mantle grown + beadless. These samples (again, see figure 27) showed all the characteristics of a product that was the result of tissue grafted into the mantle of *P. maxima*. It is possible that the host oysters were used for culturing two types of pearl at the same time: beaded, gonad-grown cultured pearls and these beadless mantle-grown products. That the baroque-shaped cultured pearls contained multiple centers joined into a single body reminded us of similar-appearing Chinese freshwater cultured pearls reported in the GNI entry that follows in this issue. As with the "twin" cultured pearl described in that entry, the samples documented here may have resulted from the mantle pieces being placed too close to one another, or the cultured pearls were left in their host mollusks for too long a period of time.

The trade has typically referred to beadless cultured pearls from *P. maxima* and *P. margaritifera* as "keshi." We expect that these new products will appear under this name on the market. While South Sea and Tahitian keshis so far have consisted of gonad-grown cultured pearls formed after bead rejection, the pearls described here are obviously mantle grown, as indicated by their flattened base which suggests formation close to the shell.

Henry A. Hänni

Twinned cultured pearl. The SSEF laboratory is seeing an increasing number of natural pearls for examination. The majority show the typical features of saltwater natural pearls: diagnostic X-ray structures and the absence of Mn as a trace element. The identification of freshwater natural pearls is more challenging because they typically lack beads, so their shape and growth structures are usually the only characteristics that offer clues for identification. LA-ICP-MS is still not a routine technique, and research and chemical sampling are in progress.

In February 2008, we received an unusual 5.61 ct "twinned" pearl (i.e., two intergrown pearls) for identification. Unlike most such pearls, though, the two parts of the intergrowth were different colors (figure 29). There was also a broken surface on one side that suggested that a third pearl was once attached to the other two. X-radiography in two perpendicular directions (figure 30) showed clear evidence that this was a beadless cultured pearl, with two typically shaped central cavities. Analysis of the Mn

Figure 29. This bicolored freshwater cultured pearl (15 × 8 × 6 mm) is actually an intergrowth of two pearls that were undoubtedly stimulated by tissue pieces taken from different areas of the mantle of the donor mollusk. They are shown on the shell of Hyriopsis cumingii, *the most common source of mantle tissue for freshwater pearls cultured in China. The surface of the shell illustrates the variety of nacre colors that can be produced by the mantle tissue. Photo by H. A. Hänni, © SSEF.*

Figure 30. X-radiographs of the twinned pearl show features typical of beadless cultured pearls, especially the characteristic complex-shaped central cavity. Image by H. A. Hänni, © SSEF.

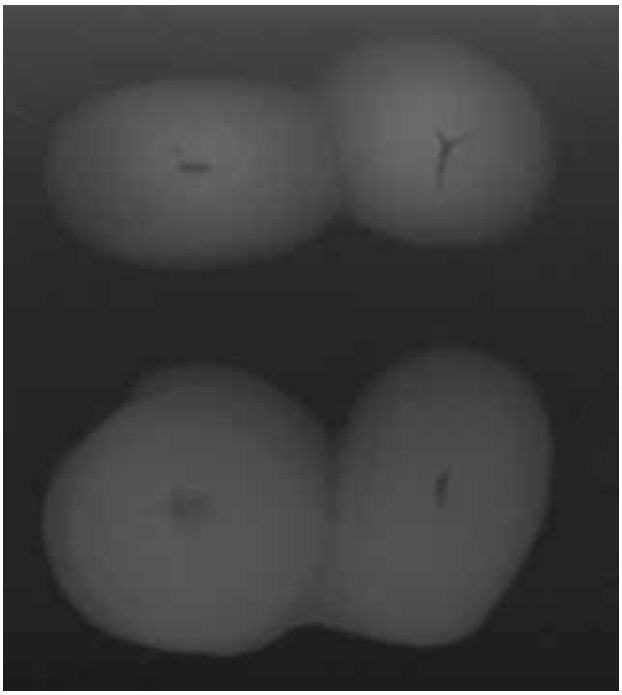

Figure 31. These pallasitic peridot specimens came from an undisclosed location in the United States. The slab measures 45 × 30 mm, and the other samples weigh 1.06, 0.50, 0.67, and 3.47 ct (from left to right; photo by Robert Weldon). The 0.36 ct cabochon in the inset shows good chatoyancy (photo by R. Stinson).

content (by luminescence to X-rays and EDXRF spectroscopy) gave results consistent with freshwater origin. We concluded that this was a beadless cultured pearl such as those produced in China.

Chinese pearl farmers typically culture freshwater pearls by grafting numerous pieces of mantle tissue in multiple closely spaced rows in the mantle of the host mollusk. The color of the resulting cultured pearl is directly related to the original location of the tissue in the donor mollusk. The bicolored nature of this sample probably resulted when tissue pieces taken from different locations of the donor mollusk were placed adjacent to one another. The "twin" resulted either because they were too close, or the cultured pearls were left in the mollusk for too long a period of time.

Henry A. Hänni

Interplanetary cat's-eye peridot. Pallasite, a type of stony-iron meteorite first described in the 18th century, is known for the yellowish green olivine that can be extracted from it. Yet pallasitic peridot, the gem variety of olivine, is extremely rare. (For historical background and a gemological examination of nine faceted samples, see J. Sinkankas et al., "Peridot as an interplanetary gemstone," Spring 1992 *Gems & Gemology*, pp. 43–51.)

At the 2008 Tucson gem shows, meteorite hunter Steve Arnold of Kingston, Arkansas, showed the *G&G* editors five pallasitic specimens: one faceted peridot, one oval peridot cabochon showing chatoyancy, a rough piece of peridot, an irregularly shaped cabochon, and a slab of pallasite containing gem-quality peridot (figure 31). Using a metal detector, Mr. Arnold discovered several kilograms of the material in 2006 near a known meteorite location in the United States. He took the rough to Rick Stinson (Stinson Gemcutting Inc., Wichita, Kansas), who observed that some of the peridot was chatoyant (figure 31, inset), a phenomenon that is very rare in terrestrial peridot. According to Mr. Arnold, the American Museum of Natural History in New York later identified the cause of chatoyancy as parallel, tube-like hollow inclusions.

Peridot is a relatively soft gem material (6.5 on the Mohs scale), and the pallasitic material seems more fragile than peridot mined on Earth, perhaps due to the stress of its passage through the atmosphere and subsequent impact. In fact, a small piece of the peridot cabochon chipped off as the stone was being prepared for photography in Tucson.

Because extracting the gem-quality peridot is so difficult and destructive, Mr. Arnold estimates that less than 1% of the total weight of the recovered meteorite material will be converted into finished gemstones. So far 40 stones have been faceted, ranging from 0.20 to 1.04 ct, and only a few cabochons showing chatoyancy have been cut.

Stuart Overlin (soverlin@gia.edu)
GIA, Carlsbad

New rubies from central Tanzania. At last April's BaselWorld jewelry fair in Switzerland, the SSEF Swiss Gemmological Institute received a number of attractive rubies (e.g., figure 32) with uncommon features. The stones, which were submitted by different dealers, all had a rather saturated red hue, and their internal features indicated they were clearly unheated. The largest weighed 10.75 ct (figure 33). EDXRF qualitative chemical analysis of all the samples established that Cr and Fe were the main trace elements, while Ga was low and Ti and V were below detection limits. The client was sure of the stone's Tanzanian origin and expected to see the country identified on the test report. Because SSEF had not seen faceted rubies with such characteristics before, it was not possible to specify the origin at that time.

However, we recalled a small parcel of rough corundum

Figure 32. These unheated rubies (2.2–3.6 ct) are apparently from a new locality in Tanzania called Winza, near the town of Mpwapwa. Photo by H. A. Hänni, © SSEF.

Figure 33. This 10.75 ct ruby from Winza has no fissures and shows no indications of heating. Courtesy of Gemburi Co., Chanthaburi, Thailand; photo by H. A. Hänni, © SSEF.

(figure 34) from a new deposit in Tanzania that was supplied in January 2008 by Werner Spaltenstein, a buyer in East Africa. These samples were represented to him as coming from the village of Winza, which is located near Mpwapwa, about 85 km east-southeast of Dodoma. The crystals and fragments displayed various habits and crystal faces, the most surprising of which was an octahedron-like variation of a rhombohedral shape (compare with H. A. Hänni and K. Schmetzer, "New rubies from the Morogoro area, Tanzania," Fall 1991 *Gems & Gemology*, pp. 156–167). As with the crystals described by Hänni and Schmetzer (1991), the triangular faces of the Winza samples had fine lines visible with magnification that represented the surface expression of thin twin lamellae.

A comparison of the material from Winza with the cut stones examined during the Basel fair showed a similar chemical composition, and some of the inclusions were identical. These included bent fibers that were actually hollow channels filled with a polycrystalline substance (probably secondary minerals; figure 35, left), as well as partially healed fissures consisting of idiomorphic cavities with a polycrystalline filling of white and black grains (figure 35, right). Therefore, we concluded that the rubies seen at the fair were indeed from Winza.

The faceted gems we have seen thus far from this new deposit suggest that there is considerable potential for high-quality rubies that in some cases do not need enhancement. But as with all deposits, a considerable amount of lower-quality material is also probably present—in this case, as fractured stones with blue color zones. Such corundum will likely be subject to flux-assisted heat treatment to remove the blue spots and "heal" the fractures.

Henry A. Hänni

Ruby and sapphire mining at Winza, Tanzania. As reported in the previous GNI entry, some fine rubies were recently produced from a new deposit at Winza in central Tanzania. In April-May 2008, these contributors undertook separate field research expeditions to the mining area to document its location, mining, and geology, and also to obtain research samples for characterization. Since foreigners are prohibited from visiting the deposit, we had to obtain permission from several government officials, who also supplied police escorts. We are grateful to Dimitri Mantheakis (Lithos Africa, Dar es Salaam, Tanzania), and also to the Saul family (Swala Gem Traders, Arusha, Tanzania) and Tanzanian broker Abdul Msellem for their assistance in arranging our trips to the Winza mining area. Some preliminary observations from our visits are reported here, and further information is in preparation for an article that we plan to submit to *Gems & Gemology*.

The mining area is located approximately 10 km southwest of the village of Winza, and can be reached by four-

Figure 34. These ruby crystals from Winza display rhombohedral and prismatic habits. Some stones contain blue patches in crystallographically defined zones. The largest crystal is 25 mm wide and weighs 17.6 g. Photo by H. A. Hänni, © SSEF.

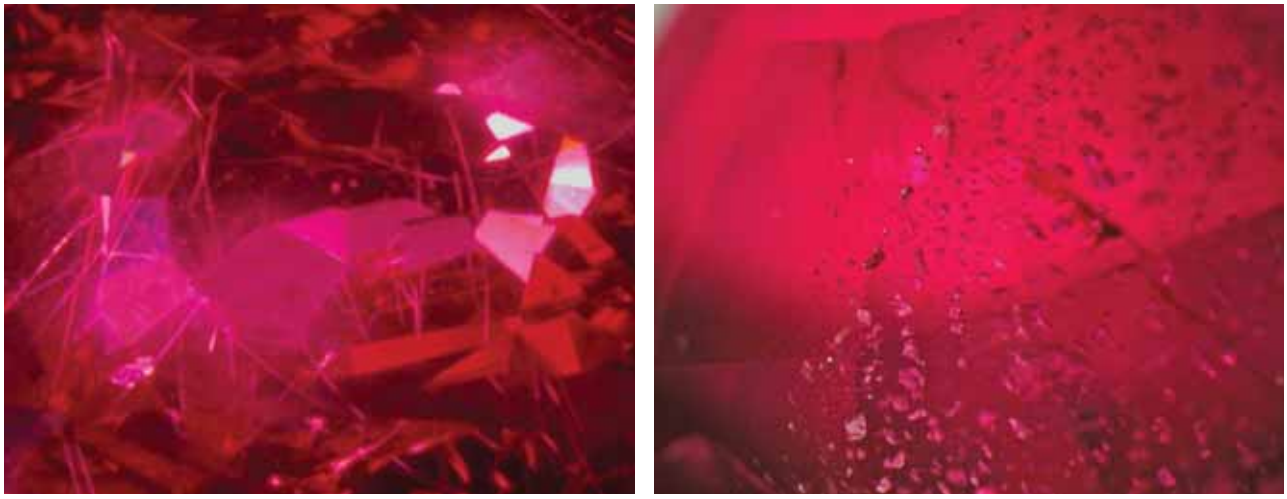

Figure 35. Bent needles, such as these seen in one of the rough Winza rubies (left, magnified 30×), were also present in the 10.75 ct faceted ruby examined at BaselWorld and appear to be characteristic of material from this locality. The partially healed fissure on the right (magnified 20×) consists of multiphase inclusions, which were also commonly seen in the rough Winza rubies and the faceted stones examined at BaselWorld. Photomicrographs by H. A. Hänni, © SSEF.

wheel-drive vehicle in about 2½ hours (much longer during the wettest season, in March-April) from the nearest small town, Mpwapwa. At least 5,000 miners have rushed to the deposit and are using hand tools to excavate shallow pits in eluvial soil (figure 36). The excavated material is loaded into sacks, carts, or trucks, and brought to the nearby stream for washing. There, the soil is wet-screened and the gems are removed by hand (figure 37). In addition, several shafts have been dug by hand to depths reaching 30 m to explore the underlying hard-rock deposits. The corundum occurs within a dark, fine-grained metamorphic host rock, as aggregates and isolated crystals that are well formed and typically color zoned (e.g., with an irregular dark blue surface layer and a pink-to-red interior). Raman analysis of a piece of corundum-bearing host rock by GIA Laboratory staff gemologist Karen M. Chadwick showed that it is composed of amphibole (and is therefore an amphibolite), and locally contains irregular areas of brown garnet that are associated with the corundum.

It appears that most of the ruby and sapphire from Winza has come from the eluvial workings. There was no evidence that any corundum has been produced from the alluvium within the stream where the material is washed. However, in one of the corundum parcels we saw gem-quality pieces of a waterworn pinkish orange mineral represented as garnet, which were reportedly recovered from the same area.

Most of the ruby and sapphire production is being routed to dozens of Thai and Sri Lankan (and a few African) buying offices in Mpwapwa. The material we were shown in Mpwapwa consisted mostly of lower-quality fragments, in a range of colors (often zoned) from blue to violet, purple (rarely), pink, and red. Due to the informal nature of the mining, it was impossible to determine how much corundum was being produced, but we estimate that at the times of our visits the miners were gathering a few kilograms per day of mixed-quality material. By early June, however, the water in the stream had grown scarce, resulting in a corresponding decrease in production (D. Mantheakis, pers. comm., 2008). So far, gem corundum from Winza has been recovered from an area measuring several square kilometers, but the overall size of the deposit is not yet known.

Brendan M. Laurs
Vincent Pardieu
Gübelin Gem Lab
Lucerne, Switzerland

Figure 36. Miners use picks and shovels to excavate shallow pits in search of ruby and sapphire at Winza, Tanzania. Photo by V. Pardieu.

Figure 37. The eluvial soils are brought to the nearby river for washing, screening, and hand-picking of the ruby and sapphire. Photos by B. M. Laurs.

A sapphire with *en echelon* inclusions. Sapphire, whether natural or treated, exhibits a wide range of inclusion features. In addition to their diagnostic value, these features often provide gemologists with interesting imagery. One such sapphire was examined recently at the Gem Testing Laboratory of Jaipur.

The RI and SG of the 11.31 ct light violetish blue mixed-cut oval (figure 38) were consistent with those of natural or synthetic sapphire. There was no reaction to long- or short-wave UV radiation, and no absorptions were seen with the desk-model spectroscope. When examined with magnification, the stone displayed some linear whitish zones of dotted inclusions, which are commonly associated with natural sapphire (heated or unheated). At higher magnification, these zones appeared to be composed of fine white pinpoints arranged *en echelon* (i.e., as subparallel overlapping or step-like features; see figure 39). We could not determine the exact orientation of these linear zones relative to the c-axis, but the optic axis was inclined to the planes containing these features. Hence, we can only speculate that the dotted inclusions were oriented along the dipyramidal faces of the crystal. Although these features did not indicate whether the sapphire had been heated, they offered conclusive proof that the stone was of natural origin, as such inclusions have not been reported in synthetic sapphires.

Other inclusions observed in this sapphire were a "burst halo" centered around a white sugary crystal (figure 40, left) and numerous surface-reaching fingerprint-like

Figure 38. This 11.31 ct sapphire contains some distinctive inclusions. Photo by G. Choudhary.

Figure 39. At relatively high magnification, linear trains of en echelon *inclusions were visible in the sapphire. Photomicrograph by G. Choudhary; magnified 85×.*

Figure 40. The presence in corundum of a white, sugary crystal with an associated stress fracture (left) is typically associated with high-temperature heat treatment. Surface-reaching fingerprint-like inclusions (right) are further evidence of heat treatment. Photomicrographs by G. Choudhary; magnified 80× (left) and 60× (right).

inclusions (figure 40, right), both of which are commonly seen in corundum that has been exposed to high-temperature heating. The latter features are essentially surface breaks into which some foreign substance (e.g., borax) penetrated the stone during heat treatment.

The exact nature of the *en echelon* inclusions could not be determined. However, our observations of the overall inclusion features led us to identify the sapphire as natural with "indications of heat treatment."

Gagan Choudhary

Serpentinite artifact resembling Libyan desert glass. In February 2008, the SSEF Swiss Gemmological Institute received an unusual object (figure 41) that was found at an archeological site in the Lop Nur dry lake bed in the Taklamakan Desert of Xinjiang Province, northwestern China. According to Dr. Christoph Baumer, a Swiss archeologist who worked on the excavation, the artifact was reportedly discovered near a 2,000-year-old jade axe.

The translucent yellow bar (56.02 ct) had a distinctly worked outline. One end was rounded while the other was irregular, suggesting that it had been broken in the past. Visually, the item resembled natural desert glass from Libya. The heavily etched surface was similar to that commonly seen on desert glasses, which have typically been exposed to prolonged abrasion by sand storms (figure 42). However, the uniform shape strongly suggested a manufactured object.

Standard gemological testing was inconclusive: hydrostatic SG—2.59; fluorescence—slightly yellow to long-wave UV radiation and no reaction to short-wave UV; handheld spectroscope—no absorption seen; polariscope reaction—always bright, indicating an anisotropic aggregate. Due to the irregular surface, no refractive index could be measured.

As a next step, the chemical composition of the item was qualitatively determined by EDXRF spectroscopy. In contrast to Libyan desert glass, which is nearly pure silica glass with some minor amounts of Fe and other trace elements, this specimen showed both Si and Mg as main constituents; minor amounts of Fe were also detected. Based on the chemical composition and the appearance between crossed polarizers, it was evident that the material was not a glass but rather a polycrystalline aggregate of a Mg-silicate such as antigorite (serpentine group). The Raman spectrum confirmed this identification, with four distinct peaks at 1045, 688, 377, and 231 cm^{-1}, which matched our reference spectrum for antigorite. In the gem trade, translucent light yellow antigorite is known as *bowenite serpentine*.

Figure 41. This unusual artifact (39.3 × 18.3 × 6.8 mm), which was discovered at an archeological site in the Taklamakan Desert of China's Xinjiang Province, proved to be antigorite (bowenite serpentine). Photo by H. A. Hänni, © SSEF.

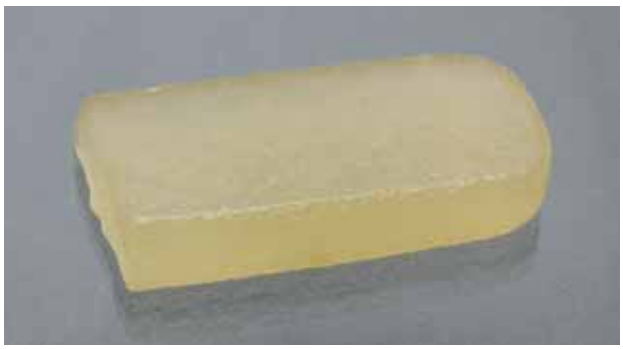

Figure 42. The serpentinite artifact's irregular surface etching is likely due to prolonged abrasion by wind-blown desert sands, as is often seen in desert glasses. Photo by H. A. Hänni, © SSEF.

As antigorite is relatively soft (5.5 on the Mohs scale), it has long been used for jewelry and carving purposes, especially in China (see R. Webster, *Gems*, 5th ed., revised by P. G. Read, Butterworth-Heinemann, Oxford, UK, 1994, pp. 275–276). The etched surface of the broken end indicated that it had been broken before it was exposed to prolonged abrasion in the dry and windy climate of the Taklamakan Desert.

Michael S. Krzemnicki (gemlab@ssef.ch)
SSEF Swiss Gemmological Institute
Basel, Switzerland

Star and cat's-eye topaz from Brazil. Topaz is a common gem, but only rarely does it occur with chatoyancy or asterism. The largest cat's-eye topaz described in the literature thus far was a 270 ct stone from Ukraine (Winter 2004 GNI, p. 346); star topaz has not been previously reported. However, in August 2005 this contributor acquired a star topaz in Brazil, and it was even larger than the 270 ct cat's-eye stone.

The egg-like cabochon (figure 43) weighed 333.27 ct and measured 38.2 × 33.5 × 28.0 mm. It was identified as topaz by standard gemological methods. The stone was filled with semiparallel flat, hollow channels, similar to a pale blue 152.15 ct cat's-eye topaz from Brazil that this contributor also described (figure 44; J. Hyršl, "Some new unusual cat's eyes and star stones," *Journal of Gemmology*, Vol. 27, No. 8, 2001, pp. 456–460).

The channels were much more common in one half of the stone, and the border between the two halves was sharp, confirming that the tubes were the result of a growth phenomenon, not etching. The stone showed two rays when illuminated with a strong spotlight (again, see figure 43). One ray was yellow and oriented perpendicular to the hollow channels. The second ray was white and oriented at an angle of about 40° from the first ray; with magnification, it showed bright iridescent colors (figure 45). The cause of the second ray was apparent only with high magnification: The channels were not smooth inside, but rather showed strong striations at an angle of

Figure 43. This extremely rare star topaz from Brazil (333.27 ct) shows asterism—composed of a vertical yellow ray and a white ray oriented at about 40° to the yellow ray—that is caused by oriented growth tubes and internal striations within the tubes. Photo by J. Hyršl.

Figure 44. This cat's-eye topaz (152.15 ct), also from Brazil, shows chatoyancy resulting from internal features similar to those causing the asterism in the stone in figure 43. Photo by J. Hyršl.

Figure 45. Striations on the inner surface of the subparallel hollow channels are the cause of the reflective white ray in the star topaz. Photomicrograph by J. Hyršl, reflected light; field of view 2 mm.

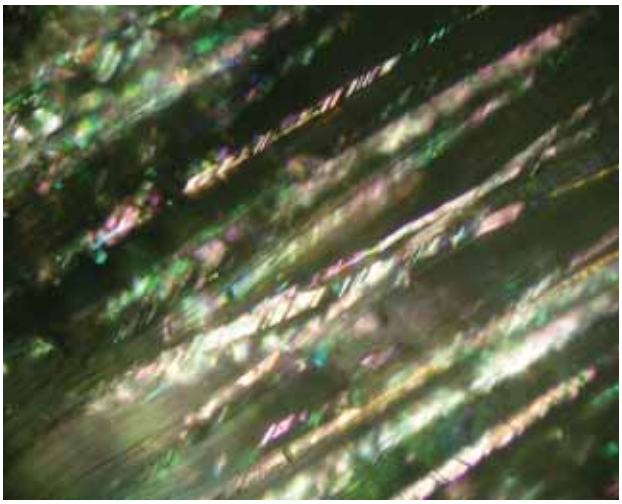

about 40° to their length. Similar striations in topaz were reported by J. I. Koivula more than 20 years ago (see figure 6 in "The rutilated topaz misnomer," Summer 1987 *Gems & Gemology*, pp. 100–103). These striations were responsible for the asterism in the 333 ct topaz and the cat's-eye effect in the 152 ct topaz. Both are likely from the same locality, said to be alluvial cassiterite deposits in the state of Rondônia.

It is interesting to note that there exists a third possible cause of chatoyancy in topaz, which was described by W. Kumaratilake ("Gems of Sri Lanka: A list of cat's eyes and stars," *Journal of Gemmology*, Vol. 25, No. 7, 1997, pp. 474–482). According to this report, chatoyancy in white topaz from Sri Lanka is caused by parallel blade-like sillimanite inclusions. Compared to the stones from Brazil, cat's-eye topaz from Sri Lanka (e.g., figure 46) is much more transparent, the internal chatoyancy-causing features are very fine, and the eye is sharper.

Jaroslav Hyršl (hyrsl@kuryr.cz)
Prague, Czech Republic

A new source of Persian turquoise: Kerman, Iran. The Iranian Neyshabur mines in Khorasan Province have historically been known for producing the finest Persian turquoise. However, in recent years these deposits have not yielded much high-quality material. In 2005, a new turquoise area was discovered in Kerman Province, 1,200 km southwest of the Neyshabur mines. This new mining area is located approximately 90 km northeast of the town of Bardsir (Mashiz), at 30°03′ N and 56°30′ E. The mine is owned by local people from Kerman City, who employ about eight workers and use an excavator. The turquoise was found accidentally while they were searching for copper. Summers in this region are dry with daytime temperatures typically over 38°C (100°F), while winters are rainy with occasional snowstorms.

Figure 47. A new source of turquoise has been discovered near Bardsir in Kerman Province, Iran. The three cabochons and two partially polished pieces (9.49–29.79 ct) were characterized. Photo by Robert Weldon.

Figure 46. In this cat's-eye topaz from Sri Lanka (28.24 ct), the chatoyancy is caused by oriented sillimanite inclusions. Photo by J. Hyršl.

Approximately 800–1,000 kg of mixed-quality turquoise (including porous chalky material) was recovered in the 2007–2008 mining season (starting in June-September and going until December). The color range is similar to that from the Neyshabur mines, varying from very light blue to "sky" blue (e.g., figure 47). Some dark greenish blue to yellowish green material has also been recovered. As much as 5% of the total production is high-quality "sky" blue material, which is usually found in small sizes ranging from 1 to 5 cm (although larger pieces have been recovered; see, e.g., figure 48).

The geology of this area is similar to that at Neyshabur. The turquoise is hosted by a deeply weathered porphyritic volcanic rock (trachyte) that contains phenocrysts of alkali feldspar and quartz, and is locally cemented by limonite (all minerals identified solely by visual means).

One piece of rough, two partially polished pieces, and three cabochons of the Bardsir turquoise were loaned to

Figure 48. Some large pieces of high-quality turquoise (here, 12 × 7 cm) have been recovered from the Bardsir deposit. Photo by M. Douman.

GIA for examination (again, see figure 47). One of us (EAF) determined the following properties on the five polished stones: color—greenish blue, with no pleochroism; spot RI—1.61–1.62; hydrostatic SG—2.65–2.75; Chelsea filter reaction—none; fluorescence—weak blue to long-wave and inert to short-wave UV radiation; and an absorption band at 430 nm visible with the desk-model spectroscope. These properties are consistent with those reported for turquoise by M. O'Donoghue, Ed. (*Gems*, 6th ed., Butterworth-Heinemann, Oxford, UK, 2006, pp. 323–328). Microscopic examination revealed inclusions of quartz, pyrite, and chalcopyrite, all identified by Raman analysis.

The higher-quality material from this new deposit does not need any treatment, and the availability of some pieces in rather large sizes is also encouraging.

Makhmout Douman (makhmout@arzawa.com)
Arzawa Mineralogical Inc., New York

Eric A. Fritz
Denver, Colorado

A rare faceted yellow vanadinite. Vanadinite [$Pb_5(VO_4)_3Cl$] is an uncommon mineral found in arid climates that forms as a result of the oxidation of primary lead minerals (W. L. Roberts et al., Eds., *Encyclopedia of Minerals*, Van Nostrand Reinhold, New York, 1974, p. 646). Faceted vanadinite is extremely rare. However, gem dealer Mark Kaufman recently loaned a 2.40 ct bright yellow round modified brilliant vanadinite (figure 49) to GIA for study. He cut the stone from rough material supplied by Dr. Rob Lavinsky (The Arkenstone, Garland, Texas), who reported that it came from a new surface prospect at an undisclosed locality in the Democratic Republic of the Congo (DRC).

Figure 49. This extremely rare 2.40 ct vanadinite was cut from material reportedly recovered from a new surface prospect located in the DRC. Photo by Robert Weldon.

The faceted vanadinite yielded the following properties: color—highly saturated yellow; RI—over the limit of the refractometer; birefringence—high, as evidenced by the strong doubling of the crown facet edges when viewed through the pavilion; hydrostatic SG—7.24; fluorescence—weak orange-red to long- and short-wave UV radiation. No absorption features were observed with the desk-model spectroscope. With the exception of the bright yellow color,

Figure 50. The faceted vanadinite contained a healed fissure consisting of minute particles in parallel formations. Photomicrograph by R. Befi; image width 1.0 mm.

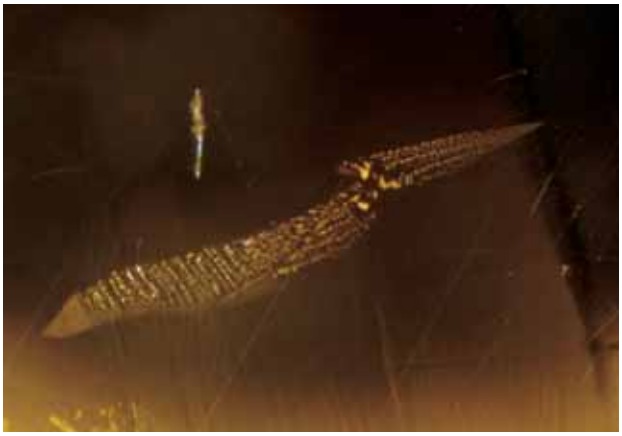

these properties are consistent with those reported for vanadinite by Roberts et al. (1974).

The faceted stone was transparent, with only a few inclusions. Microscopic examination showed two small "fingerprints" (see, e.g., figure 50) and long, thin growth tubes intersecting tiny flat inclusions. No growth banding or color zoning was observed. The girdle was chipped; the crown, table, and pavilion showed abrasions and scratches; and the facet edges were rounded rather than sharp. This was consistent with vanadinite's low hardness (2½–3 on the Mohs scale) and brittleness.

The chemical composition of the faceted stone (determined by EDXRF) was also consistent with vanadinite, with major amounts of Pb and V. The Raman spectrum, taken with 514 nm laser excitation, consisted of peaks at 828, 356, and ~324 cm^{-1}, matching our vanadinite reference. The UV-Vis-NIR absorption spectra showed that the ordinary ray and extraordinary ray had similar absorption peaks at 589, 754, and 807 nm.

Vanadinite is known from several localities, including the U.S., Mexico, Scotland, Sardinia, Austria, Russia, Algeria, Tunisia, and Morocco. To the best of this contributor's knowledge, this is the first report of vanadinite from the DRC. In addition, this is believed to be the first faceted vanadinite examined at the GIA Laboratory.

Riccardo Befi (riccardo.befi@gia.edu)
GIA Laboratory, New York

SYNTHETICS AND SIMULANTS

Experimental CVD synthetic diamonds from LIMHP. The SSEF Swiss Gemmological Institute recently studied two near-colorless (slightly gray; figure 51) slices of synthetic diamond grown by chemical vapor deposition (CVD) at the Laboratoire d'Ingénierie des Matériaux et des Hautes Pressions (LIMHP) in Paris. One sample (4.15 × 3.70 × 0.20 mm, 0.05 ct), referred to here as sample A, showed features typical of CVD synthetic diamond (P. M. Martineau et al., "Identification of synthetic diamond grown using chemical vapor deposition [CVD]," Spring 2004 *Gems & Gemology*, pp. 2–25). However, the other slice (4.01 × 3.99 × 0.35 mm, 0.09 ct; sample B) showed features that were quite distinct from those of previous CVD synthetic diamonds grown at LIMHP, which were described by W. Wang et al. ("Experimental CVD synthetic diamonds from LIMHP-CNRS, France," Fall 2005 *Gems & Gemology*, pp. 234–244).

Observed between crossed polarizing filters, the two samples showed very different reactions: Sample A displayed considerable strain, similar to the cross-hatched "tatami" patterns observed in natural type II diamonds, while sample B was nearly strain free. Microscopic examination revealed the presence of very small whitish and roundish inclusions in both samples.

In contrast to earlier reports, in which orange-red fluorescence was commonly observed in CVD synthetic diamonds (see, e.g., P. M. Martineau et al., 2004), both slices

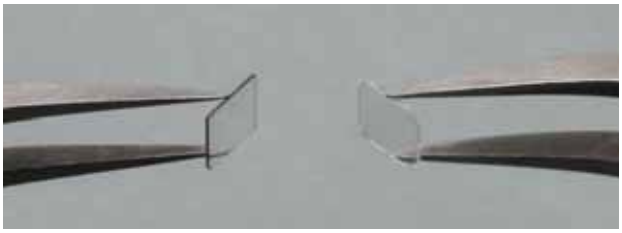

Figure 51. These thin slices of CVD synthetic diamonds (~4 × 4 mm) were grown by LIMHP in Paris. Sample A is shown on the left, and B is on the right. Photo by L. Phan, © SSEF.

were inert to long- and short-wave UV radiation, similar to the more recent samples described by W. Wang et al. ("Latest-generation CVD-grown synthetic diamonds from Apollo Diamond Inc.," Winter 2007 *Gems & Gemology*, pp. 294–312). Examination with the DiamondView instrument revealed two parallel zones in sample A when observed from the side, due to growth in layers (figure 52), which is typical for the CVD process. One zone had a bluish reaction and the other zone was inert. Sample B was entirely inert.

FTIR spectroscopy showed no nitrogen or boron above the detection limit in either sample, classifying them as type IIa. However, sample A showed two large bands centered at 4723 and 4659 cm^{-1}, which have not been previously reported. The UV-Vis-NIR spectra (200–1800 nm) of both samples matched those of near-colorless type IIa diamonds, with no absorption features except a weak progressive absorption from 450 nm to a cutoff at 225 nm.

The photoluminescence spectra, recorded at liquid-nitrogen temperature (77 K) with a 514 nm laser source, were very interesting. Sample B showed only the intrinsic diamond Raman peak at 1332 cm^{-1}; the Si-V center, usually present at about 737 nm, was notable by its absence.

Figure 52. Sample A, when observed from the side in the DiamondView instrument, shows two different fluorescence zones, a sign of growth in layers. Photo by P. Lefèvre, © SSEF.

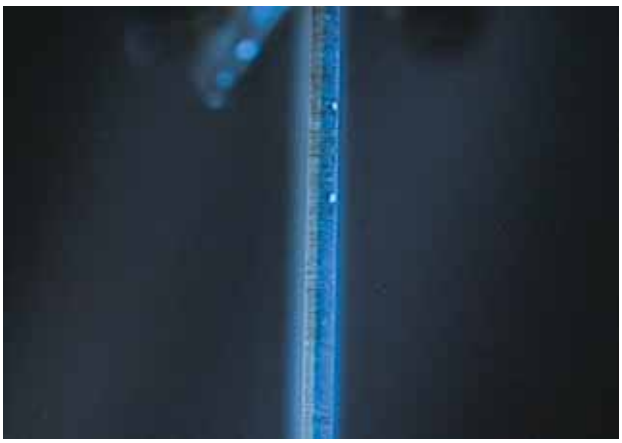

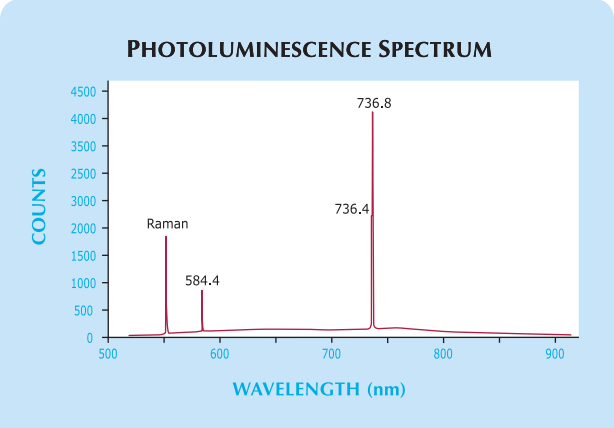

Figure 53. The photoluminescence spectrum of CVD synthetic diamond sample A shows a doublet at 736.4 and 736.8 nm, characteristic of Si-V centers.

This matches results obtained by Martineau et al. (2004) for CVD synthetic diamond grown by Element Six and by Wang et al. (2007) for samples provided by Apollo Diamond, which also did not show this defect. The PL spectrum of sample A (figure 53) showed peaks at 584.4, 736.4, and 736.8 nm; the latter two formed a doublet that is characteristic of Si-V centers.

These two samples were interesting because, although they were grown in the same plasma reactor, different experimental parameters (F. Silva, LIMHP, pers. comm., 2007) led to completely different characteristics. Sample A was relatively easy to identify as CVD synthetic diamond using the DiamondView and PL spectroscopy. The other sample was more difficult, because it did not show the typical growth and spectroscopic characteristics, especially Si-V centers in its PL spectrum at 514 nm excitation. (However, it is possible that Si-V centers could have been resolved using 633 nm excitation, but this was not available on our instrument.) Additionally, both stones lacked the orange-red UV fluorescence that previously aided identification by gemological testing.

These two samples were too thin to be cut into gemstones, but larger samples may be grown in the future that lack the typical features of CVD synthetic diamonds, similar to sample B, and these could present significant identification challenges.

Pierre Lefèvre and Jean-Pierre Chalain (gemlab@ssef.ch)
SSEF Swiss Gemmological Institute
Basel, Switzerland

Unusual glass imitation of rubellite. We recently examined a 30.12 ct gem that had been sold as rubellite in Jaipur, India. When observed face-up, it convincingly resembled a color-zoned rubellite (figure 54). When observed perpendicular to its width, however, the specimen had a very uneven coloration, with alternating colorless and vivid pink cylinders (figure 55). The sample was singly refractive (1.47 RI) and had a hydrostatic SG of 2.51. It was inert to long-wave UV radiation and fluoresced strong chalky blue to short-wave UV. With the microscope, one could see elongated bubbles parallel to the colored cylinders. In some cases, the bubbles were so elongated that they reached both sides of the faceted stone, mimicking growth channels. All these gemological properties were consistent with a manufactured glass.

To determine the exact composition of this glass and look for possible variations between the pink and colorless zones, we analyzed its chemical composition with a JEOL 5800 scanning electron microscope equipped with a high-resolution Princeton Gamma Tech IMIX-PTS germanium energy-dispersive detector. The instrument was operated

Figure 54. This 30.12 ct piece of faceted glass was sold as rubellite. The elongated straight lines are gas bubbles. Photo by B. Mocquet.

Figure 55. This side view of the sample reveals that the glass is made up of successive colorless and vivid pink cylindrical layers. Photo by B. Mocquet.

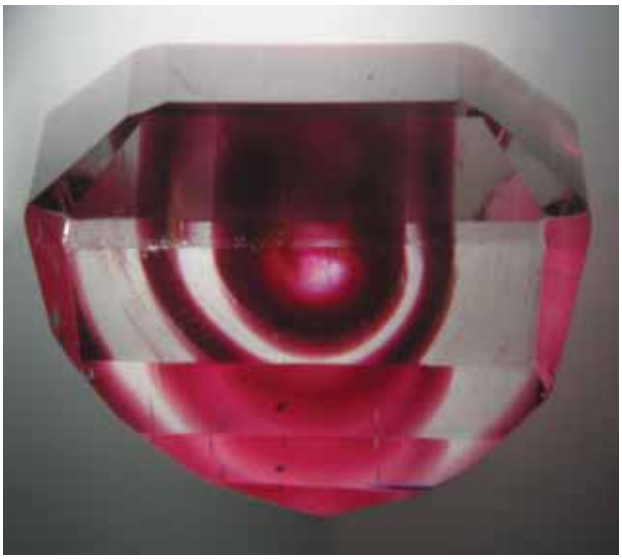

using an accelerating voltage of 20 kV, a current of 1 nA, and a 37° take-off angle. The composition was consistent with a glass, containing 78.0% SiO_2, 4.3% K_2O, 2.5% CaO, 9.7% Na_2O, 1.0% Al_2O_3, 1.0% BaO, 0.6% ZnO, 0.5% MgO, and 0.2% FeO (values expressed in wt.%). We did not detect any systematic chemical differences between the pink and colorless zones.

To understand the origin of the pink color, we measured the UV-Vis absorption spectrum of this glass with a Unicam UV4 spectrophotometer in the 350–800 nm range. The main spectral features were a broad band centered at ~540 nm and a continuum of absorption regularly increasing from the red to the UV region. A similar broad band has been observed in "ruby glass" of equivalent color (Jean-Pierre Razmoket, pers. comm., 2008). Therefore, the coloration was likely due to Mie scattering on submicroscopic metallic inclusions of either gold or copper (G. Mie, "Beiträge zur Optik trüber Medien, speziell kolloidaler Metallösungen [Contributions to optics, opaque media, especially metal colloidal solutions]," *Annalen der Physik*, Vol. 4, No. 25, 1908, pp. 377–445). We could not observe these features using the SEM because they are likely smaller than the resolution of our instrument.

This type of material, in particular the pink central cylinders, is not unlike Venetian glass, widely used for centuries as man-made jewels or gem imitations.

Benjamin Rondeau, Emmanuel Fritsch, Yves Lulzac, and Blanca Mocquet

Tourmalines and their imitations obtained in Kandahar, Afghanistan. Matthew McCann, stationed with the American forces in Kandahar, Afghanistan, purchased five gems represented as tourmalines (figure 56) in the local bazaar. He suspected that the two largest of these (10.58 and 11.35 ct) were fake, because of their relatively large sizes combined with the fact that they were eye-clean and bicolored in unusual hue combinations for tourmaline: purple/near colorless and yellow/green. Mr. McCann sent all five samples to the University of Nantes for analysis.

When observed from the side, the large yellow/green emerald cut displayed a planar colorless zone a little over 1 mm thick, with parallel yellow zones on both sides that were 3–4 mm thick (figure 57, left). Green zones flanked the yellow areas (although only one green zone is shown in figure 57, left). A series of purple and near-colorless lamellae were visible across the width of the pavilion in the other large emerald cut (figure 57, right).

Figure 56. These five gems were sold as tourmalines in a bazaar in Kandahar, Afghanistan. The two larger emerald cuts proved to be quartz, one natural (purple/near colorless, 10.58 ct) and one synthetic (yellow/green, 11.35 ct). Photo by Alain Cossard.

Both samples had RIs of 1.54–1.55, a hydrostatic SG of 2.65, no luminescence to UV radiation, and were uniaxial positive. These properties identified them as quartz rather than tourmaline. Neither sample showed twinning, and in both the optic axis was roughly parallel to the table. In addition, the colorless zone in the yellow/green emerald cut was perfectly planar, with minute inclusions bordering it on both sides, corresponding to the seed plate in synthetic quartz. The purple/near-colorless zoning of the other large stone indicated that it was a natural amethyst, as such zoning is known in natural quartz but has not been reported in synthetic quartz.

The other three stones—a dark green 1.42 ct oval, a slightly greenish yellow 0.64 ct round, and a 1.33 ct bicolored green-pink emerald cut (again, see figure 56)—proved to be tourmalines, as indicated by their RIs of about 1.62–1.64, SG of ~3.05, and uniaxial negative optic character. The last two stones actually appeared biaxial on the refractometer

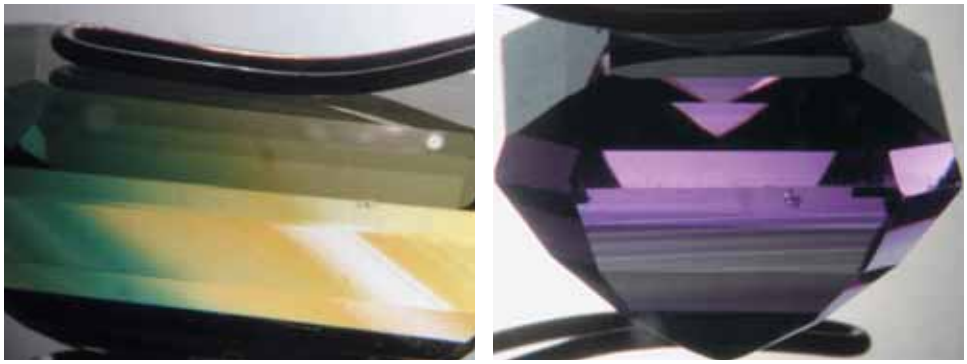

Figure 57. Symmetrical yellow and green zoning ran parallel to a colorless seed plate in the 11.35 ct synthetic quartz (left); note the pinpoint inclusions near the seed. The sharp, fine, parallel-planar zoning seen in the 10.58 ct purple/near-colorless quartz (right) has not been reported in synthetic amethyst. Photomicrographs by E. Fritsch.

(i.e., n_o = 1.633–1.641 and n_e = 1.618–1.628 for the greenish yellow stone; n_o = 1.635–1.640 and n_e = 1.620–1.640 for the bicolored tourmaline), but uniaxial with the conoscope (the optic figure in the bicolored stone could only be seen with immersion in heavy liquid). This somewhat unusual behavior might be explained in part by internal stress, which was visible between crossed polarizers as a "tatami" pattern.

This is a good example of synthetic stones being used as imitations of yet another gem variety. Also, it reinforces the fact that even buying stones close to the source can be problematic without some basic identification equipment.

Emmanuel Fritsch, Yves Lulzac, and Benjamin Rondeau

CONFERENCE REPORTS

Sinkankas Garnet Symposium. The sixth annual symposium in honor of John Sinkankas took place April 19, 2008, at GIA in Carlsbad. Co-hosted by GIA and the San Diego Mineral and Gem Society, the sold-out event had 148 people in attendance.

After opening remarks by convener Roger Merk (Merk's Jade, San Diego, California), **Lisbet Thoresen** (Beverly Hills, California) reviewed the use of gem materials (including garnet) by Bronze Age and Classical cultures. She noted that the following inclusions have been documented within garnets set in ancient objects: rutile needles, apatite, metamict zircon, monazite with tension halos, and possibly ilmenite. **Dr. William "Skip" Simmons** (University of New Orleans) covered the mineralogy and crystallography of the garnet group. Of the 15 garnet species recognized by the International Mineralogical Association, only four (pyrope, almandine, spessartine, and grossular) are important gem materials. **Si Frazier** (El Cerrito, California) reviewed the history and lore of garnets. He noted that lapidaries used heavy steel weights to break almandine garnet from western Europe, with the resulting tabular pieces aptly suited for carvings or gem inlay. **William Larson** (Pala International, Fallbrook, California) reviewed the sources and mining for Russian demantoid. Within the past two years, several small alluvial deposits have been discovered in the Ural Mountains near the historic mines.

Meg Berry (Mega Gem, Fallbrook, California) illustrated the faceting and carving of garnet, showing how the appearance of overdark rhodolite can be lightened by cutting a 40° facet at each corner, and describing the successful carving of large pieces of spessartine (80 and 137 ct) into free-form designs. **Robert Weldon** (GIA, Carlsbad) provided suggestions for getting the best photos of garnets—applicable to other gems as well—including the use of light backgrounds for dark stones (and vice versa) and diffused lighting to avoid hot spots (with the exception of capturing the phenomenon in iridescent garnets, which are best photographed using a fiber-optic light source). **Dr. William Hanneman** (Hanneman Gemological Instruments, Rio Rancho, New Mexico) discussed garnet nomenclature, and stressed the importance of correlating any new garnet trade names with their proper mineralogical equivalent.

John Koivula (GIA, Carlsbad) reviewed the wide variety of internal features found in garnet (e.g., growth zoning, strain, and inclusions such as sulfides, rutile, Cr-diopside, and forsterite), and also the occurrence of garnet as an inclusion in other minerals (e.g., spessartine in quartz, chrysoberyl, topaz, beryl, and obsidian). **Dr. George Rossman** (California Institute of Technology, Pasadena) reviewed the primary causes of color in garnets, which relate to Fe^{2+}, Fe^{3+}, Cr^{3+}, V^{3+}, Mn^{2+}, and Mn^{3+}, as well as Fe^{2+}-Ti^{4+} interactions.

The theme of next year's Sinkankas Symposium (date to be determined) will be spinel.

Brendan M. Laurs

2008 Scottish Gemmological Association conference. This conference, held May 2–5 at The Queens Hotel in Perth, Scotland, featured a variety of topics.

Dr. George Rossman (California Institute of Technology, Pasadena) delivered two talks. The first described his latest research on nanoscale features in minerals that relate to origin of color and optical phenomena. These included the cause of asterism in rose quartz (which is due to nanofibers of a new mineral related to dumortierite), star almandine from Idaho (minute hollow tubes), and star corundum (rutile in Sri Lankan and diaspore in Tanzanian material). Dr. Rossman's second talk focused on historic and modern technologies for modifying color in gem materials (beryl, zircon, corundum, amethyst, and tourmaline), and the current understanding of the atomic processes involved in such treatments.

David Callaghan (London), formerly senior director of the estate jeweler Hancocks, offered insight into jewelry from the Art Deco period leading up to the abdication of Edward VIII, and reviewed various pieces the monarch gave to the Duchess of Windsor. In particular, he described her flamingo and panther brooches, and also her charm bracelet consisting of gemstone crosses that the duke had engraved with secret messages for special occasions.

Alan Hodgkinson (Ayrshire, Scotland), the Association's president, presented methodology for "top-lighting the refractometer," in which a light beam is passed vertically down through the stone placed on the hemicylinder. He also reviewed techniques for dealing with tiny stones and uneven cabochon surfaces, and described the ideal amount of liquid used for the spot RI method.

Elisabeth Strack (Gemmological Institute of Hamburg, Germany) discussed the results of her testing of the emeralds in Mogul objects from the Gold Room at the Hermitage State Museum in St. Petersburg, Russia, which date from the 16th century. She concluded that the emeralds were Colombian, given the fact that they contained jagged three-phase inclusions. She also detected oil residue in fissures and fractures. Her tests were performed using only limited gemological techniques since she did not have access to advanced instrumentation in the museum.

Stephen Whittaker (Fellows and Sons Auctioneers,

Birmingham, UK) reviewed the wide variety of interesting and unusual items that have recently passed through the auction house. Some of the items received far more attention and higher bids than anticipated due to publicity.

In addition to the keynote talks, several short presentations were delivered. **Brian Jackson** (National Museum of Scotland, Edinburgh) discussed strong yellow and blue pleochroism in apatite from Lake Baikal, Russia. **Harold Killingback** (independent gemologist) explored asterism in rose quartz using a red laser pointer and some reflectors. **Anton Vasiliev** (LAL, Moscow, Russia) described how his Facet Design Software helps plan and predict the result of cutting colored stones by accounting for the lighting, transparency, RI, and proportions.

Rounding out the event were several workshops, on "Emerald Inclusions," "Spectra of Red Stones," "Facet Design Software," "Opals," "Filters," and "Auction Items," as well as a post-conference field trip to collect an ornamental stone called haggis rock from the Peebles area of Scotland. The group also visited Lauriston Castle to see the famous Blue John collection.

Cigdem Lule-Whipp (cigdem@gialondon.co.uk)
GIA London

ANNOUNCEMENTS

CIBJO introduces *Precious Metals Blue Book*. CIBJO, the World Jewellery Confederation, recently launched the first edition of its *Precious Metals Blue Book*. This publication, aimed at ensuring consumer confidence and promoting best practices, provides standards for precious metal alloys, finenesses, weights, colors, tolerances, solders, coatings/platings, and markings. It covers precious metal jewelry, flatware, and hollowware. The manual will soon be available in electronic format on the CIBJO website, www.cibjo.org.

Conferences

IGC 2008. Held in Oslo, Norway, on August 6–14, the *33rd International Geological Congress* will include sessions with possible applications to gemology: mineral spectroscopy; metallogeny and mineral potential of Russia, Belarus, and Ukraine; geology of Africa; and development strategies for the mining sectors of African countries. Visit www.33igc.org.

9th International Kimberlite Conference. Held August 10–15, 2008, in Frankfurt, Germany, this conference will bring together the academic and diamond exploration communities to exchange information on kimberlites, related rocks, and diamonds. Visit www.9ikc.com.

WJA "Women in the Know" conference. The Women's Jewelry Association will host its second annual West Coast "Women in the Know" conference August 15, 2008, in Los Angeles. It will include presentations on leadership skills, entrepreneurship, luxury marketing strategies, jewelry manufacturing, and more. The conference will directly precede the West Coast Jewelry Show, which runs August 16–18. Visit www.womensjewelry.org.

IUCr2008. Crystal growth, characterization, and analytical techniques will be covered at the *21st Congress and General Assembly of the International Union of Crystallography*, held in Osaka, Japan, August 23–31. Visit www.congre.co.jp/iucr2008.

FIPP 2008 gem show and mine tour. The International Gem Fair known as FIPP (Feira Internacional de Pedras Preciosas) will take place in Teófilo Otoni (Minas Gerais, Brazil) August 26–30, 2008. Following the show, a 10-day tour will visit various gem deposits in Minas Gerais. There will be an optional four-day extension to the amethyst mines of Rio Grande do Sul State. Visit http://customgroup.travel/brazil/tour.htm. An 11-day Brazilian gem tour can also be scheduled through www.tourguidebrazil.com/mineraltour.html.

6th International Conference on Mineralogy and Museums. Held September 7–9, 2008, at the Colorado School of Mines, Golden, Colorado, conference themes are the relationships between museums and research, collection management, and society. Gems will form a significant part of the program, and pre- and post-conference field trips are being planned to kimberlite and pegmatite sites in Colorado. Visit www.mines.edu/outreach/cont_ed/ICMM6.

Diamond 2008. The *19th European Conference on Diamond, Diamond-like Materials, Carbon Nanotubes, and Nitrides* will be held in Sitges, Spain, September 7–11. Program topics include the growth, processing, and characterization of diamond. Visit www.diamond-conference.elsevier.com.

Rapaport International Diamond Conference. Taking place September 8, 2008, in New York, this conference will cover diamond finance, rough supply, manufacturing, commoditization, and fair trade jewelry. E-mail IDC@diamonds.net.

ICAM 2008. Gems will be one of the subjects covered at the *9th International Congress for Applied Mineralogy*, held September 8–10 in Brisbane, Australia. Visit www.icam2008.com.

World of Gems. The inaugural session of this conference, addressing current developments in gem treatments, identification, diamond grading, and appraisal issues, will be held September 13–14, 2008, in Chicago, Illinois. Visit www.worldofgemsconference.com.

GemFest Asia Hong Kong 2008. The GIA Alumni Association will host GemFest Asia on September 19, during the Hong Kong Jewellery & Watch Fair at the Hong Kong Convention and Exhibition Centre, Room 601. This

free educational event will feature a keynote presentation by Dr. James Shigley titled "Adventures on the Gem Trail: How GIA Research Uncovers Country of Origin." Continental breakfast will be served from 8:30 to 9:00 a.m., followed by GemFest from 9:00 to 10:30 a.m.

Gem-A Centenary Conference and 2008 European Gemmological Symposium. The Gemmological Association of Great Britain (Gem-A) will hold its annual conference October 25–26 in London. In conjunction with its centennial celebration, Gem-A will also be hosting this year's European Gemmological Symposium. Day one will highlight the history of gemology and the jewelry trade, and day two will discuss practical tips and new technologies for the modern gemologist. Visit www.gem-a.info/membership/conferences.htm.

Gems in objects of cultural heritage. An international conference titled *Geoarchaeology and Archaeomineralogy: Impact of Earth Sciences in the Study of Material Culture* will take place in Sofia, Bulgaria, October 29–30, 2008. One of the conference topics will be "Archaeomineralogy and Gemmology." A field trip will focus on the "Role of Bulgaria in the History of World's Jewellery Art." Visit http://mgu.bg/docs/CircularEN.doc.

GIT 2008. The Gem and Jewelry Institute of Thailand will host the *2nd International Gem & Jewelry Conference* December 11–14 in Bangkok. The program will feature a two-day technical session, with oral and poster presentations, followed by a two-day excursion to the Kanchanaburi sapphire deposits. Abstracts are welcomed. Visit www.git.or.th/eng/eng_index.htm.

IDCC-2. The 2nd International Diamond Cut Conference will take place in Lausanne, Switzerland, March 22–25, 2009, just before the Basel World 2009 Jewelry and Watch Fair. A diamond cut exhibition will take place at the fair. Visit http://idcc2.octonus.com.

Exhibits

Exhibits at the GIA Museum. From now through December 2008, "Facets of GIA" explains the various gemological services that GIA provides, including diamond grading, gem identification, education, and public outreach. The exhibit is illustrated with superb gems, crystals, and jewelry. Also currently on display in the Rosy Blue Student Commons are photo essays by Robert Weldon, manager of photography and visual communications at the GIA Library, and *Gems & Gemology* editor Brendan Laurs, depicting emerald mines in Colombia and the Paraíba-type tourmaline deposit in Mozambique, respectively (for more on the latter, see the article in the Spring 2008 issue of *G&G*). Advance reservations are required; to schedule a tour, call 760-603-4116 or e-mail museum@gia.edu.

IN MEMORIAM
GEORGE S. SWITZER (1915–2008)

Distinguished mineralogist George S. Switzer died March 23 at the age of 92.

Dr. Switzer was born in Petaluma, California, and graduated in 1937 from the University of California at Berkeley. He received a master's degree in mineralogy in 1939 and a doctorate in 1942, both from Harvard University.

After teaching at Stanford University and Harvard, Dr. Switzer served as GIA's director of research from 1946 to 1947. He published a dozen articles and news items for *Gems & Gemology* during this time and wrote several others after he left to work at the U.S. Geological Survey.

Dr. Switzer joined the Smithsonian Institution's National Museum of Natural History in 1948, where he was associate curator in the Mineralogy and Petrology Division until 1964 and chairman of the Mineral Sciences Department from 1964 to 1969. He was curator emeritus until his retirement in 1975. In 1979, he and Dr. Cornelius S. Hurlbut published the classic book *Gemology*.

During his tenure at the Smithsonian, Dr. Switzer was instrumental in building the museum's National Gem Collection. In 1958, he persuaded Harry Winston to donate the legendary Hope diamond. Another highlight of his career at the Smithsonian was the purchase of one of the first electron microprobes to analyze lunar rock samples brought back from Apollo missions during the early 1970s.

In retirement, Dr. Switzer pursued his hobby of azalea propagation, eventually serving as director of the Azalea Society of America and assistant editor of its quarterly journal.

Dr. Switzer is survived by his wife of 68 years, the former Sue Bowden; two sons, Mark and James; eight grandchildren; and 12 great-grandchildren.

BOOK REVIEWS

Henry Dunay: A Precious Life

By Penny Proddow and Marion Fasel, 223 pp., illus., publ. by Harry N. Abrams [www.hnabooks.com], New York, 2007. US$60.00

This beautiful work is not only a gift to inspire the collector but also a must-read for the designer, master goldsmith, and jewelry enthusiast. The reader will be transported into an American dream story of drive and passion that produced one of the great jewelry designers of our time. The book is divided into four sections, with essays by journalists Penny Proddow, Marion Fasel, and Jeryl Brunner, and by curator George Harlow.

Henry Dunay, who began his life in 1935 as Henry Loniewski, became a messenger to a New York jewelry workshop at the age of 14. From there, his dedication and perseverance earned him a promotion to jeweler's apprentice. During these years in the Bowery, he worked nonstop to master every aspect of diamond setting.

Henry was born with design and precision in his blood. Growing up in the midst of Manhattan's world-famous retail jewelers—names like Harry Winston, Van Cleef & Arpels, and Tiffany & Co.—he gained a keen awareness of the elements used in fine jewelry making, and mastered the techniques of contemporaries such as David Webb. Yet Dunay took everything he touched to a new level of beauty and design, producing imaginative, magnificent, truly distinctive jewelry.

In 1967, Dunay got his first real break as a designer when he won the De Beers Diamonds International Award. The road to success, however, was not an easy one. During the 1970s, when times were difficult in New York, he set his sights on other areas of the country. He eventually networked his way into the famed Neiman Marcus department store in Dallas, Texas, where some of his wealthiest and most faithful followers can still be found. Soon, Dunay's pieces were sold before they even appeared on the sales floor.

Stephen Magner, vice president of Neiman Marcus's jewelry division from 1984 to 2005, wrote in the introduction, "Through the endless public appearances, conversations with followers, as well as vast travel experience in sourcing materials, the collections came to truly reflect Henry's heart, soul, and personality." His relationship with Neiman Marcus has lasted more than 30 years, and the stories of a number of top Neiman Marcus clients are recounted in Brunner's section titled "Suntanned Ladies: Henry's Muses Sing a Song of Beauty." Some of his clients have Dunay collections larger than the Neiman Marcus inventory, and in their interviews they share their favorite pieces with the reader and describe why Henry Dunay is a part of their style. Dunay's creations have adorned presidents' wives, famous actors, and dignitaries throughout the world, and their stories come to life here through beautiful photographs and delicious details.

Harlow's section, "Coloring Henry: An Education on Colored Stones," compares Dunay to famed mineralogist George Frederick Kunz, who was Tiffany & Co.'s gem expert in the late 19th and early 20th centuries. Even in a diamond-driven market, Dunay realized that colored gemstones other than the big three (ruby, emerald, and sapphire) could be combined with his designs to create less-expensive pieces. Using his keen eye for the combination of fineness and form, and how they fit his designs, Dunay started his own line of colored stone jewelry.

As a designer, Dunay quickly saw opportunities in both fashioned gems and natural crystals, and this early work inspired him to further his education in colored gems by traveling to the market in Idar-Oberstein, Germany. This section also describes his special relationship with mentor and business partner Hans Jurgen Henn. From his travels with Henn in the Himalayas to his annual pilgrimage to the coral capital of Torre del Greco in Italy—as well as trips to Tanzania, Myanmar, Russia, and Ukraine—Dunay has spanned the globe. His ability to combine metals with gem finds from his travels leaves the reader captivated.

Dunay's passion has permeated his family's everyday life, and his son and daughter share delightful stories of how they've seen their father's designs come from a deep inner place, from his soul. The craft was always paramount in their family life—Paul Dunay began joining his father on business trips at the age of 12—but it is evident that Dunay, now a grandfather, treats his family with the love he gives his creations.

Full-page museum-quality photographs and original renderings of these collectible pieces glitter on each

page. The book will help the reader appreciate how Henry Dunay's autonomous craftsmanship has defined him as a modern-day Fabergé. Before reading this book, I was not necessarily a fan of Dunay. This book inspired me so much that it sent me on my own search for Dunay pieces in the secondhand market, and what a delightful treasure hunt it has been!

MELINDA ADDUCCI
Joseph DuMouchelle International Estate Buyers & Auctioneers
Grosse Pointe Farms, Michigan

Russian Gemstones Encyclopedia

By Vladimir V. Bukanov, 472 pp, illus., publ. by Granit Publishing, Prague, 2006. €79

Russian Gemstones Encyclopedia is a single book, but it includes enough text, photos, and illustrations to have been published as two or more volumes without looking sparse. Much is covered in its eight main chapters, the first of which appears to be unique in a publication such as this: "To the History of Jeweler's Art & Gemology." It is commendable that this chapter was included and that it mentions many important people—not all of whom are Russian—as this is a worldwide history. That being said, some major contributors to the science of gemology are conspicuous by their absence here. This first chapter is followed by two pages characterizing different kinds of materials that are used in jewelry and for other ornamental purposes.

A chapter explaining the structure of the *Encyclopedia*, its chapters, and their topics and subheadings follows, including a list of abbreviations. The third chapter, and probably the most important one, is "Best Known Gemstones," though this also includes lesser-known gems such as scapolite. There are many subtopics for each gem, with the most important gems commanding the most attention. For diamond alone, there are 10 subtopics, such as Composition and Properties, Deposits, Quality Improvements, Legends, and more. Interestingly, this "gemstone" chapter includes metals such as gold, platinum, palladium, silver, copper, and iron.

Five more chapters follow: "Less Known Gemstones" (e.g., apatite, dioptase, and variscite), "Gemstones for Collectors" (e.g., apophyllite, diaspore, and sinhalite), "Minerals and Rocks as Ornamental Stones" (e.g., calcite, the feldspar family, magnesite, and the serpentine group), "Bioorganic-Jewelry-Ornamental Materials" (pearls, amber, ivory, and the like), and "Synthetic Gemstones." Following these chapters is an appendix that covers some two dozen other useful topics (such as unique diamonds, jade, and Russian gem deposits). There is also a useful general index.

This book holds an abundance of information, illustrations, and good-quality photographs, and the paper, binding, and handsome hardcover produce a reference that will last. However, this work is also compact in nature with small, hard-to-read print and relatively small illustrations. The title is also a bit deceptive, as it is not solely about Russian gemstones but is rather a general work with an emphasis on Russian material. Regrettably, some of the information appears outdated (such as equating the values of fancy-colored diamonds to colorless brilliants of the highest quality) or even incorrect (blue diamonds are type IIb, not type Ib). In addition, the translation into English was hard to follow and often resulted in broken syntax. I had to pay close attention in many instances to understand the author's intended meaning.

Despite some drawbacks, I like this book overall. It encompasses a wealth of information that is hard to find in most other texts. I would have enjoyed the volume even more had it limited itself exclusively to Russian gemstones, as the title implies.

MICHAEL EVANS
Gemological Institute of America
Carlsbad, California

Volodarsk-Volynski: Mineralogy of the Volynian Chamber Pegmatites, Ukraine

By Vladimir Ivanovich Pavlishin and Stanislav Alekseevich Dovgyi, Mineralogical Almanac, Vol. 12, 125 pp., illus., publ. by Mineralogical Almanac [http://webcenter.ru/~minbooks], Littleton, CO, 2007. US$45.00

A most welcome and long-awaited publication finally made it to press and in English, too. This work reviews the history and mineralogy of one of the most famous and widely studied pegmatite districts in the world, the Volodarsk chamber pegmatites in Ukraine. My first impression was that this issue is just as remarkable as the beryl and topaz the mines have produced.

The Volodarsk pegmatites were known as early as the 1900s, but only in 1931 did the Soviet government begin serious prospecting and mining for piezoelectric quartz. The area eventually became one of the most closely studied gem pegmatite regions in the world: A 22 km long, 1–3 km wide belt of the Korosten Pluton in Ukraine was core-drilled from 100 m down to 600 m in a very tight grid to detect pegmatites containing the large quartz crystals sought by the Soviet military. In its heyday, the mine employed some 1,000 miners and 60 geologists. Topaz and beryl were mere by-products of the mine until the breakup of the Soviet Union. Only 10% or so of the pockets contained topaz, and only 2% held beryl. But the pockets were gigantic, often several meters in size, with each one producing anywhere from a few tons to more than 100 tons of quartz, though usually only a small portion of the quartz crystal terminations were of good piezoelectric quality.

The various studies of the deposit and its geologic-petrographic characteristics are covered in chapter 2, while chapter 3 addresses the position, morphology, and structure of the pegmatites. The gem species and non-gem minerals that occur are well described and richly illustrated in

chapter 4. Cross-sections of individual pegmatites and good geologic maps add to the richness of information. Perhaps the highlight of the book is the detailed description of the conditions of formation (and dissolution) of individual minerals. A comprehensive and well-selected bibliography adds to the value of the volume.

Somewhat weaker are the descriptions of individual finds (year, location in the mine, and depth), but such information is known only to a small handful of people. The book also lacks photographs of the faceted and carved gems and the jewelry made from them, which poured into the European and North American markets for a few years but disappeared as quickly as they arrived. In fact, many large and beautifully colored flawless stones were cut from Volodarsk beryl and topaz.

Since 1995, small-scale exploration and mining has been conducted (sometimes clandestinely) by pumping out huge volumes of water and silt from the old shafts and galleries, at great expense, but production has been very limited and most of the gem-quality material is cut and sold in jewelry in Ukraine. This reviewer was the first foreigner allowed to enter these mines in the post-Soviet era. That was in 1995, just when they were about to be closed. When I last visited the mines in the spring of 2008, only small-scale digging was taking place, in a single open pit just above water level. Some pockets described by geologists in the 1970s as still containing significant amounts of untouched beryl have proved to be unproductive, while other pockets that were once overlooked have shown some beryl mineralization.

This work was undoubtedly written and edited by experts and lovers of this deposit. However, I would have liked to see much more information about the production and discovery of magnificent gem minerals from the 1970s to the 1990s. More importantly, there was much detailed scientific research by the mine geologists conducted during this period that is not fully reflected in the book. Finally, there are some mistakes in the translation from the excellent Russian version that sometimes make the text unclear or even contradictory. For instance, page 61 (line 12 from the bottom), "presence of strong base solutions" should read "absence of . . . ."

Nevertheless, this is truly a marvelous publication deserving much respect, and it should prove extremely valuable for anyone curious about the Volodarsk deposit. It also offers some insight into the tremendous (and very costly) efforts of the former Soviet Union to exploit the pegmatites, as information about the deposit was considered a state secret during the Soviet era and even today is guarded closely. The publication is an absolute must for anyone seriously interested in gemstone deposits, pegmatites, and minerals.

PETER LYCKBERG
Luxembourg

OTHER BOOKS RECEIVED

Laboratory Grown Diamonds, 2nd Ed. *By Branko Deljanin and Dusan Simic, 86 pp., illus., publ. by Gemology Headquarters International [www.ghilab.com], Mumbai, 2007, US$20.00.* This is a revised and updated version of *Laboratory Created Diamonds* by Sharrie Woodring and Branko Deljanin (see review in the Summer 2007 *Gems & Gemology*). Sections on standard identification techniques have been expanded, and new information on identifying small synthetic diamonds and synthetic diamond grading has been added.

TWO

Diamond Ring Buying Guide, 7th Ed. *By Renee Newman, 156 pp., illus., publ. by International Jewelry Publications [www.reneenewman.com], Los Angeles, 2007, US$18.95.* This is a revised and updated version of the sixth edition (reviewed in the Summer 2002 *Gems & Gemology*), covering new information on diamond cut grading, diamond treatments, and synthetics. New for this edition is a discussion on the use of palladium in jewelry.

TWO

Tables of Gemstone Identification. *By Roger Dedeyne and Ivo Quintens, 309 pp., illus., publ. by Glirico [www.gemmologie.be/GEMMOEN/BooksEN.htm], Ghent, Belgium, 2007, €89.* Designed as a reference for laboratory and other working gemologists, this large-format (A4) hardbound book contains detailed lists of commonly used gemological properties. The information is organized in five separate tables sorted by refractive index (transparent and opaque gems), specific gravity, spectrum, and alphabetical order, respectively. Also included are a graph of RI vs. SG for glass, and two tables to assist with identifying garnet group gems and diamond simulants.

TWO

Verdura: The Life and Work of a Master Jeweler. *By Patricia Corbett, 224 pp., illus., publ. by Thames & Hudson [thamesandhudsonusa.com], New York, 2008, US$34.95.* This is a paperback edition of the 2002 book chronicling the life and work of Fulco Santostefano della Cerda, Duke of Verdura (1898–1978). An impoverished Sicilian nobleman with a talent for drawing, Verdura caught the eye of Coco Chanel in the 1920s. He came to the United States in 1934, and his jewelry designs quickly became a favorite of Hollywood stars and wealthy Americans. The book is well illustrated with numerous photos of Verdura's signature pieces and the famous clientèle who wore them.

TWO

GEMOLOGICAL
ABSTRACTS

COLORED STONES AND ORGANIC MATERIALS

^{57}Fe Mössbauer spectroscopy, X-ray single-crystal diffractometry, and electronic structure calculations on natural alexandrite. S.-U. Weber [sven.weber@sbg.ac.at], M. Grodzicki, W. Lottermoser, G. J. Redhammer, G. Tippelt, J. Ponahlo, and G. Amthauer, *Physics and Chemistry of Minerals*, Vol. 34, No. 7, 2007, pp. 507–515.

Two crystals of alexandrite from Malysheva, near Sverdlovsk in the Ural Mountains of Russia, were characterized by several techniques to better determine the oxidation state and location of iron in the crystal structure. Most of the iron was Fe^{3+}, and a small percentage was Fe^{2+}. Both ions occupy octahedral (M1 and M2) sites where they substitute for aluminum—there is no evidence of their presence in tetrahedral sites that contain beryllium. Trivalent iron appears to favor the M2 site, and chromium substitutes for aluminum mainly in this same position. The article also presents chemical composition data by electron microprobe and unit-cell parameters refined by single-crystal X-ray diffraction.

JES

Fossil pearls: Very old, very rare. R. Torrey, *Pearl World*, Vol. 17, No. 3, 2008, pp. 3–5.

The article discusses a collection of more than 1,000 fossil pearls from long-extinct bivalves. A small number (29) were round and still showed nacre, while the remainder were blister pearls still attached to shells. Most were collected around Florida. The article also includes photographs of fossil pearls held by other collectors. *RS*

This section is designed to provide as complete a record as practical of the recent literature on gems and gemology. Articles are selected for abstracting solely at the discretion of the section editors and their abstractors, and space limitations may require that we include only those articles that we feel will be of greatest interest to our readership.

Requests for reprints of articles abstracted must be addressed to the author or publisher of the original material.

The abstractor of each article is identified by his or her initials at the end of each abstract. Guest abstractors are identified by their full names. Opinions expressed in an abstract belong to the abstractor and in no way reflect the position of Gems & Gemology *or GIA.*

Infrared spectroscopic study of modern and ancient ivory from sites at Jinsha and Sanxingdui, China. L. Wang [wangling@cdut.edu.cn], H. Fan, J. Liu, H. Dan, Q. Ye, and M. Deng, *Mineralogical Magazine*, Vol. 71, No. 5, 2007, pp. 509–518.

Ancient ivory, buried for several thousand years at the Chengdu Jinsha and Guanghan Sanxingdui sites in China, was compared to modern ivory using IR spectroscopy in the 4000–400 cm^{-1} range. By combining these results with XRF data, the authors determined the crystallinity and crystal chemistry of the apatite component, as well as the structural characteristics of the ivories. The ancient ivory consisted almost entirely of hydroxyl-carbonate apatite. Compared to modern ivory, the PO_4^{3-} and CO_3^{2-} bands were stronger, the νPO_4 IR bands were obviously greater, and an extra OH^- band at 3569 cm^{-1} was observed. These results imply that there is a greater degree of crystallinity in the ancient apatite, and that there has been incorporation and recrystallization of CO_3^{2-} in the apatite during burial. Positive correlations were found between apatite crystallinity, CO_3^{2-} and OH^- contents, and burial time. Loss of organic matter from the ancient ivory may be the main reason why it is easily dehydrated and readily friable after being unearthed. *RAH*

"Keshis" et nouvelles perles de culture d'eau douce de Chine ["Keshis" and new Chinese freshwater cultured pearls]. E. Strack, *Revue de Gemmologie*, No. 162, 2007, pp. 9–10 [in French].

For more than two years, China has been exporting freshwater cultured pearls in a variety of flat, slightly curved shapes, ranging from subround to baroque; they may also be rectangular or form a joined pair. These cultured pearls may exhibit impressive orient, and have colors varying from white to pink, orange, violet, golden gray-brown, and green-brown. They are known commercially as "corn flakes," "petals," or—incorrectly—as "keshis."

The Japanese word *keshi*, which refers to a very small particle (e.g., a poppy seed), was originally applied to minute pearls found in the oyster next to cultured pearls. These small pearls are an accidental result of the cultivation process, and may develop either when the implanted mantle tissue fractures and forms separate pearl sacs, or following the oyster's rejection of the implanted bead. Keshis can also form when small chips from the mollusk's shell break off and fall inside the organism during bead insertion. Akoya keshi pearls are usually off-round to baroque in shape. Since 1980, the name *keshi* has also been applied to white and black non-nucleated saltwater cultured pearls.

The Chinese product is in fact not a true keshi but a planned freshwater cultured pearl that formed after the second harvest. Because these flat cultured pearls are the product of a collapsed pearl sac, they tend to be baroque in shape.

Also from China are freshwater cultured pearls with large beads that recently came to market from Zhuji, Zhejiang Province. Called *Ikecho*—a Japanese name given to the Chinese freshwater mollusk *Hyriopsis cumingii*—they have baroque shapes and can reach 15 mm long. They have excellent luster and exhibit typical colors associated with Chinese freshwater cultured pearls: white, pink, orange, and violet. *Francine Payette*

DIAMONDS

A contribution to the understanding of pink color in diamond: The unique, historical "Grand Condé." E. Fritsch, B. Rondeau [benjamin.rondeau@univ-nantes.fr], T. Hainschwang, and M.-H. Quellier, *Diamond and Related Materials*, Vol. 16, No. 8, 2007, pp. 1471–1474.

This study documents, for the first time, the Grand Condé, a 9.01 ct faceted pink diamond that has been kept since 1862 at Château de Chantilly in Oise, France. It is a somewhat irregular, flat pear shape measuring approximately 20 × 14 × 5 mm. With magnification, the pink color appeared to be evenly distributed. Between crossed polarizing filters, it exhibited intense anomalous double refraction consisting of a combination of a cross-hatched "tatami" pattern and broad regions of low-order interference colors. The diamond had weak yellowish green fluorescence to long-wave UV radiation, and very weak whitish yellow fluorescence to short-wave UV.

The Grand Condé is a type IIa diamond, as confirmed by its mid-infrared spectrum, which also exhibited several very weak absorption features of uncertain identity (and not previously reported) between 1156 and 860 cm^{-1}, and by its relative transparency to short-wave UV. The visible spectrum (recorded at 77 K) had a broad absorption band centered at about 550 nm and a group of weak but sharp bands at 573, 586, 594, 600, and 609 nm (named here the "609 nm system"). All of these features were superimposed on an absorption continuum that rose toward the UV region. The spectrum also contained a very weak 741 nm band caused by the diamond's exposure to a small amount of natural radiation. No photoluminescence features were excited by illumination with a 532 nm laser.

One surprising feature of the Grand Condé was the association of the broad 550 nm absorption band with an evenly distributed pink color. This band is normally seen in diamonds with distinct pink graining in bands parallel to the octahedral planes. The UV fluorescence reactions of the diamond were also quite unusual. *JES*

In the cut. R. Murphy, *W*, Vol. 37, No. 3, 2008, pp. 282–284.

The article details the large diamonds that have come from Lesotho's Letšeng mine, including the 603 ct Lesotho Promise and the 493 ct Letšeng Legacy. London jeweler Laurence Graff fashioned 26 D-Flawless diamonds, total-

ing 224 carats, from the Lesotho Promise after paying US$12.4 million for the rough. The author interviewed Graff about the cutting of the stone, which took nine months. *RS*

Detection of diamond in ore using pulsed laser Raman spectroscopy. G. H. Lamprecht [gert.lamprecht@debeersgroup.com], H. G. C. Human, and L. W. Snyman, *International Journal of Mineral Processing*, Vol. 84, 2007, pp. 262–273.

This study suggests that extracting diamond from ore by detecting its Raman signal with a laser is more effective than sorting by X-ray luminescence. The authors analyzed the Raman and luminescence signals of diamond and associated minerals (18 total) found in diamondiferous ore. The samples included four diamonds (one each of type Ia, Ib, IIa, and IIb) for analysis in the broad spectral region, and a set of 203 diamonds (in a variety of types and qualities) for the narrow spectral region.

When excited by pulsed lasers, the fluorescence of diamond and its associated minerals shows a nonlinear relationship with incident irradiation density. This saturation effect suggests that pulsed lasers offer an advantage over continuous wave lasers in diamond extraction. The 308, 355, and 532 nm pulsed lasers and the 532 nm continuous wave laser were found suitable for use in a detection apparatus. However, the 266 and 1064 nm pulsed lasers and the 488 and 632 nm continuous wave lasers did not perform well, because their strong fluorescence overwhelmed the Raman signals, their poor detection resulted in weak Raman signals, or a combination of both. Based on the statistics, the 532 nm pulsed laser was found to be the most reliable for diamond sorting applications.

KSM

Les diamants de couleur naturelle [Natural fancy colored diamonds]. T. Haddad and A.-F. Fourre, *Revue de Gemmologie*, No. 162, 2007, pp. 11–14 [in French].

Almost all colors of the rainbow have been found in diamonds, with brown being the most common and red the rarest. Thirteen hues have been noted in all: pink, red, orange, yellow, brown, "olive," green, blue, violet, purple, white, gray, and black. The origin of color is related to changes in internal structure caused by substitution of a carbon atom by another type of atom (as a single atom or as aggregates), structural defects (e.g., graining), natural radiation, fluorescence, or the presence of inclusions.

There is no standard nomenclature for colored diamonds. Most laboratories use either the Munsell color system or the color grading terminology formulated by GIA. Because the intensity of color plays such a significant role in determining value, fancy-colored diamonds are described by their saturation using seven classifications ranging from *faint* to *dark*. Clarity is usually less important than color in determining the value of a colored diamond.

Twenty years ago, fancy-colored diamonds were not in demand, and many were relegated to industrial grade. However, such diamonds are now more popular than ever and command high prices. Black and brown diamonds usually sell for less than near-colorless stones, while red, blue, intense purple, and intense green diamonds command the highest prices. Larger fancy-colored diamonds are much rarer than their colorless cousins and significantly more valuable. *Francine Payette*

Investigating large vacancy clusters in type IIa diamond with electron energy loss spectroscopy (EELS). R. Barnes [rachelbarnes1983@hotmail.com], U. Bangert, and A. Scott, *Physica Status Solidi (a)*, Vol. 204, No. 9, 2007, pp. 3065–3071.

The origin of brown color in diamonds continues to attract scientific attention. Type IIa brown diamonds commonly contain very low amounts of chemical impurities, which indicate that their coloration results from lattice defects. Past theories that their color is due to dislocations resulting from plastic deformation are no longer viable, since such deformation also occurs in colorless diamonds. Recent investigations have suggested that the brown color is linked to vacancies (missing carbon atoms) and vacancy-related extended defects (or vacancy clusters of perhaps 50–60 vacancies). Calculations indicate that such extended defects will give rise to a featureless optical absorption spectrum similar to that of brown type IIa diamonds. The present study uses a spatially resolved EELS technique, which can provide information on the local electronic structure of extended defects in materials. Examination of several diamonds, including one with alternating colorless and brown bands, suggests that the brown-colored areas contain a greater percentage of carbon atoms linked by pi (π) bonds (a type of covalent bonding present in polymeric materials in which the greatest overlap between atomic orbitals occurs along a plane that is perpendicular to the line joining the atomic nuclei). Such bonding is thought to be a feature of the extended defects in brown diamonds.

JES

La mine de Williamson [The Williamson mine]. S. Scalie, M. Philippe, and D. Sirakian, *Revue de Gemmologie*, No. 159, 2007, pp. 21–25 [in French].

This article reviews the history of the Williamson mine in Tanzania, which is one of the few sources of pink diamonds, among them the 54 ct Williamson Pink. The diamondiferous pipe at Mwadui was discovered by John Thorburn Williamson in 1940 and was exploited by him until his death in 1958. The mine was acquired by De Beers, then nationalized by the Republic of Tanzania, and sold again. Since 1994, it has been jointly owned by De Beers (75%) and the Tanzanian government (25%).

The diamond-bearing kimberlite at Mwadui erupted some 52 million years ago. The formation of tuffs and caving in of the granites surrounding the pipe, together with

erosion, has partly filled the crater so that diamonds are found today not only in their original kimberlite but also in multilayered sediments of kimberlite mixed with tuffs, granitic debris, and breccias.

Williamson only exploited the surface layer of the pipe and produced one million carats per year (10–14 carats per 100 tonnes). Today, mining has extended 85 m below the upper rim. With increasing depth, production has increased, but the quality of the stones has decreased. In 1988, prospective drilling explored to a depth of 668 m.

Since 1967, when 927,000 carats were recovered, diamond production has dropped considerably (e.g., 260,000 carats in 2004). It is hoped that new technologies will help increase production over the next 25 years. *RT*

On the role of nitrogen in stiffening the diamond structure. S. G. Nailer, M. Moore [m.moore@rhul.ac.uk], J. Chapman, and G. Kowalski, *Journal of Applied Crystallography*, Vol. 40, No. 6, 2007, pp. 1146–1152.

Three rough diamonds (4–7 mm) from the Argyle mine in Australia were examined for their nitrogen content and crystalline perfection. These diamonds were interesting because each was half brown/half colorless with a well-defined boundary separating the color zones along a (111) plane. Since the two halves experienced identical geophysical conditions of time, temperature, pressure, and shear forces, and those factors influence the extent of plastic deformation believed to cause brown coloration, these samples were ideal specimens to see what other features could affect diamond color.

The authors investigated the crystal distortion by a number of different methods, including synchrotron Laue photographs, synchrotron topographs, and double-crystal rocking curves. In all tests, the brown sections of the crystals showed significantly higher distortion than the colorless sections. From IR spectroscopy, the authors calculated the nitrogen concentration and its extent of aggregation in the brown and colorless halves. They observed a correlation between color and total nitrogen content, but not with the presence of A and B aggregates. In two samples, the colorless sections of the stones had at least 1.6 times more nitrogen than the corresponding brown halves. The authors also calculated the average platelet radii in these samples and found no obvious correlation with nitrogen concentration or the degree of deformation. *SE-M*

GEM LOCALITIES

La colline aux aigues-marines d'Opanayake, Sri Lanka [The aquamarine hill of Opanayake, Sri Lanka]. P. Algier [pascal@planetgem.com], *Revue de Gemmologie*, No. 161, September 2007, pp. 15–21 [in French].

The author reports on a trip to two gem deposits in Sri Lanka. The first part describes a visit to a sapphire mine near Ratnapura (including a descent underground) and the primitive mining conditions there. This is followed by a visit to Opanayake, where a large pegmatitic quartz outcrop contains aquamarine and is also mined by artisanal methods. The aquamarines are of "ocean" green to blue color and can be very brilliant after cutting. Some gemological data are given, together with photos of rough and cut samples. *RT*

Il mistero delle dendriti indiane [The mystery of Indian dendrites]. M. Campos Venuti and M. Pantò, *Rivista Gemmologica Italiana*, Vol. 2, No. 3, 2007, pp. 181–191 [in Italian].

Dendritic agates were very popular in the 18th and 19th centuries and were generally known as *mocha stones*. In recent years, they have reappeared on the market.

This article traces the agates back to their origin: A region near Bānda in southern Uttar Pradesh, India. Here, agates with flat banding (Uruguay-type) formed in the vast basalts of the Deccan Plateau. Black, brown, and reddish dendrites subsequently developed parallel to these flat layers. The agates are found in alluvial deposits or in weathered basalt. The stones are recovered by local villagers, who also fashion them by hand into flat cabochons using methods largely unchanged since the 18th century. Only about one out of 100 agate geodes contains dendrites, and truly attractive specimens are very rare and highly prized. Also discussed are dendritic agates and quartz from other sources, especially Brazil and Kazakhstan. *RT*

Noble gases in corundum megacrysts from the basalts in Changle, Shandong Province, eastern China. W. X. Hu [huwx@nju.edu.cn], Y. C. Song, X. M. Chen, M. X. Tao, and L. P. Zhang, *Chinese Science Bulletin*, Vol. 52, No. 3, 2007, pp. 380–387.

The occurrence of corundum crystals in basalts is still somewhat of a geologic enigma. Noble gases such as He, Ar, and Xe trapped in mineral inclusions act as isotopic tracers that can provide unique information on the properties and evolution of the Earth's mantle and identify mantle-derived materials. This study of sapphire megacrysts from Changle was undertaken to better understand their origin. These crystals displayed noble gas isotopic compositions (particularly He and Ar) similar to pyroxene and anorthoclase megacrysts from the same area, and also similar to mantle-derived peridotite xenoliths from this and other areas of eastern China. This indicates that the noble gases trapped in the corundum originated from a mantle source that appears to represent a "mixed fluid" produced by the interaction between the lithospheric mantle and fluids released from a subducting plate. Furthermore, the noble gas isotopic compositions, and the oxygen isotopic composition of the corundum itself, are not characteristic of a crustal source. The authors conclude that the corundum megacrysts formed from a mantle-derived magmatic source with minimal crustal contamination.

JES

JEWELRY HISTORY

The Treasure of Guarrazar: Tracing the gold supplies in the Visigothic Iberian Peninsula. M. F. Guerra, T. Calligaro, and A. Perea, *Archaeometry*, Vol. 49, No. 1, 2007, pp. 53–74.

An early (6th–7th century AD) Visigothic gold hoard known as the treasure of Guarrazar was found in 1858 near the Spanish village of Guadamur, outside Toledo. The 10 crowns, 9 crosses, 16 pendants, and multiple chains and parts of votive jewelry that have survived a century and a half of looting consist of a combination of sapphires, garnets, mother-of-pearl, emeralds, and glass set in gold. These artifacts represent some of the finest workmanship from Germanic goldsmiths that is still preserved in Europe. Stylistically, the sophistication of design indicates trade links with the Byzantine world.

This article reports on attempts to identify the source of the gold, aided by comparison with contemporary gold coins from the same areas. Forty-six samples were subjected to elemental analysis using PIXE (particle-induced X-ray emission) and PIGE (particle-induced gamma-ray emission). Difficulties arose from the small sizes of the gold samples used for testing (which was by necessity restricted to nondestructive methods) and the fact that the gems could not be unset. The minute samples taken from the crowns and crosses of the treasure were also too small to be analyzed by PIXE alone. The combination of PIXE and PIGE with an external 3 MeV proton beam was a good compromise.

Information given by Pliny the Elder on Iberian gold sources in his *Natural History* suggests mining of the gold district around the River Tagus. Most of the garnets probably originated from European deposits (i.e., the Czech Republic), and the emeralds probably came from the Habachtal mines in the Austrian Alps. These results suggest that the Visigoths used materials from European sources rather than from Roman commercial routes.

JEC

SYNTHETICS AND SIMULANTS

HPHT synthesis of large single crystal diamond doped with high nitrogen concentration. Y. Zhang, C. Zang, H. Ma [maha@jlu.edu.cn], Z. Liang, L. Zhou, S. Li, and X. Jia, *Diamond and Related Materials*, Vol. 17, 2008, pp. 209–211.

The authors report on the high-pressure, high-temperature (HPHT) synthesis of type Ib single-crystal diamonds (up to 3.2 mm) with nitrogen concentrations up to 1520 ppm. The goal was to grow large-size single-crystal diamonds with nitrogen concentrations similar to those found in nature and then to use HPHT treatment to convert them to the most common natural diamond type—Ia. The synthetic diamonds were grown using the temperature gradient method under HPHT conditions. The nitrogen source was NaN_3, the carbon source was pure graphite, and the catalyst was Kovar, an iron-cobalt-nickel alloy ($Fe_{59}Co_{25}Ni_{17}$). The growth conditions that produced the largest and highest-quality synthetic diamonds with high nitrogen concentration were a pressure of 5.4 GPa, a temperature of 1480 K, and growth times ranging from 2 to 20 hours. Nitrogen concentrations were calculated using FTIR spectroscopy data. Absorption peaks were seen at 1344 and 1130 cm^{-1}, corresponding to type Ib synthetic diamonds with singly substituted forms of nitrogen. The authors predict that further HPHT treatment of their synthetic diamonds may result in type Ia products with high nitrogen contents, or what they refer to as "nature diamonds." *JS-S*

TREATMENTS

On the interaction of molecular hydrogen with diamonds: An experimental study using nuclear probes and thermal desorption. A. A. Shiryaev [shiryaev@ns.crys.ras.ru], D. Grambole, R. Rivera, and F. Herrmann, *Diamond and Related Materials*, Vol. 16, No. 8, 2007, pp. 1479–1485.

Hydrogen can be an important impurity in natural and synthetic diamonds, with concentrations of up to 7000 atomic ppm (0.7 at.%) reported in the literature. In this study, 13 natural and synthetic diamonds that had been HPHT annealed and then heated in a hydrogen-rich atmosphere were investigated by several techniques. The H concentration was high near the surface of each sample (several atomic percent), but it decreased rapidly (to ~0.5 at.%) within depths of 20 nm below the surface, indicating very low diffusivity and solubility of H in diamond. More H was found in type Ia as compared to type IIa diamonds. Nitrogen defects, particularly single substitutional N atoms, act to block H diffusion, which suggests that H is trapped at this defect. Octahedral growth sectors contained higher H concentrations than cubic sectors. The presence of dislocations in diamond may promote H diffusion.

The results of this study show that it is virtually impossible to introduce an appreciable amount of H into diamond by annealing it in H_2 gas. High concentrations of this impurity found in some natural diamonds appear to result only from the trapping of H during growth. Important H reservoirs in natural diamond are primary fluid inclusions and/or hydrogen-vacancy complexes. *JES*

MISCELLANEOUS

Diamond detail and gem fraud status. J. D. Boles [bgi@bgiuk.com], *Journal of Financial Regulation and Compliance*, Vol. 16, No. 1, 2008, pp. 77–84.

Reports of criminals and terrorists using gemstones as money laundering vehicles have made headlines but are

often greatly overstated. While gems have intrinsic value, they require a great deal of expertise in buying/selling and (when rough) often arbitrary grading, which criminals and terrorists are unlikely to have. With margins on some gems as low as 4–5%, there is little room for error, so using them for money laundering could result in substantial losses. Rough stones present additional problems because of the possibility that the quality or yield of the resulting polished gem may not be as high as planned. In addition, gemstones are covered by anti-money-laundering regulations such as the USA PATRIOT Act and the Kimberley Process, further diminishing their appeal as money laundering media.

The article cites statements from consultants who advise law enforcement on money laundering activities that there is little hard evidence that diamonds or colored stones have been used regularly for such activities, noting that other commodities and illicit drugs are much more reliable trading media. *RS*

Farming miners or mining farmers? Diamond mining and rural development in post-conflict Sierra Leone. R. Maconachie [r.maconachie@ids.ac.uk] and T. Binns, *Journal of Rural Studies*, Vol. 23, 2007, pp. 367–380.

This article examines how alluvial diamond mining in previously war-torn areas of Sierra Leone can spur the revival of agricultural production in that country. The authors trace historic relationships between alluvial diamond mining and farming, and discuss the "resource curse" theory of conflicts waged over resources—particularly "lootable" resources that can be easily carried off and sold. However, the authors maintain that the revival of peaceful diamond mining in these conflict areas can serve as a catalyst for reviving food production. They describe how building infrastructure from diamond revenues serves local populations and can finance conversion of mined-out areas to agriculture. The article also discusses cooperative projects designed to help local residents derive the most benefit from diamonds mined in their locales. *RS*

Girls' best friends. C. Batchelor, *Financial World*, December–January 2007–08, pp. 50–51.

Collecting antique and modern jewelry can be rewarding if buyers know how to look for appropriate pieces. The article discusses various jewelry periods that have come into and fallen out of fashion, and the types of pieces that collectors seek. Pricing and buying at auctions, how to examine pieces for damage, and imitation and treated gems are reviewed. The author concludes by discussing how imitation jewels created in the 18th century have since taken on a value of their own as historical pieces. *RS*

An old threat in a new setting: High prevalence of silicosis among jewelry workers. N. Murgia [nicola.murgia@med.unipg.it], G. Muzi, M. dell'Omo, D. Sallese, C. Ciccotosto, M. Rossi, P. Scatoloini, A. Zingarelli, M. P. Accattoli, D. Melchiorri, and G. Abbritti, *American Journal of Industrial Medicine*, Vol. 50, 2007, pp. 577–583.

Silicosis is an incurable disease of the lungs caused by inhaling airborne crystalline silica. Although its incidence is well known and widely studied in industries such as mining, stoneworking, and glass manufacturing, there has been very little study of its effects on jewelry workers. The authors sought to determine the degree of risk in the lost-wax method of jewelry casting, in which plaster (which can contain significant amounts of crystalline silica) is cast around a wax model to create a mold that is then used to recreate the design in precious metal. They questioned and examined (including via chest X-ray) 100 jewelers who worked in artisanal shops throughout central Italy; 23 showed evidence of silicosis.

The authors speculate that the risks of silicosis in lost-wax casting might be increased because of the very fine particle sizes used in plaster. Also, very few of the workers reported using respiratory protection. However, the authors also caution against drawing broader conclusions from these results because of the relatively low response rate they encountered when recruiting participants for the study. *TWO*